The effect of inter-helix loop length and composition on the voltage sensitivity of jShak1 and mouse K$_v$1.2

By

Nazlee Sharmin

A thesis submitted in partial fulfillment of the requirements for the degree of

Doctor of Philosophy

In

Physiology, Cell, and Developmental Biology

Department of Biological Sciences
University of Alberta

ABSTRACT

The mechanism by which voltage-gated potassium ion (K_v) channels respond to changes in membrane polarization is one of the most widely studied yet least understood aspects of K_v channels. The voltage-sensing S4 helix contains 4-7 basic residues that form an electrostatic interaction network with the acidic residues in the S2 and S3 helices to stabilize the open and the closed state in response to voltage change. Previous studies have demonstrated the importance of S3-S4 loop length and composition in shaping the voltage response of K_v channels. In this thesis, I have undertaken a series of mutagenesis experiments on the mouse $K_v1.2$ (V_{50} approximately -13 mV) and a jellyfish K_v1 channel jShak1 (V_{50} approximately +26 mV) to evaluate how the S3-S4 loop affects the voltage sensitivity and regulates the interaction within the VSD in two different channel backgrounds. I have mutated the S3-S4 loop by changing the length and composition and have mutated an acidic residue on the S2 helix that stabilizes the open state by forming salt bridges with basic residues of the S4 helix. In most K_v1 family channels this residue is glutamate (E226 in mouse, E283 in *D. melanogaster* Shaker), but in the jellyfish channel it is asparagine (N227). I have also made pairwise combinations of the loop-mutants and the S2 mutants to evaluate how their effects interact. Our study found that the effects of the loop mutations on the two channels are significantly different, both in terms of loop length and composition, indicating that the loops affect the propensity for channel opening through factors other than simple constraints on relative movement of S3 and S4. Mutations in the S2 residue reveal the packing of the helices in the two channels differs significantly - in the mouse $K_v1.2$ mutations of E226 to shorter and less

charged residues creates an omega pore through the voltage sensing domain, whereas mutation of N227 in jShak1 leads to strong interactions between the effects of shortening the S3-S4 loop and increasing the size of the residue 227 side-chain, indicating a tighter packing of the helices in jShak1 than in mouse $K_v1.2$.

PREFACE

The part of the thesis presented in Chapter 3, is an extension of our previous study published as Sand et al., 2013 (attached in appendix). Some of the mutants used for this chapter were previously made by Rheanna Sand for the paper published as Sand et al., 2013. An international summer intern, Matthias Ostermaier, helped to make some of the mutants used in the study presented in chapter 4. Aside from the material presented in the Appendix, no part of this thesis has been previously published.

DEDICATION

I would like to dedicate this thesis to my dear ones who have inspired me the most to achieve my goal. To my parents, Mrs. Saleka Begum and Mr. A.N.M. Nurul Haque, for unconditional love and support. To my supervisor Dr. Warren J. Gallin, for guiding me, teaching me and for walking so patiently beside me on this journey. Most of all, I dedicate this thesis to my dear husband, Abunaser Chowdary, who stood by me through the best and the worst of it. My humble gratitude is all yours.

ACKNOWLEDGEMENTS

I would like to acknowledge the following people who directly or indirectly assisted me in the completion of this work: Dr. Warren Gallin, Dr. Declan Ali, Dr. Peter Light, Dr. Rheanna Sand, Donna Atherton, Patrick Boutet, Carla Morgan, Matthias Ostermaier, Danial Phan and the staff in the University of Alberta Biological Sciences Department and Aquatics Facility.

TABLE OF CONTENTS

LIST OF TABLES

LIST OF FIGURES

LIST OF SYMBOLS AND ABBREVIATIONS

Δ	change in
$\Delta 23$	first 23 amino acids removed (inactivation-removed)
ΔG	change in Gibbs free energy between closed and open states
AP	action potential
b	Boltzmann slope factor
DIDS	diisothiocyanatostilbene-2,2′-disulfonic acid
I	current
G	conductance
G-V	conductance-voltage
K^+	potassium ion
K_v	voltage-gated potassium channel
Na^+	sodium ion
Ca^{2+}	calcium ion
Na_v	voltage-gated sodium channel
ND96	*Xenopus laevis* physiological saline
MBM	modified Barth's medium
mRNA	messenger ribonucleic acid
ORF	Open Reading Frame
PCR	polymerase chain reaction
PD	pore domain
PDB	Protein Data Bank
S1	1st transmembrane helix in K_v channels
S2	2nd transmembrane helix in K_v channels
S3	3rd transmembrane helix in K_v channels
S4	4th transmembrane helix in K_v channels (voltage sensor)
S5	5th transmembrane helix in K_v channels
S6	6th transmembrane helix in K_v channels
T1	tetramerization domain
TEV	tobacco etch virus (protease)
TM	trans membrane
V	voltage (across the membrane)
V_{50}	half activation voltage
V_{rev}	potassium reversal potential
VSD	voltage sensing domain

Chapter 1: Introduction

K$^+$ channels are the most diverse group of ion channel family

The neurons and muscles of our body are specialized by their unique ability to generate electrical signals and are commonly known as excitable cells. Like all other cells of living systems, an excitable cell maintains a difference in ion concentration between the intracellular and extracellular environment, which creates a small electrical potential across the plasma membrane. The cellular excitability of these excitable cells is mostly mediated by a family of membrane proteins, called the voltage gated ion channels that have three crucial functional elements: (i) an ion conduction pore distinguishing between K$^+$, Na$^+$ and Ca^{2+}; (ii) a gate that regulates the flow of ions through the pore and (iii) a voltage sensor that can detect the change in membrane voltage and trigger the opening and closing of the gate in response to voltage change (Hille, 2001). Voltage gated ion channels can be defined as pore-forming multi-subunit proteins with the ability to open and close in response to membrane voltage. The two most important features of ion channels that distinguish them from other ion transporters are: the rate of ion transport through the channel is very high (often 10^6 ions per second or greater) and ions are passed through the channels down their electrochemical gradient, without the direct involvement of metabolic energy (Hille, 2001).

The excitable cells (neurons, muscles and endocrine cells) use the voltage gated ion channels to generate and propagate action potential- a short-lasting event, in which the electrical membrane potential rapidly rises and falls, in a consistent trajectory (Cole and Curtis, 1939). In response to appropriate stimulation, the membrane voltage in the dendrite of the neuron becomes depolarized (less negative than the resting state), which causes the voltage-gated sodium channels (Na_v) to open (Hodgkin and Katz, 1949). The rapid influx of Na^+ through Na_v causes the membrane potential to raise, Na_vs to inactivate and the voltage gated potassium channels (K_v) to activate. The resulting outward current of K^+ begins to repolarize the membrane potential back toward its rest state (Hodgkin and Huxley, 1952). The repolarization typically overshoots the resting potential as the potassium channels remain open until the membrane potential becomes more negative than the resting potential. This transient period of hyperpolarization, also known as refractory period, is essential to prevent an action potential from traveling the wrong direction. An action potential typically lasts a few milliseconds and is crucial for mediating cell-to-cell communication in neurons. In skeletal muscle cells, an action potential is the first step in the chain of events leading to muscle contraction (Fenn and Cobb, 1939). Most, but not all, smooth-muscle cells can generate action potentials in their plasma membrane upon membrane depolarization. Some smooth muscles generate action potentials spontaneously, in the absence of any external input, because of pacemaker potentials in the plasma membrane that repeatedly depolarize the membrane to threshold (Widmaier et al., 2014).

K$^+$ channels can be divided into four major structural classes, depending on the trans- membrane (TM) segments (Fig-1.1): (i) K$^+$ channels with 2TM helices, that includes inward rectifiers (K$_{ir}$) (ii) The two-pore K$^+$ channels (K2P) with 4TM domains (iii) K$^+$ channels with 6TM segments and one pore domains. This group includes the voltage gated channels and the small conductance Ca^{2+} activated K$^+$ channels. Voltage gated potassium (K$_v$) channels are a member of 6TM domains class, that also includes KCNQ (K$_v$7.x), ether-a-go-go (K$_v$10.x), egr (K$_v$11.x) and elk (K$_v$12.x) subfamilies (Fig-1.1). K$_v$1.x to K$_v$4.x corresponds to Shaker, Shab, Shaw and Shal channels respectively in *Drosophila*. Besides having conducting 6TM channels (KCNA, KCNB, KCNC, KCND, KCNQ and KCNH), K$_v$ family also includes the non-conducting group of gating modulator: KCNF (K$_v$5), KCNG (K$_v$6), KCNV (K$_v$8), and KCNS (K$_v$9). To be fully functional, K$_v$ channels require a minimal tetrameric organization, with the ion conduction pore lying in the axis of a 4-fold symmetric structure. This research is focused on K$_v$1 family (KCNA) channel from two evolutionarily distant organisms: K$_v$1.2 from mouse (*Mus musculus*) and jShak1 from jellyfish (*Polyorchis penicillatus).*

Voltage gated Potassium (K$_v$) channels: Structure and function

Each α subunit of a K$_v$ channel tetramer contains six transmembrane segments (S1-S6). The S5 and S6 helices and their connecting P loops from each subunit
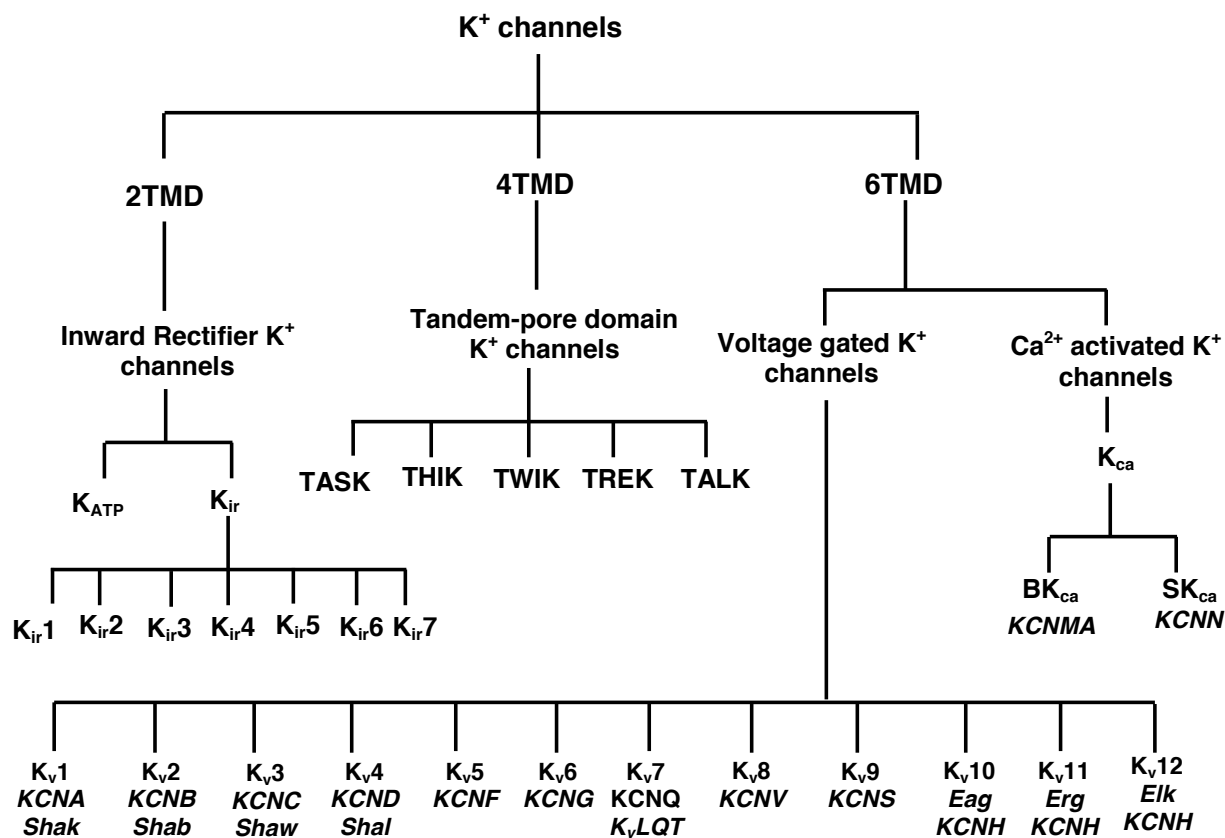
Figure 1.1: Potassium (K^+) channel families arranged according to their trans-membrane (TM) domains (modified from Zhong et al., 2013). K^+ channel families can be grouped in those having two transmembrane segments (2TM; Kir), 4TM (2-pore domain) and 6TM (voltage gated and Ca^{2+} activated channels). Subdivisions of the voltage-gated K_v channels into 12 subfamilies are presented here. The nomenclature proposed by HUGO Gene Nomenclature Committee (HGNC) is followed in this diagram.

form the central pore at the interface between the subunits. Helices S1 through S4 form the voltage sensing domain (VSD). Depending on channel type, S4, the voltage sensing helix, contains four to seven positively charged amino acid residues (usually Arg), also known as gating charges (Fig-1.2). Several negatively charged residues (usually Asp and Glu) that play a role in voltage sensitivity are distributed on the S2 and S3 helices. Gating of the channel is conferred through the attachment of the VSD to the pore domain (PD). In response to change in membrane voltage, the S4 helix undergoes a conformational change, causing the opening of central pore domain. The crystal structure of mammalian $K_v1.2$ channel resolved at 2.9Å (Long et al., 2005) shows that the VSD of one subunit is located near the PD of the adjacent subunit. The connection between the pore and the VSD is made by the S4-S5 linker, which runs parallel to the intracellular membrane surface. Besides having vast sequence diversity within the family, all the K_v channels carry an extremely conserved signature sequence of TTVGYGD that forms the structure of the ion selective filter. This sequence of the PD allows K_v channels to selectively conduct K^+ ions hundreds of times over the Na^+, where the Na^+ has only 0.4 Å smaller radius than K^+. The crystal structure of a bacterial K^+ channel KcsA at 3.2 Å resolution showed two zones in the PD region that K^+ ions must transit in their trajectory trough: the selectivity filter, containing two cations, and the internal vestibule (cavity), having one cation beneath the entrance of the selectivity filter (Doyle et al., 1998). They proposed that in a 4-fold symmetry, the oxygen atoms of the peptide backbone carbonyl groups can
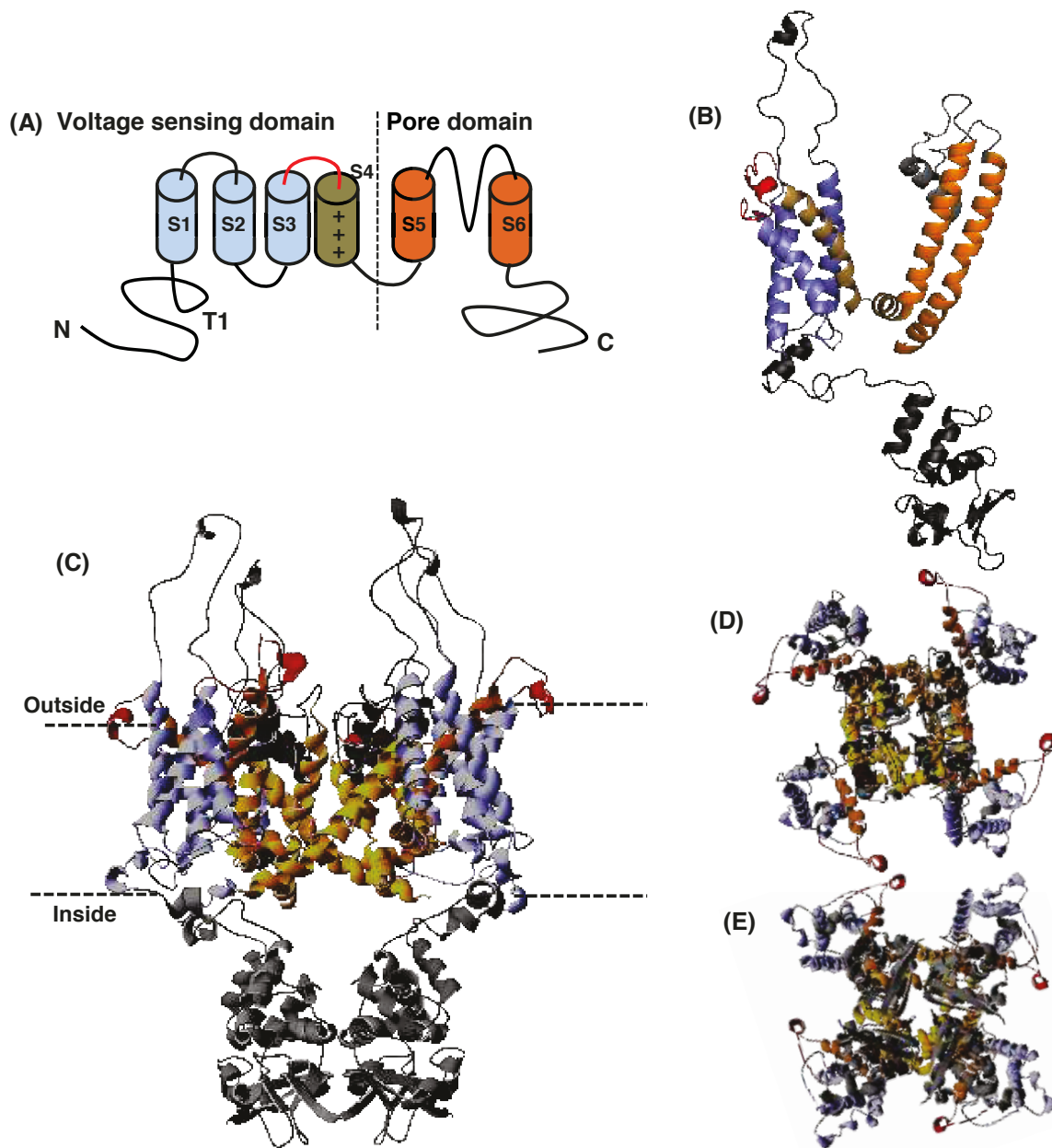
Figure 1.2: Schematic diagram of an ∝ subunit of K_v channel (A), showing an intracellular N-terminus which sometimes contains an inactivation particle (not shown), a tetramerization (T1) domain, six trans-membrane helices (S1 through S6) and their linkers, a re-entrant loop between S5 and S6 that forms a filter region highly selective to dehydrated K^+ ions, and an intracellular C-terminus. Functionally, K_v subunits can be broken down into the voltage-sensing domain (VSD) and the pore domain (PD). The S4 helix carries four to seven positively charged residues at every third position, providing the primary electromotive force that drives pore opening and closing in response to changing membrane electrical potentials (A). The 3D model of rat $K_v1.2$ (3LUT; Chen et al., 2010) (B). Note that rat and mouse $K_v1.2$ have identical protein sequence. Tetramer of mouse/rat K_v 1.2 channel, viewed from the side (C), top (D) and bottom (E). Each subunit has the same colour scheme, and it is the same as that presented in (A). Molecular model images were made in PyMOL.

stabilize the dehydrated K^+ ions by acting as water "surrogate" (Doyle et al., 1998).

Mammalian genomes contain on average ~40 genes that encode the primary or α subunits of K_v channels (Millar, 2000). The functional diversity of the K_v channels in different cell types arises from the differential expression of the genes of K_v channels. The multiplicity of K_v channels is further increased through: (i) Hetero-multimerization: Different monomers of the same family can form hetero-tetramers with novel functional properties not seen in the parental homomeric channels. (ii) Hetero-multimerization with silent subunit families: K_v2 family-form heterotetramers with K_v5, K_v6, and K_v8, subunits that do not form functional channels as homotetramers (Gutman et al., 2005). (iii) Multimerization of $K_v\alpha$ tetramers with accessory β-subunits: $K_v1.1$, $K_v1.2$, $K_v1.3$, and $K_v1.5$ are delayed rectifiers but when expressed with $K_v\beta1.1$, become rapidly inactivating as the Shaker channel in *Drosophila* (Heinemann et al., 1996). (iv) Alternative splicing: For example, Shaker gene in *Drosophila* contains 23 exons and alternative splicing of these exons lead to 10 different channel variants (Schwarz et al., 1988). Alternative splicing occurs in rat K_v3 family (Perney et al., 1992) (v) mRNA editing: Human $K_v1.1$ channels changes the kinetics of $K_v\beta1$-induced inactivation by adapting a hairpin structure, caused by mRNA editing by human adenosine deaminase acting on RNA 2 (hADAR2) (Bhalla et al., 2004). (vi) Posttranslational modifications: $K_v1.2$ is extensively phosphorylated in

mammalian brain, where the phosphorylation causes disruption of $K_v1.2$ interaction with the cytoskeletal protein cortactin (Hattan et al., 2002).

In general, K^+ currents can be classified into showing A-type (fast inactivation) or delayed rectifier behaviour (non-inactivating). At a sustained depolarized pulse, A-type channels activate and then rapidly inactivate, producing a transient response. This type of fast inactivation is thought to play a role in setting the action potential interval. The name 'delayed rectifier' was used by Hodgkin and Huxley (HH) to describe the giant squid axon mostly outward K^+-current that activated later than the Na^+ currents (Hodgkin and Huxley, 1952). This current does not show inactivation in the millisecond time scale. Delayed rectifiers play roles in shaping and terminating the action potential. For example in cardiac action potential, the inward rectifier current I_{K1} participates in the latter part of repolarizing phase, together with I_{Kr} and I_{Ks}, in driving the membrane potential towards the equilibrium potential of potassium and thereby terminating the action potential (Thomas et al., 2006).

Dynamics of the voltage sensing domain (VSD)

During voltage-dependent activation, the VSD performs mechanical work that allows the PD to change its conformation between the closed and open states. The S4 helix, with positively charged residues executes the mechanical work by translocating through the changing electric field of the membrane to drive the

activation of the channel. In *Drosofila melanogaster* Shaker channel, 12-14 electronic charges are estimated to be transferred across the transmembrane electric field during the activation process, which corresponds to around 3 charges transferred per subunit (Schoppa et al., 1992). Mutational studies show that the positively charged residues of the S4 helix make different contributions to the mechanism of activation, rather than simply moving through the electric field (Perozo et al., 1994 and Papazian et al., 1991).

In *Drosophila* Shaker, the mutation of the first arginine of the S4 helix (R362) to histidine (R362H mutation) allowed permeation of cations through the VSD at hyperpolarized potential. This conduction through the mutated VSD of the Shaker channel was coined the "omega (ω) - current" by Tombola et al., (2005). In their paper, Tombola et al. suggested a possible conformational change in the S4 helix at a hyperpolarized potential that may correlate to the opening of the omega pore (Tombola et al., 2005). In a follow up paper Tombola et al. used a quadruply mutated Shaker K_v channel (R362S/ S357C/ E283D/ M256D) in conjunction with cysteine mutagenesis and thiol-reactive agents to characterize the residues in the VSD lining the omega pore (Tombola et al., 2007). They showed that the pore is lined by residues originating mainly from transmembrane helices S1 and S2 (Tombola et al., 2007). R371H mutation in Shaker generated a proton flux at depolarized potential (Starace et al., 2001). Studies have identified naturally occurring mutations in the VSDs of Na^+ channels that can cause omega currents and can lead to a human disease known as hypokaelemic periodic

paralysis (Sokolov et al., 2007). In a K_v3 family channel from platyhelminth (N.at-K_v3.2) the 1st and 3rd arginines of the S4 helix is replaced by histidine and glycine respectively and this channel produces natural omega current. H325R and G331R mutation in N.at-K_v3.2 produced current passing through the canonical pore (Klassen and Spencer, 2008). All these studies indicate the involvement of the 1st and 2nd arginines (R1 and R2) and also S2 and S3 helices in preventing omega current in K_v channel. In a recent paper, Tarek et al. (2013) has proposed that the charge-charge interaction within the VSD is crucial for preventing the omega current. In K_v channels, a water crevice penetrates the structure from the intracellular and extra cellular region, both in the active and the resting state (Krepkiy et al., 2009; Jogini et al., 2007; Treptow et al., 2006 and Freites et al., 2006). Tarek et al. proposed that the state-dependent interaction within the charged residues of the VSD makes a constriction that prevents communication between the extracellular and intracellular media through the water crevice. Any mutation in residues of this region that disrupts the constriction is most likely to generate omega current (Tarek et al., 2013).

Besides preventing the omega current through the VSD, the charged residues of the S4 helix also participate in stabilizing the open and closed state of the channel, as shown by several studies. The neutralization mutation K374Q and R377Q in the S4 helix of *Drosophila* Shaker failed to produce a functional channel. Those non-functional mutant channels were rescued by second mutations at E293Q and

D316N in S2 and S3 helices, suggesting an interaction network between these charged residues (Papazian et al., 1995).

Later studies have identified other electrostatic interactions within VSD that play a role in stabilizing the open and closed state of the channel. In the *Drosophila* Shaker channel, the closed conformation is stabilized by salt bridges formed between Lys374 (K374) in S4 and Glu293 (E293) and Asp316 (D316) in S2 and S3, respectively (Durell et al., 2004; Li-Smerin et al., 2000; Tiwari-Woodruff et al., 1997 and Papazian et al., 1995) (Fig-1.3B). The open conformation, on the other hand is stabilized by the interaction of Arg368 (R368) and R371 in S4 with E283 in the S2 transmembrane helix, whereas E293 in S2 and D316 in S3 interact with R377 (Silverman et al., 2003 and Papazian et al., 1995) (Fig-1.3A). According to a recent model proposed by Jensen et al., (2012), the S4 helix, together with the C-terminal region of the S3-S4 linker is pulled down, in between the negatively charged residues of the VSD and the PD turret, when the channel closes. A homology model of mouse $K_v1.2$, made using the inferred closed state model of Jensen et al. clearly shows the large displacement of the S4 helix and the S3-S4 loop in a downward direction (Fig-1.3D).

The charged residues that regulate voltage sensitivity of K_v channel are conserved is most K_v channels. However, the specific voltage that causes a channel to open is quite variable among and within the families of K_v channel in different species, indicating involvement of other factors in fine-tuning this behaviour of the

11
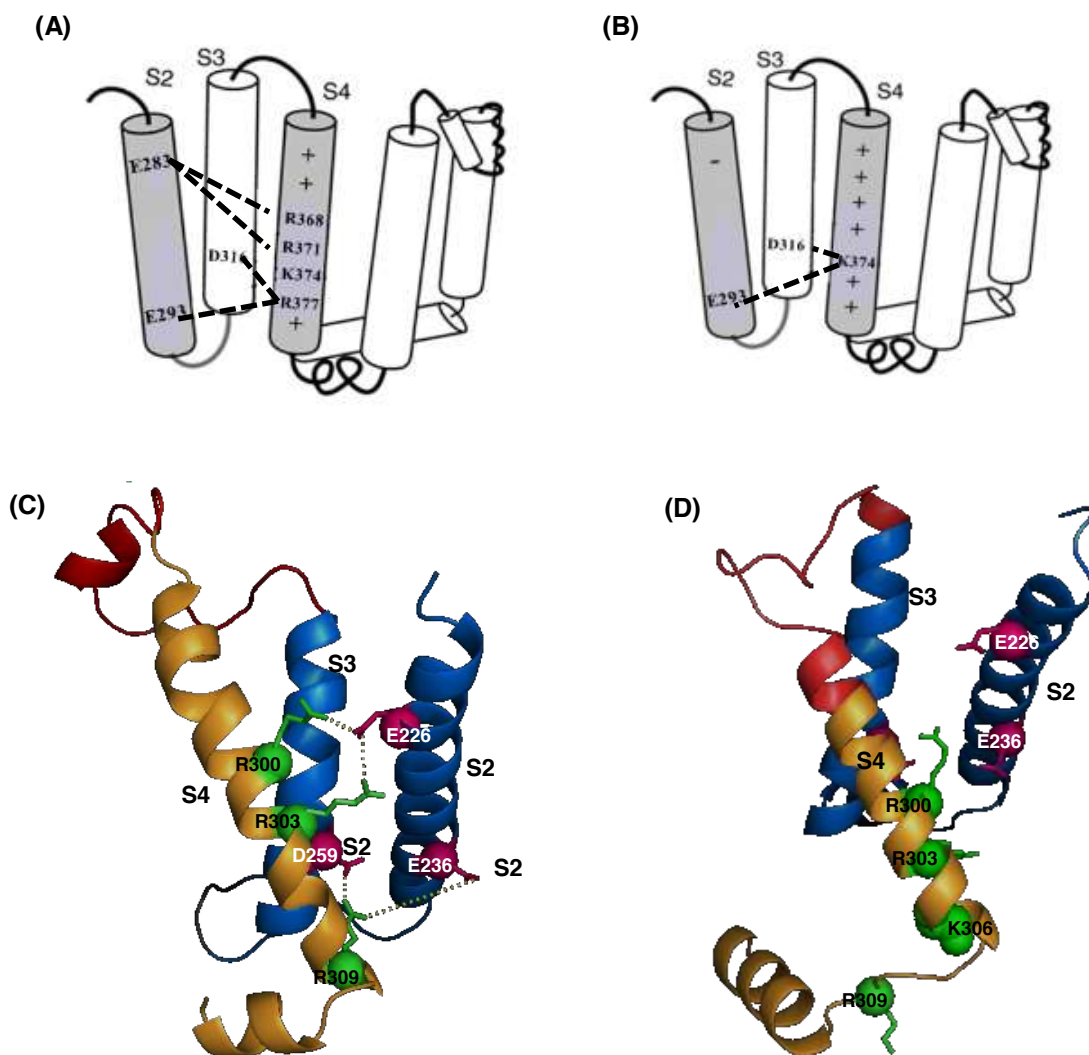
Figure 1.3: Schematic of interactions occurring within the VSD to stabilize the open (A) and closed (B) state of Drosophila Shaker channel (Silverman et al., 2003 and Papazian et al., 1995). The open conformation in Shaker is stabilized by the interaction of R368 and R371 in S4 with E283 in the S2 helix, whereas E293 in S2 and D316 in S3 interact with R377 (A). The closed conformation is stabilized by salt bridges formed between Lys374 (K374) in S4 and Glu293 (E293) and Asp316 (D316) in S2 and S3, respectively (Durell et al., 2004; Li-Smerin et al., 2000; Tiwari-Woodruff et al., 1997 and Papazian et al., 1995) (B). 3D model of mouse $K_v1.2$ VSD in open state (3LUT; Chen et al., 2010), showing possible interaction within the charged residues of the VSD. The homology model of mouse $K_v1.2$ VSD made using the inferred closed state model of Jensen et al. (2012) as template (D). According to Jensen's model, the S3-S4 linker is pulled downward when the channel closes (Jensen et al., 2012). The colour scheme of the helices is same as presented in fig-1.2. Molecular model images were made in PyMOL.

channel. From the crystal structure it becomes apparent that one of the factors that might affect the movement of the S4 helix across the membrane is the length and flexibility of the S3-S4 loop, connecting the S3 and S4 helices. In Shaker, Δ (330-360) mutation to make a channel with 0aa linker caused a large right-shift in the half-activation voltage (V_{50}) as well as a significant decrease in the gating charge (Gonzalez et al., 2000). The conformational changes associated with the activation of K_v channels result in the transfer of some electric charges across the membrane electric field, which is known as the gating charge. This charge transfer is measured as a transient capacitive current, known as gating current. Theoretically, the gating charge of a single channel can be determined by recording the gating current of a single channel (using a patch clamp amplifier) and integrating this current over time. However, the gating currents generated by a single channel are lost in the noise generated from patch clamp systems. An alternate way to measure the gating charge is to use channel-specific radio-ligand to count the number of channels expressed in a *Xenopus* oocyte. This allows a measurement of total gating charge in an oocyte membrane to be converted into a determination of charge per channel (Aggarwal et al., 1996). Decrease in the gating charge of a channel can be the result of the less number of charges in the voltage sensor (S4 helix); the presence of a wider, more diffuse potential field such that the charges traverse a smaller proportion of the potential field or a constrain in the movement of the voltage sensor. For the mutant channels made for the study by Gonzalez et al., (2000), the sequence of the S4 helix and the

13

membrane electric field were invariable. So, a decrease in the gating charge indicates a possible constraint on the motion of the S4 helix, caused by the 0aa S3-S4 linker (Gonzalez et al., 2000). The role of the S3-S4 linker in regulating the movement of the S4 helix is also supported by fluorescent studies by Sorensen et al., (2000). Sequential truncation of the S3-S4 linkers in Shaker shows that the V_{50} of the mutant channel becomes a periodic function of the S3-S4 linker of 4 to 6aa in length , where the C-terminal region of the loop was sequentially deleted (Gonzalez et al., 2001). The S3-S4 loops shorter than 3aa failed to form a functional channel *Drosophila* Shaker (Gonzalez et al., 2001). However, this study failed to differentiate between the effect of loop length and the effect of loop composition on the V_{50} of the channel. Studies with cnidarian K_v1 channel, jShak1, also indicate a possible constraint on the movement of the S4 helix, caused by the natural short length of the S3-S4 loop (Klassen et al., 2008). Our studies with mouse $K_v1.2$ (Sand et al., 2013) indicate a potential role of S3-S4 loop length and composition is setting the specific V_{50} of activation of the channel. The results of this study implied a possible energetic constrain on the movement of S4 helix caused by extreme short length of S3-S4 linker. Depending on composition, the C-terminus of the mouse $K_v1.2$ S3-S4 linker was found to stabilize either the open or the closed state of the channel by interacting with the negatively charged turret of the PD (Sand et al., 2013), as this part of the linker is positioned to close-proximity to the negatively charged residues of VSD and PD, during channel closure (Jensen et al., 2012) (Fig-1.3D).

14

All the above mentioned studies indicate a significant role of the S4 helix in preventing omega current and in setting the voltage sensitivity of the channel. It is also apparent that the S3-S4 loop length and composition constrains the movement of the S4 helix, affecting V_{50}, kinetics and the gating charge of the channel. However, no direct studies have been done to investigate the effect of the S3-S4 loop length and composition on the electrostatic interaction with in the VSD. In this context, I aimed to evaluate the effect of S3-S4 loop length and composition on the dynamics of the VSD an aspect of K_v channel that has not been reported before.

Outline of the thesis

The work presented for my thesis here is aimed to analyze the effect of the S3-S4 loop length and composition on the interaction within the VSD of K_v channel. The study is conducted in K_v1 family channels from two distantly related species: jellyfish (*Polyorchis penicillatus)* and mouse (*Mus musculus*).

The hydrozoan jellyfish *Polyorchis penicillatus* is a member of the Phylum Cnidaria and lacks a central nervous system. They use a diffuse nerve net to transmit photo-sensory information from the ocelli in the bell margin to the swimming muscles lining the bell (Spencer, 1978; Spencer, 1979). The nerve nets of *P*. *penicillatus* are coordinated by two nerve rings in the bell margin (Lin et al., 2001; Spencer, 1979; Spencer and Arkett, 1984) and the nerve rings are

functionally divided into the inner motor center and an outer integrating center. *Polyorchis penicillatus* were collected from Bamfield Inlet or Pachena Bay, near Bamfield, BC, Canada. The normal water temperature these jellyfishes experience range from 7 to 20°C throughout the year ((Lin and Spencer, 2001). So far two K_v1 family channels, jShak1 and jShak2 (Jegla et al., 1995), a K_v3-type channel jShaw1 (Sand et al., 2011) and a K_v4 with an associated gamma subunit (Jegla and Salkoff, 1997) have been isolated and characterized from *P. penicillatus*. Phylum Cnidaria is positioned far from mammals on the evolutionary tree, and is classified as a sister group to all bilaterally symmetrical animals.

The mammalian K_v1 channel used in this study is from house mouse, *Mus musculus*, which is a member of the Phylum Chordata and order Rodentia. They were originally a Palaearctic species, but have been widely introduced across the globe (Musser and Carleton, 2005). The species is now widespread over all continents, except Antarctica (Macholán 1999). House mice are typically commensal, and are found in a very wide range of man-made habitats including houses, farm outbuildings; other types of buildings, and even coal mines and frozen meat stores (Macholán 1999, Wilson and Reeder 2005). Under normal conditions, the body temperature of house mouse range from 34 to 39°C (Gordon, 1993). Most of the K_v1 channel α subunit is found to express in fetal mouse hippocampus (Grosse et al., 2000). The primary goal of this study is to evaluate how the role of S3-S4 linker in the voltage sensitivity has been adapted in two evolutionary divergent K_v1 channels. Mouse and jellyfish are evolutionary widely

16

divergent and habitant of different environments with different temperatures. The K_v1 channels ($K_v1.2$ from mouse and jShak1 from jellyfish) from these two species also possess some interesting differences at the protein sequence. Comparing the results of similar experiments from two different channels would help to identify the general as well as the channel-specific role of the S3-S4 loop in voltage sensitivity of K_v channel.

Chapter 2 contains the materials and methods used for the research. Chapter 3 includes my studies of analysing the effect of S3-S4 loop length and composition on the dynamics of the S4 helix. The work presented in this chapter is an extension of our previous study with mouse $K_v1.2$ loops, published as Sand et al., 2013 (Attached in appendix). In that previous study, we replaced the natural S3-S4 linker of mouse $K_v1.2$ with a wide range of synthetic homopolymeric loops, varying both in length and compositions (Sand et al., 2013). Since the current model of closing process indicates a possible role of the last three amino acid residues (QQA) in biasing the open to close transition of the channel (Jensen et al., 2012), some loops were also made by modifying only the last three residues, which were found to stabilize either the open or the closed state depending on their composition (Sand et al., 2013). The results showed that (i) the length of the loop is responsible for an energetic constraint on the transition between the opened and closed states; (ii) the nature of the side chain of the loops affects its interaction energy with the rest of the channel and this energy varies significantly between the open and closed state and (iii) the three amino acid residues in the C

terminus of the S3-S4 loop that translocate into the negatively charged vestibule of PD, can stabilize either the open or the closed state depending on its composition (Sand et al., 2013).

In addition, the work presented for the thesis in chapter 3 analyzes the interaction of the above stated 'loop-effect' with mutations of the negatively charged glutamic acid (E226) in the S2 helix. I made point mutations by replacing glutamic acid, E226 by aspartic acid, D, which has a shorter side chain length than E, neutral N and Q. E226D mutant channels significantly affected the V_{50} and the slope factor of the channel, compared to the wild-type mouse $K_v1.2$. Both E226N and E226Q mutation produced a leaky channel and treatment of the mutant channels with pore blocker clearly showed that the leak current is an omega current, through the VSD. I made double mutants by combining mouse $K_v1.2$ synthetic loop mutants presented in Sand et al., (2013), with 226D mutants. The synthetic loops used to make double mutants were varied in length (3aa, 5aa and 10aa) and compositions (glutamic acid, serine, and glycine). To analyze the role of the C-terminal amino acids (QQA) and its possible effect on the dynamics of the S4 helix, I also made double mutants by combining hetero-polymeric loops (G7QQA, S7QQA, E7QQA) and E226D.

The results with mouse $K_v1.2$ show that the stable salt-bridge formation between E226 and the positively charged residues of the S4 helix is important for stabilizing the open state as well as for preventing the omega current passing

through the VSD. I have proposed a mechanism in chapter 3 explaining how the different E226 mutations tested might affect the dynamics and the salt-bridging within S2 and S4 helices, causing omega current. Based on the results presented in chapter 3, I also propose the pattern of interaction between the S3-S4 loop of mouse $K_v1.2$ with the rest of the channel.

Chapter 4 contains my study entitled 'The effect of S3-S4 loop length and composition on the voltage sensitivity of jShak1-a K_v1 channel from jellyfish *Polyorchis penicillatus*'. The work presented in this chapter is conducted on a cnidarian K_v1 channel jShak1 from jellyfish *Polyorchis penicillatus*. jShak1 is evolutionary highly divergent from mouse $K_v1.2$. Moreover, jShak1 possess some structural features, unique from most of the K_v channel, making it worth studying and comparing with mouse $K_v1.2$. jShak1 opens at a much higher membrane potential (V_{50} = +26.6mV) compared to mouse $K_v1.2$ (V_{50}= -13.3mV). In jShak1, although one of the conserved acidic residues of the S2 helix (E283 in *Drosophila melanogaster* and E226 in mouse $K_v1.2$) is replaced by a neutral asparagine, N227, no omega current is observed in this channel. Also, jShak1 has one less positively charged motif in the S4 region and a very short S3-S4 linker, consisting of only five amino acid residues (Klassen et al., 2008 and Grigoriev et al., 1997).

In this study, I replaced the natural short S3-S4 linker of jShak1 with synthetic homopolymers varying both in length (3aa, 5aa and 10aa) and compositions (glycine, serine and glutamic acids). Similar synthetic loops that are used with mouse $K_v1.2$ (Chapter 3) is expected to show similar length effect in jShak1.

However, the absence of a negatively charged residue at 227 of jShak1 might prevent the longer loops from shifting the V_{50} values of the loop-mutant channels as negative as were observed for mouse $K_v1.2$ in Sand et al., 2013. To evaluate the role of the C-terminus of the S3-S4 linker in stabilizing the closed state (Jensen et al., 2012) the last positively charged lysine (K) was mutated in both natural and synthetic loops. C-terminus of the S3-S4 loop was shown to affect V_{50} by interacting with the negatively charged residues of the PD turret (Sand et al., 2013). In jShak1 the positively charged lysine (K278) in the C-terminus of the S3-S4 loop is expected to stabilize the relative closed state by interacting with the negatively charged residues of the PD turret. I also replaced the neutral N at 227 of jShak1 with both E and D. N227D and N227E mutations were combined with all synthetic loops to make double mutant channels, with an aim to analyze the effect of S3-S4 loop length and composition on the interaction between the S2 and S4 helices.

The results from jShak1 indicate that mouse $K_v1.2$ and jShak1 have evolved distinct mechanisms to both prevent the omega current and to respond to change in membrane voltage. Based on the results presented in chapter 4, I propose that in jShak1 the S3-S4 linker affects the V_{50} by constraining the movement of the S4 helix and by interacting with the channel. I have found that unlike mouse $K_v1.2$, the interaction between the S3-S4 loop and the channel in jShak1 can regulate the voltage sensitivity even in the absence of a negatively charged residue at 227 of the S2 helix.

Chapter 2: Materials and Methods

Mutant constriction

  (a) Mouse K$_v$1.2

The full-length mouse K$_v$1.2 plasmid was purchased from OpenBiosystems, Huntsville, AL, USA. The channel ORF was amplified by PCR with sense and antisense primers designed with Xho I and Spe I sites, respectively, for restriction digestion and ligation into the *Xenopus laevis* oocyte expression vector pXT7 (Dominguez et al., 1995).

E226D, E226N and E226Q mutant channels were made by overlapping PCR (Ho et al., 1989), using appropriate primers listed in Table 2.1. The final PCR product with the desired mutation was digested with NsiI and NheI. The resulted fragment was ligated with mouse K$_v$1.2 WT vector digested with the same enzymes (Fig-2.1A).

The loop mutants in mouse K$_v$1.2 were made for our previous experiments presented in Sand et al., 2013. To make double mutations between E226D and the loop vectors, both the plasmids were digested with PasI restriction enzyme. To avoid re-ligation of the vector, the digested loop vector was dephosphorylated using Shrimp Alkaline Phosphatase (SAP). Ligation was performed between the PasI digested insert fragment with E226D mutation and PasI digested and SAP treated vector containing desired loop sequence (Fig-2.1B).

(A)

PCR with primers A1 and A2

PCR with primers B1 and B2

Over lapping PCR with primers A2 and B2

Restriction digestion with NsiI and NheI

Ligation with mouse K$_v$1.2 (in PxT7) vector previously cut with NsiI and NheI

(B)

Digestion with PasI

Dephosphorylation with SAP

Ligation
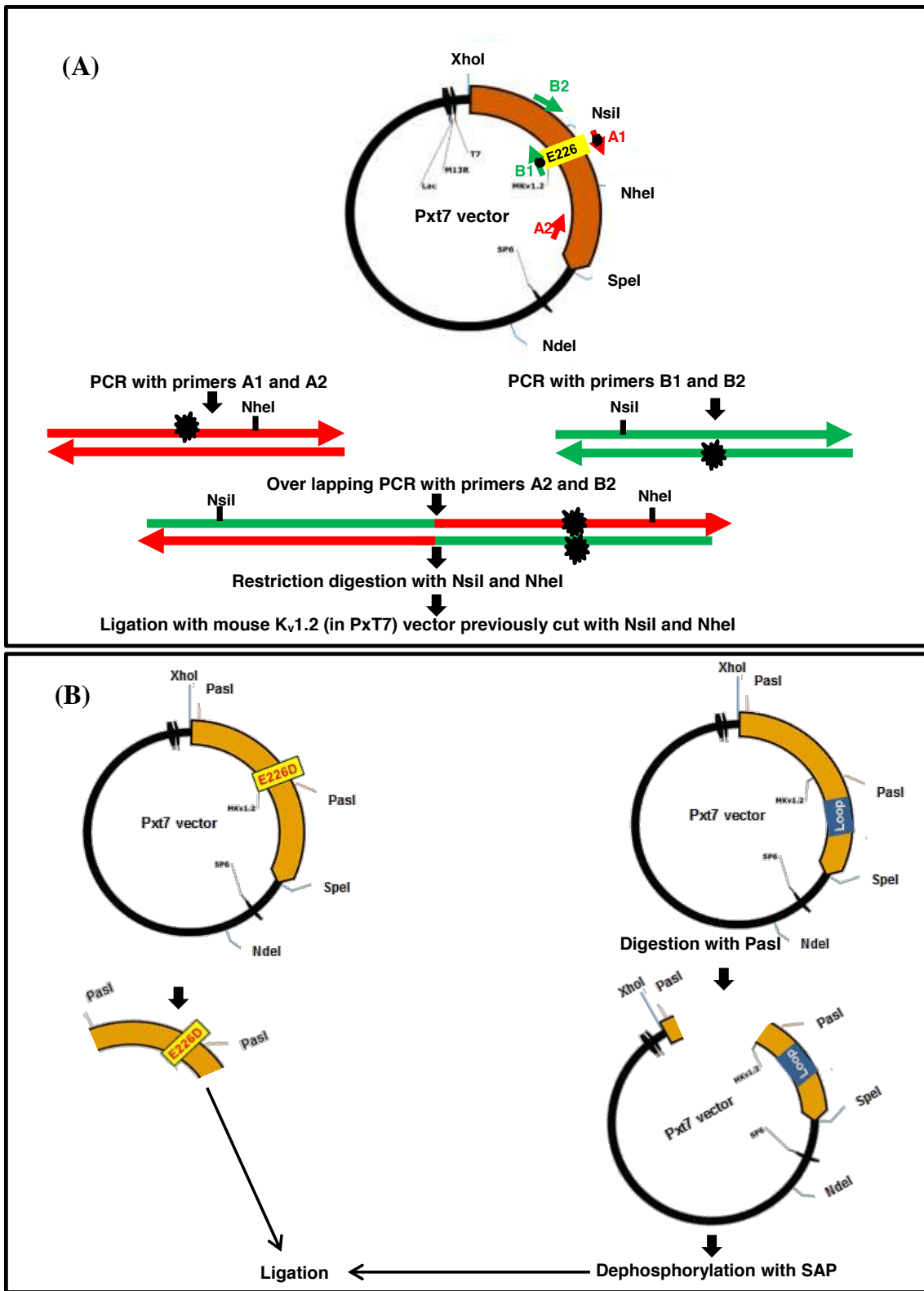
Figure 2.1: Procedure of making point mutation at 226 position using overlapping PCR method (A). Procedure of making double mutants by combining E226D and loop mutants (B).

22

(b) Polyorchis penicillatus jShak1

For the work presented in chapter 4, non-inactivating (Δ23N) jShak1 in pXT7 (Klassen et al., 2008) was used to create a construction vector with silent BsrGI and BclI cutting sites in the S3/S4 loop, using overlapping PCR with appropriate primers listed in Table 2.1. To make the homo, hetero and K278 mutant loops, synthetic oligonucleotides were designed with desired loop sequence and overhangs of BsrGI and BclI sites (Table-2.1). The annealed oligonucleotides were ligated into the BsrGI and BclI digested construction vector. To make double mutations both N227D and N227E single mutant (Klassen et al., 2008) and jShak1 loop mutants were digested with ClaI, and HpaI restriction enzymes and the relevant fragments were recombined (Fig-2.2).

TEV loop mutants were constructed by inserting TEV protease cut site (ENLYFQG) in the S3-S4 loop. Three types of TEV loop mutants were made-(i) Short TEV loop mutants, where the entire natural loop of jShak1 was replaced with one TEV cut site (ii) Short TEV-K loop mutant, where the natural loop of the channel was replaced with one TEV cut site, leaving the C-terminal K (K278) unchanged (iii) Long TEV loop mutant, where the loop was replaced with double TEV cut sites.

Sequences of all the plasmids (both mouse $K_v1.2$ and jShak1 mutants) were confirmed by Sanger sequencing. For expression in *Xenopus laevis* oocytes, all the wild type and mutant plasmids from mouse $K_v1.2$ and jShak1 were linearized

(A) Making synthetic loops mutants

T7 Promoter

jShak1

Pxt7 vector

BclI

AmpR

Digested with BsrGI and BclI

Annealed oligoneucleotides
(with desired mutation, BsrGI and BclI overhang)

5' GTACTAGTAAGTAGCAGTGACG
       ATCATTCATCGTCACTGCCTAG 5'

+

Ligation and transformation

(B) Making double mutants

T7 Promoter

HpaI

ClaI

Loop mutation

Pxt7 vector

AmpR

Digested with HpaI and ClaI

+

T7 Promoter

HpaI N227D/E

ClaI

Pxt7 vector

AmpR

Digested with HpaI and ClaI

Ligation and transformation

Figure 2.2: Procedure of making synthetic loop mutants in jShak1 (A) and the procedure of making double mutant channels by combining N227D/E with the synthetic loop mutants (B).

Table 2.1: List of Primers used to make mutant channels of mouse K$_v$1.2 and jShak1

Primer ID	Primer Description	Types	Primer Sequence
WJG2544	Mouse K$_v$1.2 E226D	Sense	GACCCTTTCTTCATTGTAGACACTCTCTGCATCATCTGG
WJG2545	Mouse K$_v$1.2 E226D	Antisense	CCAGATGATGCAGAGAGTGTCTACAATGAAGAAAGGGTC
WJG2546	Mouse K$_v$1.2 E226N	Sense	GACCCTTTCTTCATTGTAAACACTCTCTGCATCATCTGG
WJG2547	Mouse K$_v$1.2 E226N	Antisense	CCAGATGATGCAGAGAGTGTTTACAATGAAGAAAGGGTC
WJG2548	Mouse K$_v$1.2 E226Q	Sense	GACCCTTTCTTCATTGTACAGACTCTCTGCATCATCTGG
WJG2549	Mouse K$_v$1.2 E226Q	Antisense	CCAGATGATGCAGAGAGTCTGTACAATGAAGAAAGGGTC
WJG2283	jShak1 S3/S4 loop replacement vector	Sense	CAAGCAGCATGATCATTCAGCATGTTACGCGTC
WJG2282	jShak1 S3/S4 loop replacement vector	Antisense	TGATCATGCTGCTTGTACAAGGCTTAAATAATATGGTAAAATC
WJG2284	jShak1 Loop Insert: G3	Sense	GTACTAGGAGGAGGAG
WJG2285	jShak1 Loop Insert: G3	Antisense	GATCCTCCTCCTCCTA
WJG2286	jShak1 Loop Insert:G5	Sense	GTACTAGGAGGAGGAGGAGGAG
WJG2287	jShak1 Loop Insert: G5	Antisense	GATCCTCCTCCTCCTCCTCCTA
WJG2288	jShak1 Loop Insert: G10	Sense	GTACTAGGAGGAGGAGGAGGAGGAGGAGGAGGAGGAG
WJG2289	jShak1 Loop Insert: G10	Antisense	GATCCTCCTCCTCCTCCTCCTCCTCCTCCTCCTA
WJG2296	jShak1 Loop Insert: E3	Sense	GTACTAGAGGAGGAGG
WJG2297	jShak1 Loop Insert: E3	Antisense	GATCCCTCCTCCTCTA
WJG2298	jShak1 Loop Insert: E5	Sense	GTACTAGAGGAGGAGGAGGAGG
WJG2299	jShak1 Loop Insert: E5	Antisense	GATCCCTCCTCCTCCTCCTCTA
WJG2300	jShak1 Loop Insert: E10	Sense	GTACTAGAGGAGGAGGAGGAGGAGGAGGAGGAGGAGG
WJG2301	jShak1 Loop Insert: E10	Antisense	GATCCCTCCTCCTCCTCCTCCTCCTCCTCCTCTA
WJG2302	jShak1 Loop Insert: S3	Sense	GTACTAAGTAGTAGTG
WJG2303	jShak1 Loop Insert: S3	Antisense	GATCCACTACTACTTA
WJG2304	jShak1 Loop Insert: S5	Sense	GTACTAAGTAGTAGTAGTAGTG
WJG2305	jShak1 Loop Insert: S5	Antisense	GATCCACTACTACTACTACTTA
WJG2306	jShak1 Loop Insert: S10	Sense	GTACTAAGTAGTAGTAGTAGTAGTAGTAGTAGTAGTG
WJG2307	jShak1 Loop Insert: S10	Antisense	GATCCACTACTACTACTACTACTACTACTACTTA
WJG2984	jShak1 Loop Insert:K278D	Sense	GTACTAGTAAGTAGCAGTGACG
WJG2985	jShak1 Loop Insert: K278D	Antisense	GATCCGTCACTGCTACTTACTA
WJG2986	jShak1 Loop Insert: K278E	Sense	GTACTAGTAAGTAGCAGTGAAG
WJG2987	jShak1 Loop Insert: K278E	Antisense	GATCCTTCACTGCTACTTACTA
WJG2988	jShak1 Loop Insert: K278N	Sense	GTACTAGTAAGTAGCAGTAACG
WJG2989	jShak1 Loop Insert: K278N	Antisense	GATCCGTTACTGCTACTTACTA
WJG3014	jShak1 Loop Insert: K278Q	Sense	GATCCTTGACTGCTACTTACTA
WJG2991	jShak1 Loop Insert: K278Q	Antisense	GATCGAACTGACGATGAATGAT
WJG2992	jShak1 Loop Insert: K278A	Sense	GTACTAGTAAGTAGCAGTGCCG
WJG2993	jShak1 Loop Insert: K278A	Antisense	GATCCGGCACTGCTACTTACTA
WJG2994	jShak1 Loop Insert: K278G	Sense	GTACTAGTAAGTAGCAGTGGGG
WJG2995	jShak1 Loop Insert: K278G	Antisense	GATCCCCCACTGCTACTTACTA

Table 2.1: (continued)

Primer ID	Primer Description	Types	Primer Sequence
WJG2996	jShak1 Loop Insert : K278S	Sense	GTACTAGTAAGTAGCAGTAGCG
WJG2997	jShak1 Loop Insert: K278S	Antisense	GATCCGCTACTGCTACTTACTA
WJG2998	jShak1 Loop Insert: E9K	Sense	GTACTAGAGGAGGAGGAGGAGGAGGAGGAGAAAG
WJG2999	jShak1 Loop Insert: E9K	Antisense	GATCCTTTCTCCTCCTCCTCCTCCTCCTCCTCTA
WJG3000	jShak1 Loop Insert: E4K	Sense	GTACTAGAGGAGGAGGAGAAAG
WJG3001	jShak1 Loop Insert: E4K	Antisense	GATCCTTTCTCCTCCTCCTCTA
WJG3006	jShak1 Loop Insert: S9K	Sense	GTACTAAGTAGTAGTAGTAGTAGTAGTAGTAAAG
WJG3007	jShak1 Loop Insert: S9K	Antisense	CTTTACTACTACTACTACTACTACTACTTAGTAC
WJG3008	jShak1 Loop Insert: S4K	Sense	GTACTAAGTAGTAGTAGTAAAG
WJG3009	jShak1 Loop Insert: S4K	Antisense	CTTTACTACTACTACTTAGTAC
WJG3010	jShak1 Loop Insert: G9K	Sense	GTACTAGGAGGAGGAGGAGGAGGAGGAGGAAAAG
WJG3011	jShak1 Loop Insert: G9K	Antisense	CTTTTCCTCCTCCTCCTCCTCCTCCTCCTAGTAC
WJG3012	jShak1 Loop Insert: G4K	Sense	GTACTAGGAGGAGGAGGAAAG
WJG3013	jShak1 Loop Insert: G4K	Antisense	CTTTTCCTCCTCCTCCTAGTAC
WJG3002	jShak1 Loop Insert: Long TEV (2 cut sites)	Sense	GTACTAGAAAATCTTTATTTTCAAGGTGAAAATCTTTAT TTTCAAGGTG
WJG3003	jShak1 Loop Insert: Long TEV (2 cut sites)	Antisense	GATCCACCTTGAAAATAAAGATTTTCCACTTGAAAATAA AGATTTTCTA
WJG3035	jShak1 Loop Insert: Short TEV (1 cut site)	Sense	GTACTAGAAAATCTTTATTTTCAAGGTG
WJG3036	jShak1 Loop Insert: Short TEV (1 cut site)	Antisense	GATCCACCTTGAAAATAAAGATTTTCTA
WJG3037	jShak1 Loop Insert: Short TEV with K (1 cut site)	Sense	GTACTAGAAAATCTTTATTTTCAAGGTAAGG
WJG3038	jShak1 Loop Insert: Short TEV with K (1 cut site)	Antisense	GATCCCTTACCTTGAAAATAAAGATTTTCTA

by NdeI digestion, gel-purified and were used to make mRNAs by in vitro transcription using a mMessage mMachine (Ambion, Austin, TX, US) T7 polymerase kit and stored at -80°C.

Oocyte preparation and mRNA injection

A lobe of ovary was extracted from 2 year + female *Xenopus laevis*. Before performing the ovarian lobectomy, the *X. laevis* females were anaesthetized in 0.2% ethyl 3-aminobenzoate methanesulfonate salt (MS-222; Sigma-Aldrich, Oakville, ON, CAN) for 40 minutes. To access the ovarian lobes, a small incision was made approximately 1 cm lateral to the ventral midline and 1 cm caudal to the pelvic girdle. Once removed, the lobe was collected in and rinsed with modified Barth's medium (MBM) [in mmoll^{-1}: NaCl 88, KCl 1, Ca(NO$_3$)$_2$ 0.33, CaCl$_2$ 0.41, MgSO$_4$ 0.82, NaHCO$_3$ 2.4, HEPES 10, penicillin G 0.1 g l^{-1} and gentamycin sulphate 0.05 g l^{-1}] and separated into small clumps. The clumps were incubated on a rotating shaker in 2 mg ml^{-1} collagenase in MBM at room temperature for 2 hours. After this collagenase treatment, eggs were washed with MBM and were de-folliculated by immersion in a hypo-osmotic phosphate buffer [in mmoll^{-1}: K$_2$PO$_4$100 (pH 6.5 with HCl)] for 30 min. After the treatment the eggs were washed several times in MBM and stored at 17°C. Eggs were injected with mRNA and were incubated at 17°C (Grigoriev et al., 1997). To cut the TEV loop, eggs injected with jShak1 TEV mutant loops were incubated throughout post injection incubation with MBM and TEV protease enzyme at 17°C.

Data Recording and Analysis

Two electrode voltage clamp recording was performed 24-36 hours after injection of mRNA using a GeneClamp 500B Amplifier (Molecular Devices, Sunnyvale, CA, USA), connected to a PC (Dell, Austin, TX, USA) running pClamp9 software (Molecular Devices). Pipettes were pulled from 1.5 mm outside diameter borosilicate filament capillary tubing using a PMP-102 automatic puller (MicroData Instrument, Inc., South Plainfield, NJ, USA). Data were acquired through a 1322A analogue-to-digital converter and analyzed using Clampfit 9.2 (Molecular Devices) and SigmaPlot (Systat Software, Inc., Point Richmond, CA, USA). Voltage clamp protocols were implemented using pClamp9 (Molecular Devices).

Using oocyte system in two electrode voltage clamp (TEVC) has some advantages as well as some disadvantages. The expression of low number of endogenous channels and receptors makes the oocyte a useful medium to study the function of ion channels without any significant contaminations. However, one of the major limitations of using oocyte system is that the channels are being expressed in a non-native environment of membrane, temperature and possibly ionic composition, which might affect the natural function of the channel (Goldin, 2006). Another consequence of oocyte not being the native tissue is that cellular trafficking is different, which might affect the surface expression of the channel. Also, many pharmacological agents are found to be less potent on channels in

oocytes compared to the channels in mammalian cells or native tissues (Goldin, 2006).

For mouse $K_v1.2$ mutant channels, oocytes were subjected to a voltage protocol that held the cells at -90mV before stepping to increasing voltages from -80 to +80mV in 2mV steps for a depolarization phase of 50ms. Then the cells were repolarized to -50mV for 50ms, which produced outward tail currents. Current traces were filtered at 1 kHz and collected with P/4 leak subtraction. When characterizing possible leak currents (E226N and E226Q) no leak subtraction was used. Oocytes were bathed in ND96 (in mM: NaCl 96, KCl 2, $CaCl_2$ 1.8, $MgCl_2$ 1, HEPES 5) at room temperature during recording. To block the chloride currents native to *X. laevis* (Miledi and Parker, 1984) oocytes were treated with 1mM diisothiocyanatostilbene-2,2′-disulfonic acid (DIDS), present in the bath solution with ND96 during the voltage protocols. To block the pore current, eggs were exposed to 10μM agitoxinI added to the bath solution for 3 minutes before recording.

To record from the jShak1 wild type and mutant channels, oocytes were held at -90mV before stepping from -80 to + 50mV, in 2mV steps for 50ms. Then the cells were repolarized to -50mV for 50ms, same as I did with mouse $K_v1.2$ mutants. As DIDS is known to interfere with jShak1 and jShak2 channels (Grigoriev et al., 1997), recording was performed at room temperature with only ND96 as the bath solution. Data were filtered at 1 kHz and collected with P/4 leak subtraction.

In our previous study (Sand et al., 2013), channel conductance was calculated from the tail currents. Recording from uninjected eggs has shown that the tail currents are often corrupted by a transient that stabilized with in 2ms of depolarizing pulse. Some of the mutant channels showed C-type inactivation over time, affecting the tail currents as well. jShak1 is a very fast deactivating channel, with extremely fast tail currents, which makes them unreliable for GV analysis. Considering the above issues, I took the peak current value from individual traces and used the average of the peak currents in the formula:

$$G=I/(V-V_{rev})\ldots\ldots\ldots\ldots\ldots\ldots.. \text{ (i)}$$

I have used -70mV as the reversal potential (V_{rev}) of K^+ to calculate G from equation (i), as previous recordings from other K_v channels have found an average value of -70mV for the V_{rev} of K^+. I have found that even a 20mV change (-70 to -90) in the V_{rev} value used for calculation causes only a 3% change in the calculated V_{50} of a channel. Individual G-V curves were normalized and fitted to a 4th order Boltzmann equation:

$$G/G_{max} = 1/(1+\exp((V-V_{50})/b)^4) \ldots\ldots\ldots..\text{(ii)}$$

The single subunit V_{50} obtained from eq (ii) was used to calculate whole channel V_{50} by solving for V when

$$G/G_{max} = 0.5. \ldots\ldots\ldots..\text{(iii)}$$

The V_{50} values of several mouse $K_v1.2$ mutant channels presented in chapter 3(S3, S5, S10, G3, G5 and G9) differ from our previous studies presented in Sand et al., (2013). Homo-polymeric loop mutant channels with serine, G3 and G5

loops showed C-type inactivation, which also affected the tail current. When I used the peak current method to calculate the conductance, I found 5-10 mV positive shift in V_{50} values only for the above mentioned channels, compared to what I found using tail currents. Only 1-2 mV variation in V_{50} values, calculated in two different methods were found for the other homo and hetero loop channels. I consider the method of using peak current to calculate conductance is more reliable, as I addressed both the mechanical (transient effect) and electrophysiological (inactivation) issues.

The statistical differences between the V_{50} values of different channels were calculated using a two-tailed t-test.

Molecular Modeling

Rat and mouse $K_v1.2$ have the same protein sequence. For the open state model of mouse $K_v1.2$, I used the crystal structure of the open state of rat $K_v1.2$ (Chen et al., 2010) from the protein data bank, PDB (PDB ID: 3LUT). I made a homology mode of the closed state of mouse $K_v1.2$ using the inferred closed state model of $K_v1.2$ from Jensen et al., (2012) as template in SWISS MODEL.

The open state homology model of jShak1 was also made in SWISS MODEL using 3LUT (the enhanced crystal structure of rat $K_v1.2$ (Chen et al., 2010) as

template. A similar approach was taken to model the closed state of jShak1, using an inferred closed state model of $K_v1.2$ from Jensen et al., (2012) as template.

Most of the currently available computer programs make homology models based on sequence homology and with relatively simple energy minimization, indicating that the resulting model is not necessarily representing its most favourable energetic state. Such type of heuristic models are useful for identifying and representing possible molecular interactions, might not be accurate in minor details.

Chapter 3:

The role of inter-helix salt bridge formation and the effect of S3-S4 loop on the dynamics of the S4 helix in mouse $K_v1.2$

Background

Voltage gated potassium (K_v) channels are transmembrane proteins specialized to transport K^+ across the membrane in response to change in membrane voltage. K_v channels are ubiquitous among electrically excitable cells and are responsible for generation and propagation of action potential (Cole and Curtis, 1939), regulation of firing frequencies (Pongs, 1999), pacemaker activity (Li et al., 2013 and Leao et al., 2012), release of neurotransmitters (Katz and Miledi, 1969; Augustine, 1990) and many other important cellular processes. A K_v channel is composed of four subunits, each containing six transmembrane domains (S1-S6). The voltage sensitivity of this channel is conferred by a structural module known as the voltage sensor domain (VSD), which consists of helices S1 through S4. The S5 and S6 helices and their connecting P loops from each four subunits form the pore domain (Fig-1.2A).

The S4 helix, commonly known as the voltage sensing helix contains four to seven positively charged amino acid residues depending on the channel type. Change in membrane potential alters the force acting on the charged residues of the S4 helix causing it to move in response to voltage (Lee et al., 2005; Long et al., 2005). The S4 helix affects the rest of the channel behaviour by non-covalent

interactions with the acidic residues of the S2 and S3 helices and covalent interactions with the extracellular loop that joins the S3 and S4 helices, triggering the channel to open and close (Papazian et al., 1995). Studies have identified three conserved negatively charged residues (E283, E293 and D316 in *Drosophila* Shaker) in the S2 and S3 helices that interact with the positively charged residues of the S4 helix. In *Drosophila melanogaster* Shaker channel, the neutralization mutation K374Q in the S4 helix failed to produce a functional channel. That non-functional mutant channel was rescued by second mutations at E293Q and D316N in the S2 and S3 helices, suggesting a strong interaction network between these charged residues (Papazian et al., 1995). In Shaker, the closed state is found to be stabilized by electrostatic interaction between K374 in the S4 and E293 and D316 in the S2 and S3 respectively (Durell et al., 2004; Li-Smerin et al., 2000, Tiwari-Woodruff et al., 1997 and Papazian et al., 1995). The open conformation of the channel is found to be stabilized by salt-bridge formation between R368 and R371 in the S4 with E283 in the S2 helix (Papazian et al., 1995).

The negatively charged residues of the S2 and S3 helices are conserved in most K_v channel families (Fig-3.1B). Neutralization mutation of E283 shifts the voltage sensitivity of the mutant channel in a depolarizing direction compared to the wild type Shaker channel (Papazian et al., 1995). In jellyfish channel jShak1, and in Portuguese Man-o-War, *Physalia physalis* K_v1 channel, ppK_v1 the first conserved glutamic acid in S2 helix (E283 in *Drosophila*) is replaced by neutral residues N and S (Fig-3.1B). In jShak1 mutations replacing neutral N with acidic E and D at
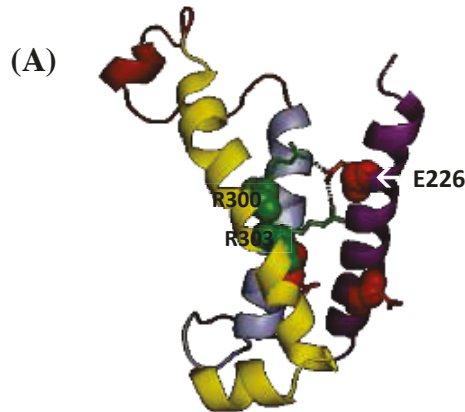
(B) Multiple Sequence Alignment


```
Mouse_Kv2.1  ----------TDNPQLAHVEAVCIAWFTMEYLLRFLSSPKKWKFFKGPLNAIDLLAILPY    273
Human_Kv2.1  ----------TDNPQLAHVEAVCIAWFTMEYLLRFLSSPKKWKFFKGPLNAIDLLAILPY    273
Shaker       GTKIEEDEVPDITDPFFLIETLCIIWFTFELTVRFLACPNKLNFCRDVMNVIDIIAIIPY    323
Mouse_Kv1.2  NSTIGYQQSTSFTDPFFIVETLCIIWFSFEFLVRFFACPSKAGFFTNIMNIIDIVAIIPY    266
Human_Kv1.2  NSTIGYQQSTSFTDPFFIVETLCIIWFSFEFLVRFFACPSKAGFFTNIMNIIDIVAIIPY    266
PpKv1        ---------NENESWMFMVSTAVIAWFTSEFMLRLICCPSKIKFFTNLSNIIDLLSIVPY    271
jShak1       ---------SEHATWMFTVNTAVICWFTIEFILRLICCPNKIKFFLNTGNIIDFLSILPY    267
                       :  :.:  *  **:  *  :*::..*.*  *     *  **::*:**

Mouse_Kv2.1  SLGFTLRRSYNELGLLILFLAMGIMIFSSLVFFAEKDEDDTKFKSIPASFWWATITMTTV    378
Human_Kv2.1  SLGFTLRRSYNELGLLILFLAMGIMIFSSLVFFAEKDEDDTKFKSIPASFWWATITMTTV    378
Shaker       ILGRTLKASMRELGLLIFFLFIGVVLFSSAVYFAEAGSENSFFKSIPDAFWWAVVTMTTV    443
Mouse_Kv1.2  ILGQTLKASMRELGLLIFFLFIGVILFSSAVYFAEADERDSQFPSIPDAFWWAVVSMTTV    375
Human_Kv1.2  ILGQTLKASMRELGLLIFFLFIGVILFSSAVYFAEADERESQFPSIPDAFWWAVVSMTTV    375
PpKv1        ILGDTLKASFHELLMLAFFLLIMILLFGSCVYYAEYQVEGTKFTSIPAASWWAIVTMTTV    369
jShak1       ILGNTLKASFNELMMLAFFLFVMILIFGSCVYYAEYKEPGTKFISIPSSFWWAIVTMTTV    363
                ** **: * .** :* :** : :::*.* *::**     : * *** : *** :*****

Mouse_Kv2.1  GYGDIYPKTLLGKIVGGLCCIAGVLVIALPIPIIVNNFSEFYKEQKRQEKAIKRREALER    438
Human_Kv2.1  GYGDIYPKTLLGKIVGGLCCIAGVLVIALPIPIIVNNFSEFYKEQKRQEKAIKRREALER    438
Shaker       GYGDMTPVGVWGKIVGSLCAIAGVLTIALPVPVIVSNFNYFYHRETDQEEMQSQNFNHVT    503
Mouse_Kv1.2  GYGDMVPTTIGGKIVGSLCAIAGVLTIALPVPVIVSNFNYFYHRETEGEEQ--AQYLQVT    433
Human_Kv1.2  GYGDMVPTTIGGKIVGSLCAIAGVLTIALPVPVIVSNFNYFYHRETEGEEQ--AQYLQVT    433
PpKv1        GYGDMYPTTLLGKLIGFVAVVCGVLTIALPVPVVVSNFEYFYTKERNRRKTEEVRKEHEK    429
jShak1       GYGDMHPVTFWGQIVGSMAVVCGVLTIALPVPVVVSNFEYFYTKERNRRKTEEARKEQAK    423
             ****: *   . *::* :. :.***.****:*::*.**. **  .:   .:     .
```

Figure 3.1 The 3-D model of mouse $K_v1.2$ VSD from 3LUT; (Chen et al., 2010) (A). E226 forms salt bridge with R300 and R303 to stabilize the open state. Molecular model images are made in PyMOL. Multiple sequence alignment from several K_v family members (B). The conserved negatively charged residues, PD and the PD turret are highlighted.

227 of the S2 helix stabilized the open state more compared to the wild-type channel (Klassen et al., 2008).

The S3-S4 loop length and composition is shown to play a role in shaping the V_{50} of mouse $K_v1.2$ (Sand et al., 2013) by interacting with the rest of the channel as well as by constraining the movement of the S4 helix (Sand et al., 2013 and Klassen et al., 2008). According to Jensen et al., (2012) when the channel closes, the C-terminus of the S3-S4 linker is pulled closer to the negatively charged PD turret and the charged residues of the VSD. The nature of the C-terminus of the loop is found to affect the V_{50} values of mouse K_v12, possibly by intercting with the PD turret (Sand et al., 2013).

In summary, the voltage sensitivity and open probability of K_v channels are regulated and affected by an electrostatic interaction between the charged residues of the S2 and S4 helices. The length and composition of the S3-S4 loop can also affect the V_{50} of the channel possibly by interacting with the pore domain turret (Sand et al., 2013) and constraining the movement of the S4 helix (Sand et al., 2013 and Klassen et al., 2008). In this study I focused to evaluate the role of the negatively charged glutamic acid (E) in setting the specific V_{50} of mouse $K_v1.2$ and how the interaction between the S2 and S4 helices is affected by S3-S4 loop length and composition in this channel.

I shortened the side chain length at position 226 by E226D mutagenesis and neutralized the charge at 226 position by replacing E226 with N and Q. My results show that E226D mutation significantly affects both the V_{50} and the slope factor of the channel; E226N and E226Q mutations produce leaky channels. Treatment of the mutant channels with a pore blocker confirms a non-canonical omega current passing in small amounts through E226D and in large amounts through E226N and E226Q. In our previous study with mouse $K_v1.2$ (Sand et al., 2013) I made synthetic S3-S4 loops varying in both length and compositions. In this study, I made double mutations by combining E226D with different synthetic S3-S4 loops to study how the interaction between the S2 and S4 helices are affected by the S3-S4 loop length and compositions.

Our previous studies with mouse $K_v1.2$ (Sand et al., 2013) showed that for the glycine loop series, the V_{50} values reached a plateau at a length of 6 aa and there were no significant differences between the V_{50} values of G6 through G9 loop-mutant channels. For the serine and glutamic acid loops the V_{50} values reached a plateau with S7 and E8 loops respectively. The study of interaction energy between the loop and the channel showed that the shorter loops of 2-4 aa had a high values of ΔG, which lowered with increasing loop length and reached a plateau at a length of 5 to 8 aa depending on composition (Sand et al., 2013). Shorter loops shift the V_{50} more positive possibly by constraining the movement of the S4 helix (Sand et al., 2013 and Klassen et al., 2008). Based on the above findings I suggest that depending on composition, each loop has a specific length,

below which, the movement of the S4 helix is energetically constrained. I have chosen three loop lengths for my study: 3aa, a length at which the movement of the S4 helix is predicted to be highly restricted; 5aa from the middle zone and 10aa at which, the 'length effect' of the loop is predicted to reach a plateau, independent of its composition.

Based on my results of homo-polymeric and hetero-polymeric synthetic loop mutants in mouse $K_v1.2$, I propose that the S3-S4 linker can be divided into two regions that interact differently with different parts of mouse $K_v1.2$ channel: (i) the N-terminal region of the loop that remains outside of the VSD vestibule at closed state, mediates a charge-charge interaction with the channel to stabilize the open state (or destabilize the closed state); (ii) the C-terminal three amino acids that are pulled down in between the VSD and PD turret, probably mediate weak hydrophobic interactions with the S3 helix to stabilize the closed state. However the weak effect of the C-terminal region is overwhelmed by the stronger effect of the N-terminal region of the loop.

The salt-bridge formation between the S2 and S4 helices, which is necessary to stabilize the open state and to prevent the omega current through the VSD, is affected by both the length and composition of the S3-S4 loop in mouse $K_v1.2$. The N-terminal regions of the loops affect the dynamics of the VSD, which was evident from a significant change in the V_{50} values of the respective mutant

channels. The C-terminal region of the S3-S4 linker however, fails to cause any effect in the interaction between S2 and S4 helices.

Results and Discussion

E226D mutation in the S2 helix affects voltage sensitivity and slope factor of the channel

In mouse $K_v1.2$, the open state is stabilized by salt-bridges between E226 of the S2 helix and R300 and R303 of the S4 helix (Fig-3.1A). The V_{50} value of E226D mutation, where D has a shorter side chain than E, is +2.5mV, significantly (p = 1.1E-07) depolarized than the wild type mouse $K_v1.2$ (V_{50} = -13mV) (Fig-3.2A, Table-3.1). No significant change (p = 0.02) is found for slope factor, b for E to D mutation at the 226 position (Table-3.1).

Our previous studies with mouse $K_v1.2$ showed that both the V_{50} values and the interaction energies between the synthetic loops and the channel reached a plateau at lengths of 5 to 8 aa, depending on loop composition (Sand et al., 2013). I propose that depending on composition, each loop has a specific length, below which, the movement of the S4 helix is energetically constrained. Loops longer than the specific length do not restrict the movement of the S4 helix and do not show any additional effect on the voltage sensitivity (Sand et al., 2013). I speculate that the loops longer than 5-8 aa (depending on composition), did not show any additional effect on V_{50} values as the complete transition of the S4 helix

39
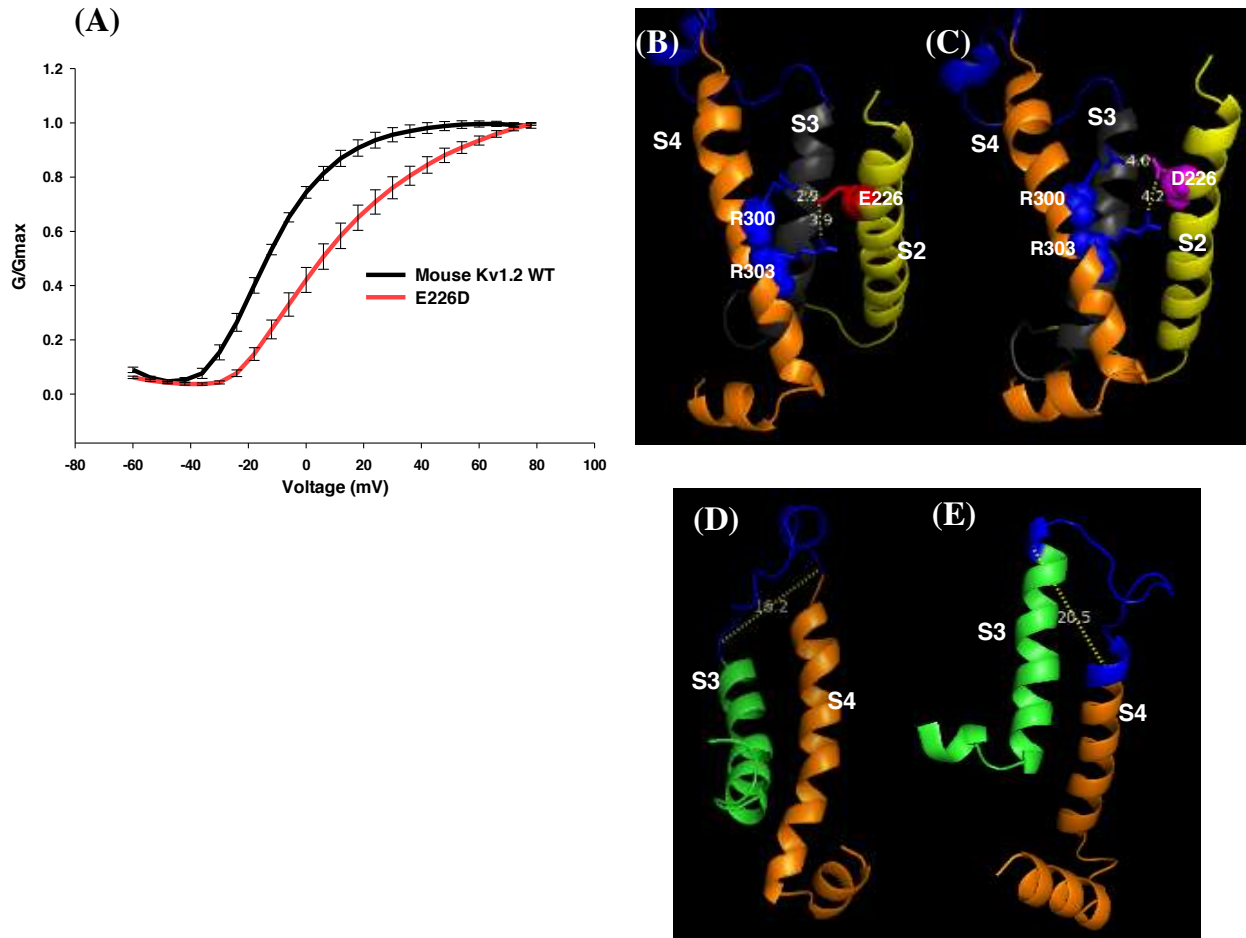
Figure 3.2 Comparison of conductance between wild type mouse $K_v1.2$ and E226D mutant (A). Individual G-V curves were normalized and fitted to the Boltzmann equation: $G/Gmax = 1/(1+\exp((V-V_{50})/b)^4)$. The distance between the side chains of E226 and R300 and R303 in open state is measured as 2.9 Å and 3.9Årespecively (B). The distance between the R300 and R303 is measured from the D226 of the E226D mutant and is found as 4Å between D226 and R300, 4.2 Å between D226 and R303 (C). The distance between the N-terminus and C-terminus of the S3-S4 loop at open state is measured as16.2 Å (D). Same end-to-end distance of the loop is measured as 20.5Å at closed state of mouse $K_v1.2$ (E). All the distances are measured using PyMOL.

Table 3.1: Half-activation voltages (V_{50}) for wild type mouse $K_v1.2$ and S3-S4 loop variants.
Channel conductance was calculated from the average peak values of each current traces by using the formula $G=I/(V-V_{rev})$, where reversal potential V_{rev} was taken as -70mV. Individual G-V curves (from -80 to + 80 mV) were normalized and fitted to the Boltzmann equation: $G/G_{max} = 1/(1+\exp((V-V_{50})/b)^4)$. The single subunit V_{50} obtained from the equation was used to calculate whole channel V_{50} by solving for V when $G/G_{max} = 0.5$

Channels	Loop sequence (5'-3') / Description	n	V_{50} (mV)	S.E.	p	Slope, b (mV/e)	S.E.	p
Mouse $K_v1.2$ WT	GTEL**AEKPEDAQQGQQA**MSLA	9	-13	0.9		14.7	1	
S3	GTEL**SSS**MSLA	9	6.6	1.6	8.6E-08	27	1.3	1.1E-05
S5	GTEL**SSSSS**MSLA	6	9.5	1.7	2.8E-06	23.2	1.5	1.6E-03
S10	GTEL**SSSSSSSSSS**MSLA	9	0.1	1.2	8.9E-08	22.1	0.9	6.7E-04
S7QQA	GTEL**SSSSSSSQQA**MSLA	9	2.6	1.1	1.6E-08	17.5	0.9	1.2E-01
G3	GTEL**GGG**MSLA	9	-6	1.4	1.2E-03	31	1	1.7E-07
G5	GTEL**GGGGG**MSLA	9	-5	2.8	2.3E-02	25.4	1.3	5.1E-05
G9	GTEL**GGGGGGGGG**MSLA	9	11.5	2.4	2.4E-06	21	1.1	3.3E-03
G7QQA	GTEL**GGGGGGGQQA**MSLA	9	2.8	0.9	1.6E-09	20	1.5	3.1E-02
E3	GTEL**EEE**MSLA	9	1.5	0.5	5.3E-09	20	2.1	6.1E-02
E5	GTEL**EEEEE**MSLA	9	-9.2	0.8	6.1E-03	26.5	1.5	3.3E-05
E10	GTEL**EEEEEEEEEE**MSLA	9	-29	1.5	4.4E-07	19.3	1.6	4.9E-02
E7QQA	GTEL**EEEEEEEQQA**MSLA	7	-26	2	1.3E-04	10	1.2	1.9E-02
E226D	Point mutation at 226 position (S2 helix)	9	2.5	0.1	1.1E-07	19.5	1.2	2.2E-02
EDS3	E226D + S3 loop	6	4.5	2.7	9.4E-04	19.1	1.9	8.5E-02
EDS5	E226D + S5 loop	7	10	1.6	1.9E-07	19.5	0.7	1.0E-02
EDS10	E226D + S10 loop	9	8.1	2	1.1E-06	23.1	1.6	1.2E-03
EDS7QQA	E226D + S7QQA loop	6	12.4	3.5	5.2E-04	26	1.3	7.9E-05
EDG3	E226D + G3 loop	9	2	0.7	1.3E-09	21.3	0.05	1.6E-03
EDG5	E226D + G5 loop	7	9.6	4.7	2.7E-03	24.5	2.9	1.4E-02
EDG9	E226D + G10 loop		Could not be made					
EDG7QQA	E226D + G7QQA loop	3	33.4	2.1	3.7E-04	19.1	2	1.4E-01
EDE3	E226D + E3 loop	5	18	1.4	5.0E-06	17	0.9	0.2
EDE5	E226D + E5 loop	7	1.7	0.8	1.7E-08	22.1	0.8	6.5E-04
EDE9	E226D + E10 loop	9	1.2	1.6	5.1E-06	15	0.9	8.4E-01
EDE7QQA	E226D + E7QQA loop	7	1.8	0.8	1.6E-08	21.5	0.2	1.3E-03

in response to voltage has already been achieve by shorter loops. Based on the results, I propose that in wild type mouse $K_v1.2$, the natural 13aa long S3-S4 loop allows the complete transition of the S4, essential for the voltage sensitivity of the channel. For this reason, when E at 226 is replaced with D, the shorter side chain of D increases the distance between the carboxyl group of D and R residues of the S4 helix, forming a weaker salt bridge compared to the wild type channel (E226). This assumption is further supported by the homology model of the mouse $K_v1.2$ open state and E226D mutant in the open state (Fig-3.2B, C). In the open state of mouse $K_v1.2$, the distance between E226 and R300 is measured as 2.9 Å and the distance between E226 and R303 is 3.9Å (Fig-3.2B). In E226D mutant channel at open state, the distance of R300 and R303 from D226 is measured as 4.0 Å and 4.2 Å respectively (Fig-3.2C). I also measured the distance between the N and C terminus of the S3-S4 linker at both open and closed state and the values are 16.2Å and 20.5Å respectively (Fig-3.2D, E). I propose that in mouse $K_v1.2$, the 16.2 Å end-to-end distance of S3-S4 loop provide the most energetically favoured conformation of the S4 helix and also an optimum distance for forming salt-bridge between R300 and R303 with E226. When the side chain of the charged residue at S2 helix (226 position) is shortened, the distance between the interacting residues increases, making the salt-bridge forming energetically unfavourable compared to the wild-type channel.

E226N and E226Q mutations produce leak current

Neutralization mutations E226N and E226Q produce instantaneous currents (Fig-3.3:C,D,G,H), which is a characteristic of two-pored K^+ channels, known as TWIK-1 (Enyedi and Czirjak, 2010). Two pore-domain potassium (K_{2P}) channels are characterized by the presence of two pore loop forming (P) domains in each subunit and are responsible for background K^+ current in mammals (Theilig et al., 2008 and Patel et al., 1998), *Drosophila* (Goldstein et al., 1996) and plants (Moshelion et al., 2002 and Czempinski et al., 1997). The most distinguishable feature of E226N and E226Q, compared to mouse $K_v1.2$ wild-type channel is the difference in open probability (P_0). When the open probability of a channel is regulated by membrane potential, the conformational change in the protein subunits followed by the change in membrane potential causes a delay in current. If a channel is independent of membrane voltage, then the probability of channel opening (P_0) should be the same for all membrane potential values. The currents of E226N and E226Q channels show an instantaneous change in the amplitude of current in response to change in membrane potential (Fig-3.3:C,D,G,H). To analyse the true nature of the leak current of the channel, recordings were performed both with and without leak-subtraction. When current traces without P/N subtraction are compared between E226 mutants and the wild type channel, no inward current in wild-type mouse $K_v1.2$ is found (Fig-3.3A, E). Small inward current at negative voltage is observed for E226D mutant (Fig-3.3B, F).
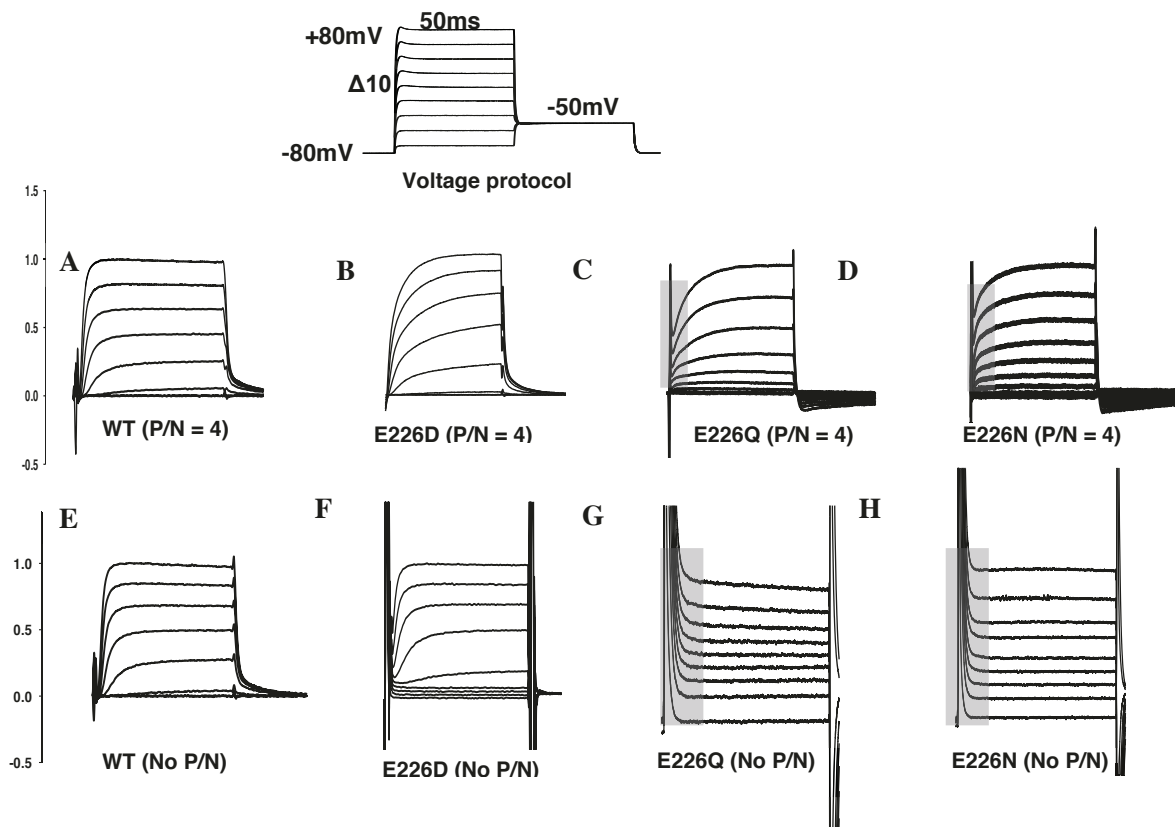
Figure 3.3 Representative two-electrode voltage clamp traces from *Xenopus laevis* oocytes expressing wild type mouse $K_v1.2$ and E226 mutant channels with (A-D) and without leak subtractions (E-H). The depicted voltage protocol (shown at the top) describes what is shown, i.e. with depolarizing pulses in 10 mV increments, but pulses were actually delivered and analyzed in 2 mV steps. All the current traces are normalized to the plateau current value at + 80mV. For each trace, y- axis represents the normalized current and the x-axis represents the time in milliseconds.

E226Q and E226N mutants show instantaneous inward current at negative voltage and outward current at depolarizing potentials (Fig-3.3: C, D, G, H). Current-voltage curve of the channels shown in Fig-3.4 clearly represent the inward currents in the mutant channels, which switch direction at -30mV for E226Q and E226N channel and at -15mV for E226D channel. This difference indicates a possible difference in the relative permeability to permeant ions - i.e. the pore shape/size might be different in these mutants.

To confirm the possible omega current, the mutants and the wild type channel are treated with agitoxin I, a $K_v1.2$ specific canonical pore blocker (Garcia et al., 1994.) AgitoxinI is a homologue of agitoxin2, which is known to interact with the extracellular surface of the pore to block K^+ transport (Takeuchi et al., 2003). Current traces are recorded from a *Xenopus* oocyte with and without agitoxinI and also with and without P/N subtraction (Fig-3.5: A-H). Further analysis was performed with current traces without a leak subtraction. 3 minutes treatment with 10μM agitoxinI blocks around 86% of the total current from the wild type channel (Fig-3.5I). For E226D mutant ~76% current is blocked by agitoxinI. For E226N and E226Q mutants, the pore blocker blocks only 27% and 2% of the total currents from the respective channels (Fig-3.5I).

AgitoxinI is a pore blocker and binds to the pore from extracellular side (Takeuchi et al., 2003 and Garcia et al., 1994). For mouse $K_v1.2$ around 86% of the total current is blocked by the toxin. As the recording is performed without leak
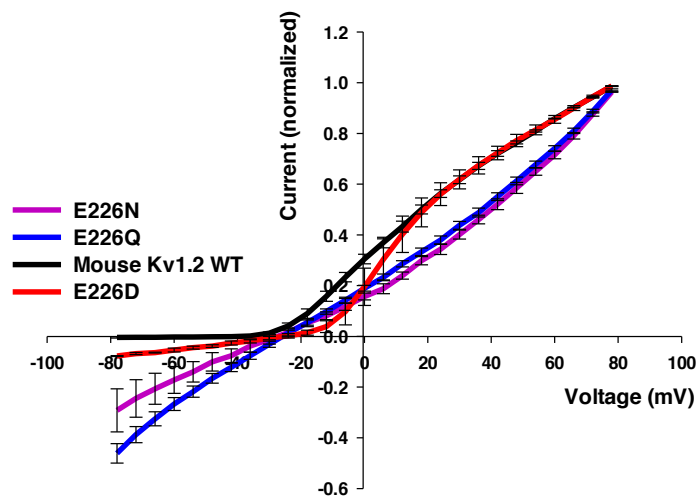
Figure 3.4: Current-Voltage (IV) graph of the wild-type and mutant channels. Current was recorded from the channels without P/N subtraction. Mouse $K_v1.2$ wild type channel (black) shows no leak current, small amount of leak current is observed in E226D mutant (red). E226N (purple) and E226Q (blue) show large leak currents at hyperpolarizing voltage. To obtain normalized current values, peak current amplitudes in response to depolarizing pulses were normalized against the maximum current amplitude at +80 mV.
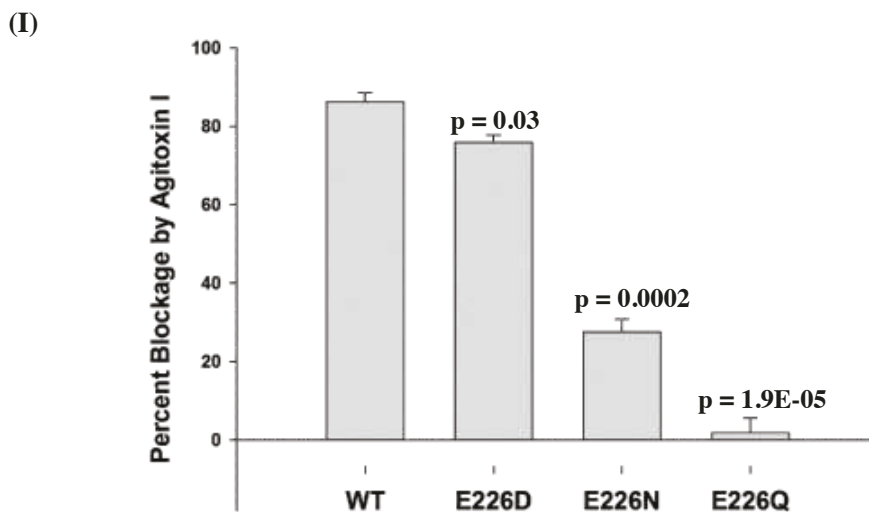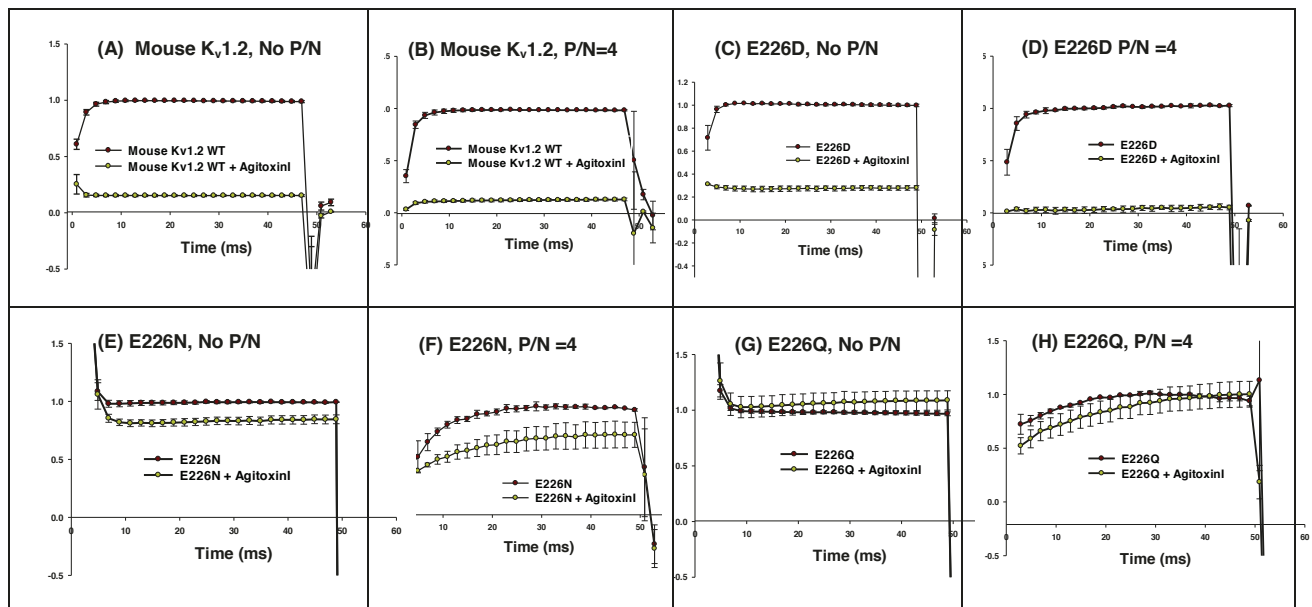
Figure 3.5: Effects of the pore-blocker agitoxinI on mouse $K_v1.2$ and E226 mutant channels (A-H). Oocytes were treated with 10 μM agitoxin I for 3 minutes before recording. Control traces from several cells were normalized to an average plateau values and was averaged. Current traces treated with agitoxin I were normalized to their own control trace and was averaged. Error bars represent s.e.m of each time point. Recordings are presented with (P/N=4) and without P/N subtraction. Percent blockage of current by agitoxinI (I). All the current traces are normalized to the plateau current value at + 80mV. For each trace, y- axis represents the normalized current and the x-axis represents the time in milliseconds in (I). Percent blockage of current was calculated from current traces of wild type and E226 mutants without leak subtractions. Error bars represent s.e.m. p values were calculated from 2-tailed t-test and indicate the significance of difference from the wild-type channel.

subtraction, I assume that the unblocked 14% current is the background leak current of the oocyte membrane. For E226D mutant, after blocking the canonical pore, around 25% current is transported, which is almost double of the assumed background leak current (~14%). The current-voltage graphs and raw recording without P/N subtraction also indicate small inward current in E226D mutant (Fig-3.3, 3.4).

The S4 helix moves in response to voltage field change. This movement is energetically stabilized and supported by several salt bridges between the basic residues of the S4 and acidic residues of the S1 through S3 helices ((Durell et al., 2004; Li-Smerin et al., 2000; Tiwari-Woodruff et al., 1997 and Papazian et al., 1995). Previous studies have found some neutralization mutations in the charged residues of the S4 helix to cause omega currents in several channels. Substitution of the 1st charged arginine, R1 with histidine in Shaker allowed proton flow at hyperpolarized potentials (Tombola et al., 2005). R4H mutation in the same channel generated a proton flux at depolarized potential (Starace et al., 2001). In sodium channel $Na_v1.4$ mutations of R2 and/or R3 with neutral amino acids caused a state-dependent flow of cations through the omega pores (Sokolov et al., 2007). A recent study by Tarek et al., (2012) proposed that the salt-bridging within the VSD is crucial for preventing the omega current. One of the major characteristics of the K_v channel VSD topology is the presence of water crevices penetrating the structure from the intracellular and extra cellular region, both in

the active and the resting state (Krepkiy et al., 2009; Jogini et al., 2007; Freites et al., 2006 and Treptow et al., 2006). Tarek et al. proposes that the state dependent interaction networks between the positively charged residues of the S4 helix and their counterparts make a constriction to prevent communication between the extracellular and intracellular media (Fig-3.6F). A mutation in residues of this region that disrupts the constriction is most likely to generate an omega current passing through the VSD (Tarek et al., 2012).

I made a homology model of mouse $K_v1.2$ in the closed state and compared with the crystal structure of the open state of the channel (PDB ID: 3LUT; Chen et al., 2010). The models show that the 226 position of the S2 helix is more exposed to the surface in closed state model compared to the open state (Fig-3.6A, 3.7A). In wild-type channel, E226 makes the opening of the omega path narrow by its longer side chain (Fig-3.6B and G). Substitution of E226 with D and N make the pore opening wider than the wild type channel (Fig-3.6 C, N, H and I). Q at 226 position in E226Q mutant clearly disrupts the constriction in the opening of the omega pore, but the pore opening is narrower in E226Q mutant compared to E226N and E226D (Fig-3.6D and J). In the open state model of the channel no obvious omega pore is found (Fig-3.7). Besides, no noticeable change in the 3D structure is observed for E226 mutations (Fig-3.7).
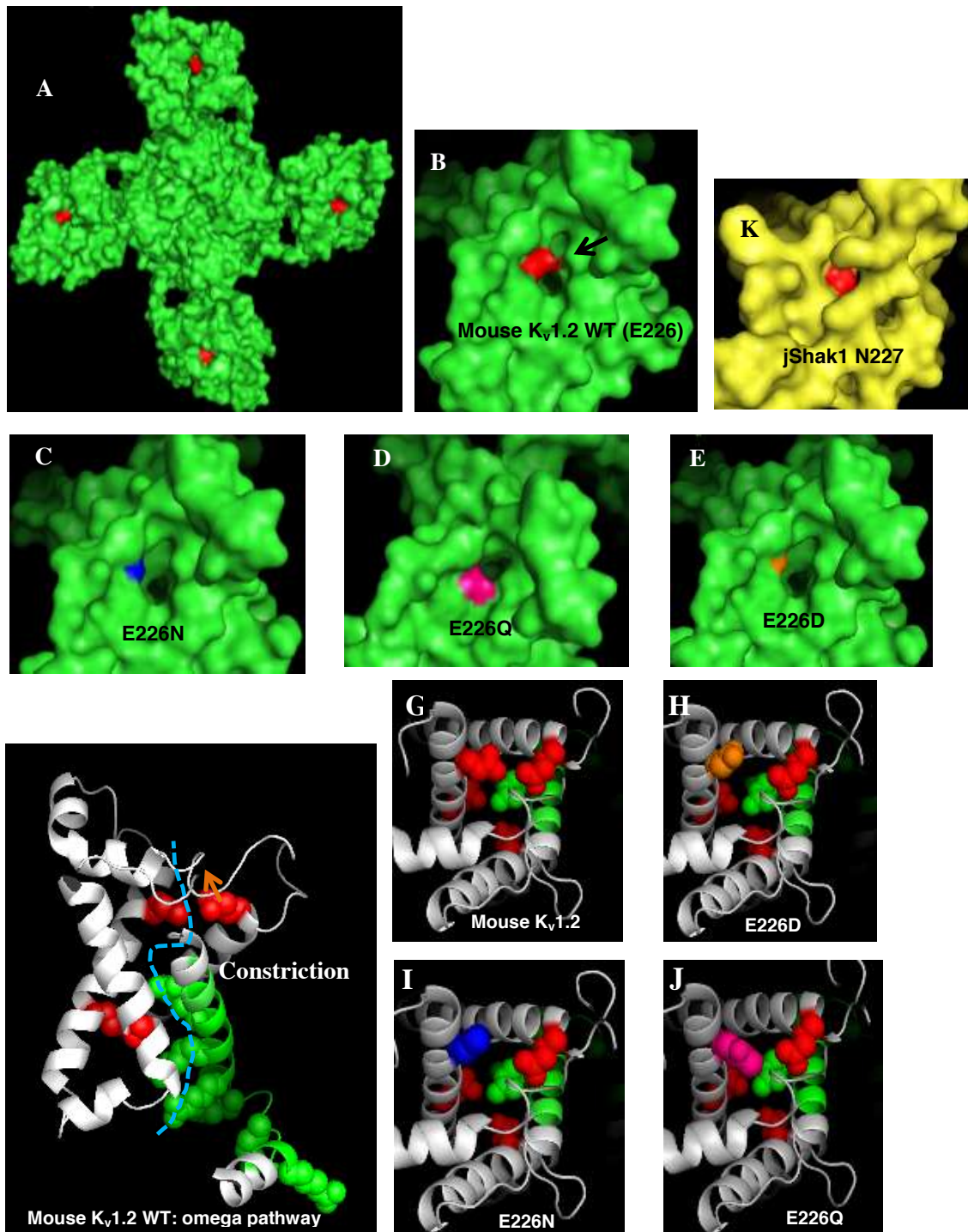
Figure 3.6: Possible omega pore of mouse K$_v$1.2 WT and E226 mutants in closed state, presented in surface (A-E) and ribbon format (F-J).The homology model was made using the inferred closed state model of Jensen et al., (2012) as a template. The omega path in VSD vestibule and the constriction by the charged residues (proposed by Tarek et al., 2012) is shown in (F). The homology model (surface) of jShak1, showing N227 region (K).

50
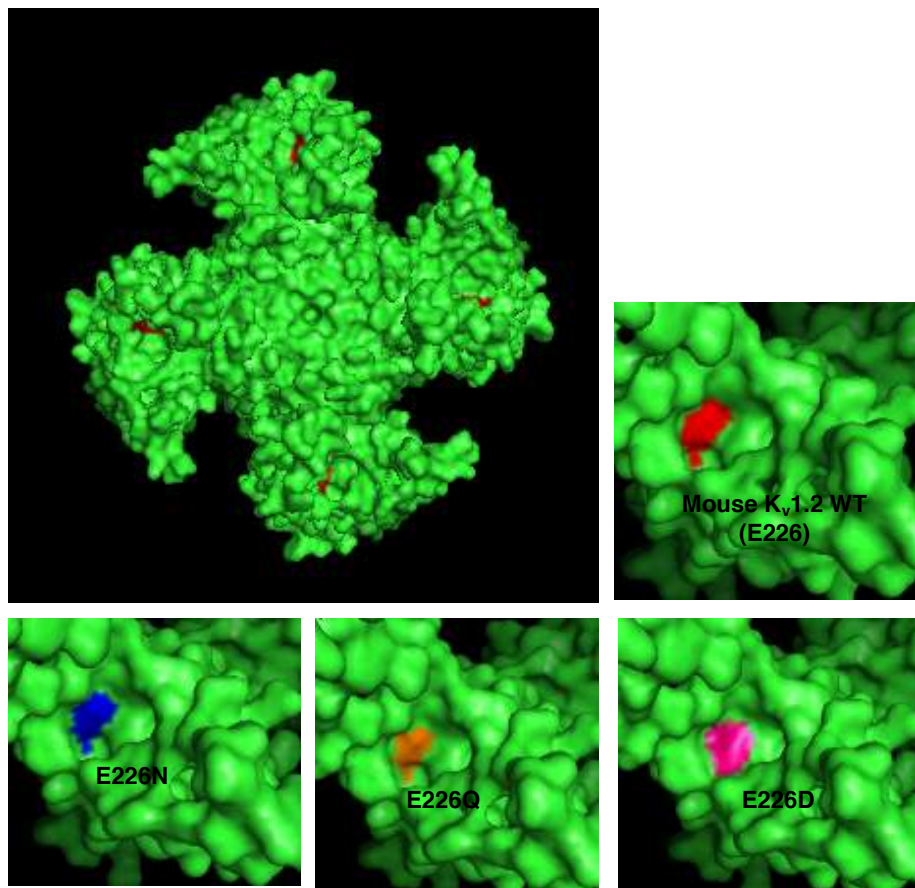
Figure 3.7: Location of possible omega pore in the open state. 3D model of mouse $K_v1.2$ in open state, modelled using PyMOL on 3LUT (Chen et al., 2010). The mutated residues in the possible omega path are highlighted with different colours.

I propose that the interaction between the positively charged residues of the S4 helix and E226 of the S2 helix is important for stabilizing the open state of the channel as well as for preventing the omega current through the VSD. All of the E226 mutants are found to generate inward currents at hyperpolarizing potentials and outward currents at depolarizing potentials (Fig-3.3 and 3.4). Experiments with the pore blocker indicate passage of larger amount of leak current through E226N and E226Q cannel compared to E226D (Fig-3.5). As aspartic acid (D) has a shorter side chain compared to glutamic acid (E), I suggest that substitution of E to D in E226D mutant channel makes the mouth of the omega pore wider compared to the wild type channel in the resting state (Fig-3.6 D, E). When the channel opens the S4 helix moves towards the S2 helix and forms salt-bridge with D at 226 position. This salt-bridging closes the omega pore and current starts to pass through the canonical pore. For this reason, only a small amount of inward current is observed for E226D mutants (Fig-3.5). During channel activation in presence of agitoxinI, the canonical pore is blocked by the pore blocker and the omega pore is blocked by salt-bridging between S4 and S2 helices, resulting about 80% blockage of the total current of E226D mutant (Fig-3.5 I).

In the E226N mutant the constriction of the omega path is disrupted by E to N mutation, which in turn made the doorway of the omega pore wider compared to the wild-type channel (Fig-3.6C, I), leading to leak current at resting state of the channel. At depolarizing potential, when the channel opens, the neutral N at 226 fails to form stable salt-bridge with the positively charged residue of the S4 helix.

As a result the omega pore remains open, passing leak current both at hyperpolarizing and depolarizing potentials (Fig-3.3D). I reason that as the salt-bridging between the S2 and S4 helices, necessary for stabilizing the open state are disrupted in E226N mutant, the complete opening of the canonical pore might also be affected. When treated with agitoxin I, I observed only 27.5% blockage, indicating that only 27.5% of the total current in E226N is passed through the canonical pore.

In the E226Q mutant, Q at 226 generate omega current at both depolarizing and hyperpolarizing potential by disrupting the omega pore constriction and by not forming salt-bridge with the S4 helix to stabilize the open state. Pore-blocker blocks only 2% of the total current passing through this channel. I infer that similar to E226N mutant channel, E226Q also fails to open the canonical pore as the open state of the channel is not stabilized by salt-bridging between S2 (226 position) and S4 helices. However, Q at 226 position might cause some conformational change in the omega pore, making E226Q leakier than E226N mutant channel.

Jellyfish channel jShak1, which is evolutionarily divergent from mouse $K_v1.2$ has evolved with a neutral N in the S2 helix (N227), but does not produce an omega current. I compared the homology model of closed jShak1 channel with the model of mouse $K_v1.2$ in closed state. In jShak1 the possible location of omega pore is closed by N227 (Fig-3.6K). Based on the structure comparison, I propose that the

helices of jShak1 are more compactly packed together than the helices of mouse $K_v1.2$. Although E at 226 position of mouse $K_v1.2$ is important for preventing omega current, this property is highly specific to channel. The overall channel sequence of jShak1 has evolved to prevent omega current differently than it is in mouse $K_v1.2$.

Homo-polymeric loops affect the V_{50} of mouse $K_v1.2$ based on loop length and composition

Besides the electrostatic interaction within the S2 and the S4 helices, the voltage sensitivity of mouse $K_v1.2$ is also affected by the S3-S4 loop length and composition (Sand et al., 2013). Shorter loops caused a positive shift in the V_{50} values compared to the wild type channel, possibly by constraining the movement of the S4 helix (Sand et al., 2013). Depending on composition, the V_{50} values of the loop mutants reached a plateau at a length of 5-8aa (Sand et al., 2013). For the study presented in this chapter, I choose synthetic loops of varying length (3aa, 5aa and 10aa long) and compositions (serine, glycine and glutamic acids) to evaluate the effect of loop lengths and compositions on the interactions between the S2 and S4 helices. The 3aa loops would constrain the complete transition of the S4 helix across the membrane in response to voltage change and the 10 aa long loops would allow flexibility to the S4 helix to move across the membrane, independent of the loop composition.

(A)

(B)
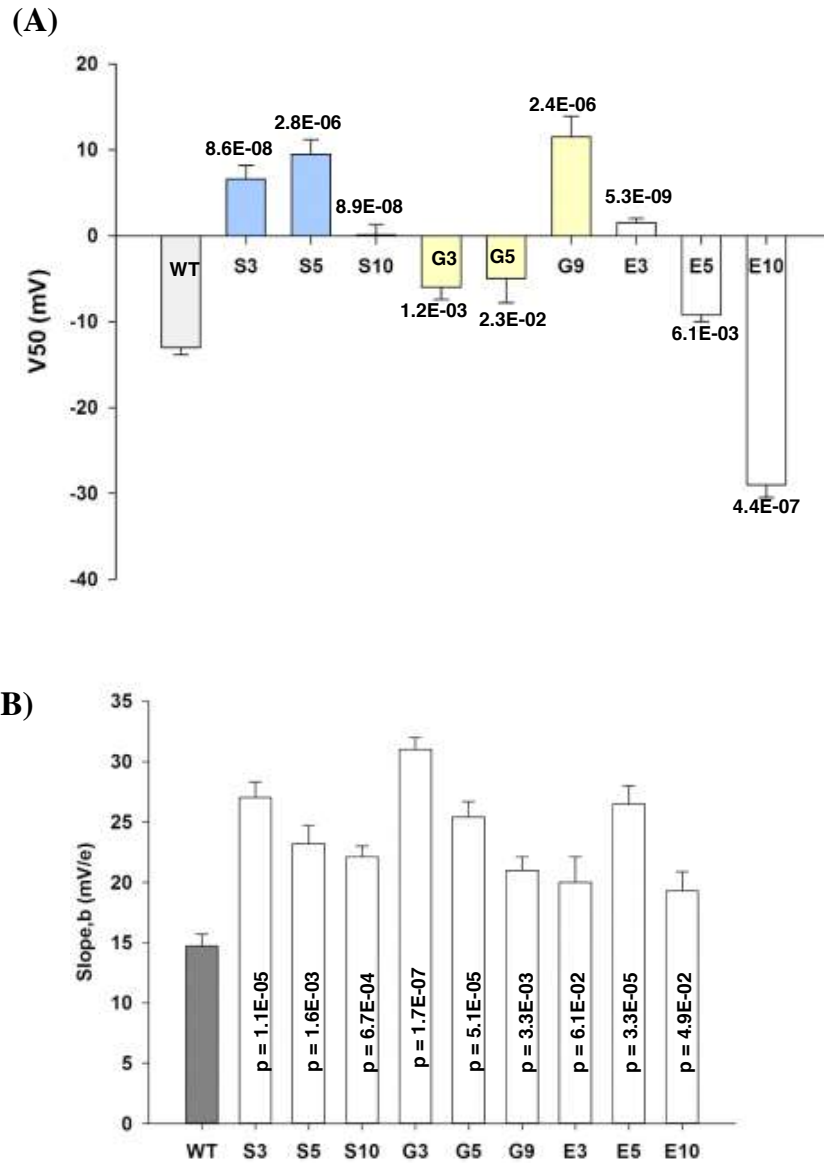
Figure 3.8: Voltage of half activation V_{50} (A) and Boltzmann slope factor, b (B) presented as a function of S3-S4 loop length and composition. The natural loop of mouse $K_v1.2$ was replaced with synthetic homoloops, varying in length and composition. Currents were recorded from two-electrode voltage clamp. Individual G-V curves (from -80 to + 80 mV) were normalized and fitted to the Boltzmann equation: $G/Gmax = 1/(1+exp((V-V_{50})/b)^4)$. The single subunit V_{50} obtained from the equation was used to calculate whole channel V_{50} by solving for V when G/Gmax = 0.5. Error bars represent s.e.m. p values were calculated from 2-tailed *t*-test and indicate the significance of difference from the wild-type channel. Colours of the bars have no

55

All the three chosen length of serine loops show positive shifts in their V_{50} values compared to the wild type mouse $K_v1.2$ channel. The V_{50} value of the S3 loop channel is +6.6 mV, significantly more positive than the wild type channel (p = 8.6E-08). S5 loop shift the channel V_{50} (+9.5 mV) is not significantly different (p = 0.2) compared to the S3 loop channels (Fig-3.8A). The V_{50} value of S10 loop mutant (+0.1mV), is significantly more negative than both S3 (p = 4.2E-03) and S5 (p = 1.1E-03) loop channels, but is more positive than the wild type mouse $K_v1.2$ (p = 8.9E-08).

The V_{50} values of mutant channels with serine and glycine loops differ from our previous study presented in Sand et al., (2013). In Sand et al., the tail currents were used to calculate conductance of the mutant channels. Later studies in our laboratory have identified a transient effect in 2ms depolarization pulse of the tail current. Furthermore, some the synthetic loops were causing C-type inactivation, affecting the tail current. Homo-polymeric loop mutant channels with serine, G3 and G5 loops show C-type inactivation, which affect their tail currents. To improve the calculation of conductance, in this study I have used the peak current of individual traces and derived the conductance of the channel from the average peak current and reversal potential (detail procedure in Material and Method section). Using the peak current method, I found 5-10 mV positive shift in V_{50} values only for the above mentioned channels, compared to what I found using tail currents. Only 1-2 mV variation in V_{50} values, calculated in two different methods were found for the other homo and hetero loop channels.

Glycine loops show a distinctive nature compared to other homo-loops in mouse $K_v1.2$. The G3 (-6mV) and G5 (-5mV) loops shift the channel V_{50} more negative compared to the G9 loop channels (+11.5mV) (p = 3.5E-05 and 5.5E-04 respectively compared to G3 and G5; Fig-3.8A). Glycine with no side chain is expected to have least interaction with its surrounding residues. However glycine might also provide the loop with structural flexibility over other sequences, which might contribute in setting the V_{50} values observed in the glycine loop-mutant channels.

Glutamic acid loop length and the V_{50} values of the mutant channels show a negative co-relation, shorter loops shifting V_{50} values more positive than the longer loops (Fig-3.8A). The V_{50} value of E3 loop mutant (+1.5mV) is significantly more depolarized compared to the E5 (-9.2 mV) loop channel (p = 1.3E-08) and the V_{50} of E10 (-29mV) is more hyperpolarized than E3 (p = 4.0E-09) and E5 (p = 6.4E-08) loop mutant channels (Fig-3.8A). Among all the other 10aa long loops, only E10 shifts the channel V_{50} more negative than the wild-type mouse $K_v1.2$.

The Boltzmann slope factor (b) of the fitted G-V curves, a measure of the inverse of the steepness of the voltage dependence, significantly (p values in Table -3.1) increased for all synthetic homoloop channels, compared to the wild type channel (Fig-3.8B). Larger b values give shallower G-V curves, indicating lower sensitivity but over a longer voltage range. Serine and glycine loop series show a

clear effect of lowering the b (slope factor) values with increasing loop length (Fig-3.8B), which indicates higher voltage sensitivity over a narrower range of voltages. Change in slope factor indicates a possible change in the core mechanism of voltage sensitivity.

The results of the homo-polymeric synthetic loops presented in this chapter are differ from our previous studies (Sand et al., 2013) as the analytical procedure has been modified in this study by considering the C-type inactivation and the transient artifacts of current recordings. However the trend of the loop behaviour is consistent among the present and previous studies with mouse $K_v1.2$.

In summary, the results of this study show that synthetic loops of same length but different sequence affect V_{50} differently in mouse $K_v1.2$. The effect of increasing loop length is also different for different loop compositions. Together, these findings indicate significant contributions of both loop length and composition in setting the V_{50} of mouse $K_v1.2$ channel. I have performed similar loop experiments with jShak1 (presented in chapter 4), which is a K_v1 family channel from jellyfish *Polyorchis penicillatus* and is widely different from mouse $K_v1.2$ in channel sequence. Synthetic loops of same length and composition is found to affect V_{50} differently in mouse $K_v1.2$ and jShak1. In jShak1, the effect of the synthetic loops are smaller than in mouse $K_v1.2$, however unlike mouse $K_v1.2$, the increasing loop length in jShak1 showed a clear effect in causing a left-ward sifts the V_{50} values of the mutant channels. The slope factor, b did not change for the

homo-loop mutants in jShak1 (chapter 4), which is also contrasting to mouse $K_v1.2$. The comparison of the synthetic loop effects in two different channel backgrounds further illustrates the effect of loop composition in setting the specific V_{50} of a channel.

__The S3-S4 loop mediates two types of interactions with the channel that differentially affect the V_{50} of the channel__

Our previous results indicate a possible interaction between the loop and the channel that significantly affects the V_{50} in mouse $K_v1.2$. In the model proposed by Jensen et al., (2012), the C-terminal region of the S3-S4 linker is proposed to pull downward, closer to the negatively charged residues of the VSD and the PD turret in the closed state of the channel. The C-terminus is found to affect V_{50} of mouse $K_v1.2$ in our previous study (Sand et al., 2013), where I calculated the interaction energy between the synthetic homo-loops and the rest of the channel and found that: (i) all synthetic loops (G,S,E) of 2-4 aa length have highly positive values of Gibbs Free energy of interaction (ΔG); (ii) glycine loops with length more than 5aa, have no interaction energy with the channel; (iii) serine loops longer than 5 aa, showed small values of ΔG compared to other synthetic loops and (iv) glutamic acid inserts of 5 and longer showed monotonically increasing negative values of ΔG, indicating strong interaction between the E loops and the rest of the channel (Sand et al., 2013)

In this study I have divided the S3-S4 loop into two functional regions: (i) the C-terminal region that is pulled down in between the VSD and the PD turret in the closed state; (ii) the N-terminal region of the loop that remains outside of the core of the VSD in the closed state. The V_{50} values are compared between the wild type channel and the hetero-loop mutants (S7QQA, G7QQA and E7QQA) that are made for the study presented in Sand et al., (2013) by replacing the C-terminus of the longest homo-polymeric loops with QQA, the natural sequence of the C-terminal region of mouse $K_v1.2$ S3-S4 loop. Both the wild type channel and the hetero loop mutants contain QQA in their C-terminal regions. The N terminal parts of the loop are the only variable among these channels.

The hetero mutant channels S7QQA and G7QQA differ from each other only the N-terminal 7 amino acids of the loop. Similar to Sand et al., (2013), no significant differences are observed between the V_{50} values of S7QQA (+2.6mV) and G7QQA (+2.8mV), indicating no differences in interactions between the N-terminal S7 and G7 parts of the loop with the rest of the channel (Fig-3.9). This finding correlates with our previous energetics studies (Sand et al., 2013) showing very small interaction energy between glycine and serine loops (5 and longer) and the rest of the channel.

The V_{50} values of wild type mouse $K_v1.2$ (-13mV) and E7QQA (-26mV) is highly negative compared to S7QQA and G7QQA (Fig-3.9). E loops longer than 5 were shown to produce negative values of interaction energy (ΔG) between the loop

60
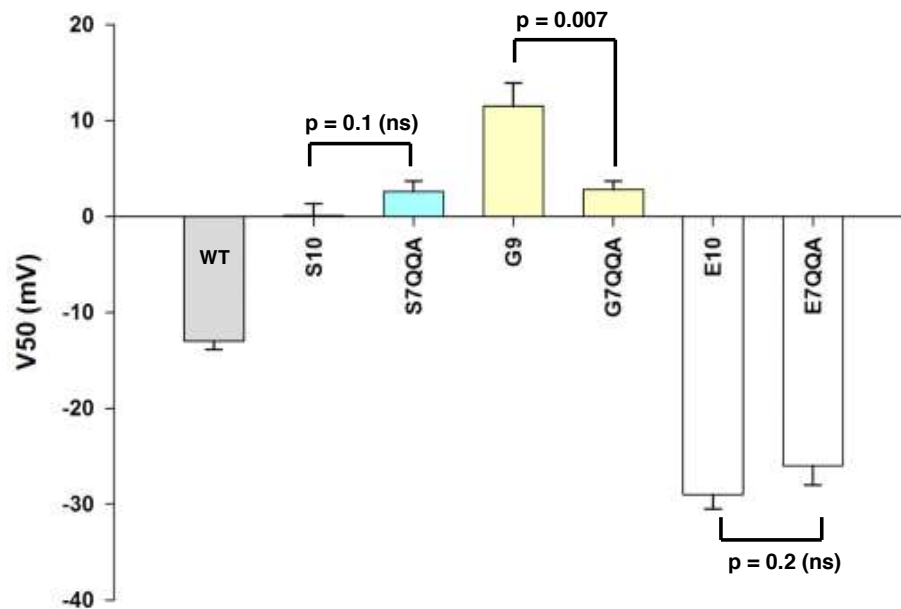
Figure 3.9: Comparison of V_{50} values between the longest synthetic homo-polymeric loops and respective hetero-polymeric loops. The hetero-polymeric loops were made by replacing the C-terminal 3aa of the homo-polymeric loops with QQA, which is the natural sequence of the C-terminus of the wild type S3-S4 loop. The method of calculating V_{50} is described in chapter 2. Error bars represent s.e.m. p values were calculated from 2-tailed *t*-test. In this graph, p values mentioned on the bar indicate the significance of difference between the two channels compared. The significance of difference from the wild type channel is mentioned in table 3.1. 'ns' means 'not significant'. Colours of the bars have no significant meaning.

and the channel (Sand et al., 2013). Comparing the V_{50} values of the hetero-loops and the wild type channel, I propose that the N-terminal region of the loop that remains outside of the VSD vestibule in the closed state interacts with the channel to affect the voltage sensitivity of the channel. The wild type loop (A**EK**P**ED**AQQG) interacts with the channel to stabilize the open state (or destabilize the closed state). The S7 and G7 loops fail to mediate any significant interaction with the channel, showing no effect in V_{50}. Negatively charged E7 loop strongly interacts with the channel to highly stabilize the open state. These results arguably indicate a possible charge-charge interaction between the N-terminal region of the loop and the rest of the channel. E7 loop being completely negatively charged mediates an interaction with the channel, stronger than the wild type loop with three negatively charged residues (marked in red above). G7 and S7 loops having no charges, fail to mediate any significant interaction with the channel.

To evaluate the effect of the C-terminal region of the S3-S4 linker in the voltage sensitivity of mouse $K_v1.2$, I have compared the longest synthetic homo-loops (S10, G9 and E10) with respective hetero-loop mutants (S7QQA, G7QQA and E7QQA) (Fig-3.9). G7QQA (+2.8mV) significantly stabilizes the relative open state compared to the G9 loop (+11.5mV) (p = 0.007), indicating that a trimer of glycine (G3) at C-terminus stabilizes the relative closed state compared to the natural QQA sequence. However, this is true only with G7 in the N-terminus of

the loop. No significant difference is observed between the V_{50} values of S10 (+0.1mV) and S7QQA (+2.6mV) loop channels (p = 0.13) and between E7QQA (-26mV) and E10 homo-loop channel (-29mV) (p = 0.2). These results suggest that trimers of serine (S3) and glutamic acids (E3) in the C-terminal region of the loop apparently make no difference compared to QQA, in S7 and E7 context respectively.

I replaced the 3 residues of the C-terminus of the wild type loop with G3, S3 and E3 to make mutant channels containing WT-G3, WT-S3 and WT-E3 loops respectively for our study presented in Sand et al., (2013). The N-terminus of these loop mutants were constant, having the wild type sequence. WT-G3 showed no significant difference from the wild type channel in the V_{50} value. The V_{50} values of WT-S3 and WT-E3 were statistically indistinguishable and were more negative than WT-G3 (Sand et al., 2013, attached in appendix). Comparison of several combinations of N and C terminal mutations suggest that the C-terminus of the S3-S4 loop affects the channel V_{50} differently depending on the nature of its side chain. However, the C-terminal effect is overwhelmed by the effect of the N-terminus of the loop and the rest of the channel (Sand et al., 2013), which probably mediate an electrostatic interaction.

According to Jensen's study (Jensen et al., 2012) when the channel closes, the S3-S4 loop is pulled downward, closer to the VSD and PD turret. From the results of the past and current studies, together with the 3D model (Fig-3.10) of the closed

63
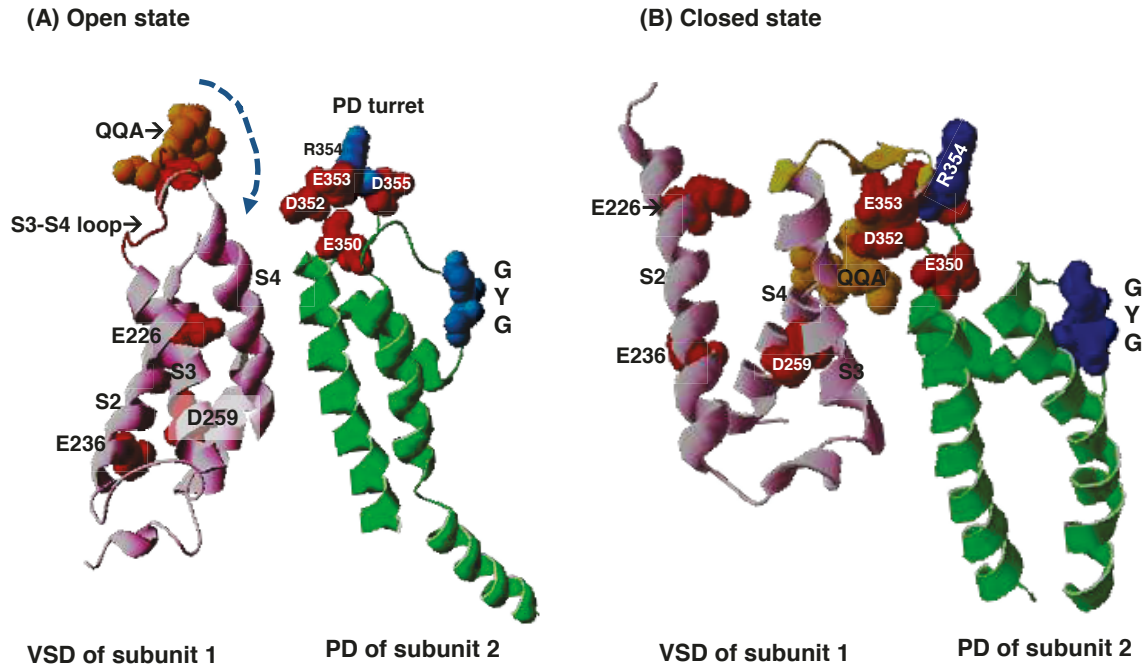
Figure 3.10: Homology model of mouse Kv1.2 in open (A) and close state (B). According to Jensen et al., when the channel closes, the C-terminal 3aa (QQA in wild type) is pulled down into a region between the VSD and the PD vestibule. The residues of the PD turret, VSD and the C-terminal region are labelled.
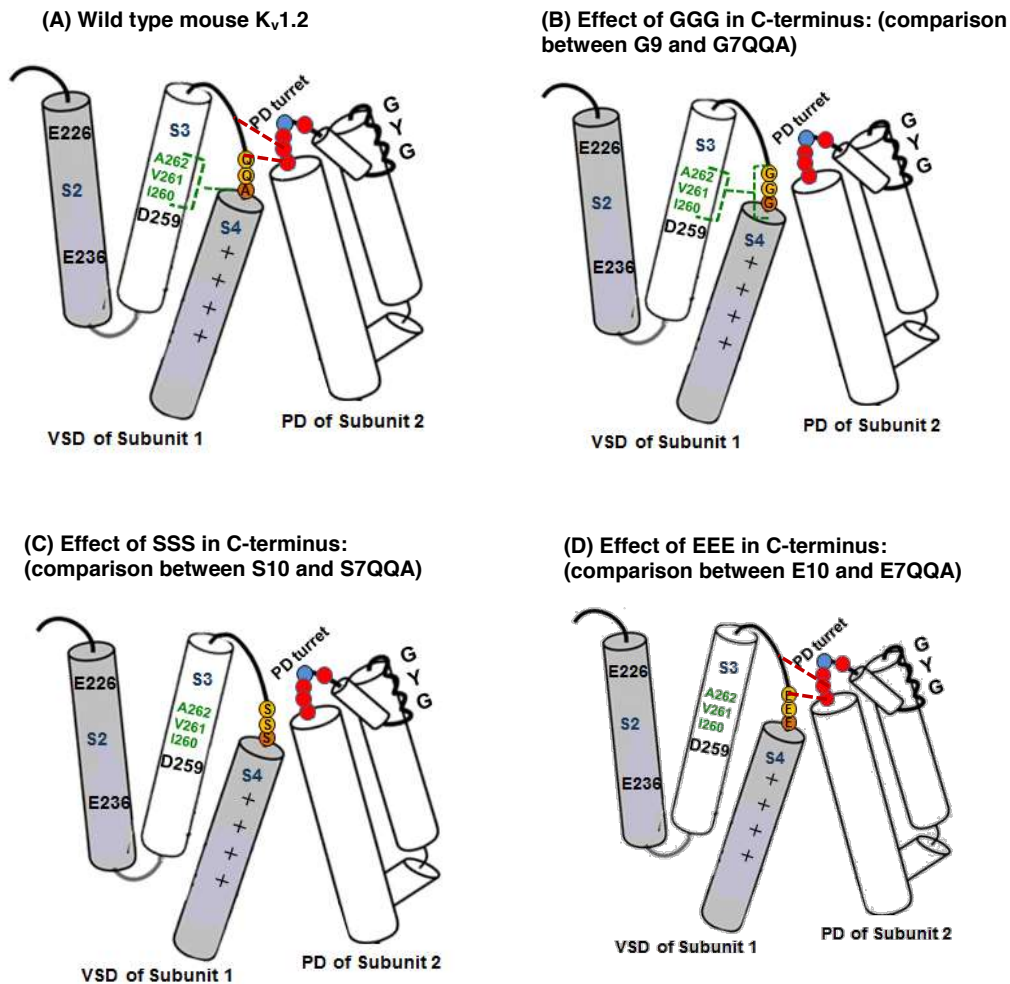
Figure 3.11: Possible interaction between the C-terminal region of the S3-S4 loop and VSD during the closed state. In wild type channel (A), alanine of QQA mediates weak hydrophobic interaction with I260, V261 and A262 of the S3 helix, weakly stabilizing the closed state. Electrostatic repulsion between the N-terminus of the wild type loop and the PD turret destabilizes the closed state. The GGG sequence mediates a hydrophobic interaction with the hydrophobic cluster (I260, V261, A262) of S3 helix (B). Three G residues mediate stronger hydrophobic interaction compared to QQA, stabilizing the closed state more than the wild type sequence. N-terminal G7 fails to mediate any interaction with the PD turret. Serine loops (C) do not conduct any interactions with either the PD turret or the S3 helix. Glutamic acid trimer (D) does not show any hydrophobic effects. However, part of the trimer repulses the negatively charged PD turret. Strong electrostatic repulsion between the E7 N-terminal region and the PD turret destabilizes the closed state.

state channel I suggest that in the closed state the C-terminus of the S3-S4 loop of mouse $K_v1.2$ is pulled down, passing most of the charge effect of the VSD and PD turret. This makes the C-terminus of the loop to be exposed to the hydrophobic residues of the S3 helix and the N-terminus to be exposed to the negatively charged region of the PD turret (Fig-3.10 and 3.11). However, the PD turret might still have smaller effect on the C-terminal region (Fig-3.11). In mouse $K_v1.2$, the conserved D259 of the S3 helix is surrounded by a cluster of hydrophobic residues (I227, I226, I229, V230, A231) (Fig-3.11, Fig-3.1B). I propose that during the closed state, the C-terminal alanine (A) of the wild type channel mediates hydrophobic interactions with I229, V230 and A231, which energetically stabilize the closed state of the channel (Fig-3.11A). However, this C-terminal effect is suppressed by the stronger electrostatic interaction between the negatively charged residues of the N-terminal region of the wild type loop and the negatively charged residues of the PD turret. The repulsion between the negatively charged residues of the loop and the PD destabilizes the closed state, shifting the V_{50} more negative and overwhelming the effect of the weak hydrophobic effect of the C-terminal of the loop.

The G9 loop shows a V_{50} value more positive than the G7QQA loop mutant (p = 0.007). I suggest that a glycine trimer (G3) in C-terminus, mediates stronger hydrophobic interactions with the hydrophobic residues of the S3 helix, stabilizing the closed state more compared to the wild-type QQA sequence (Fig-3.11B). G7 in the N-terminus of these channels fail to interact with the charged

66

residues of the PD turret, making the C-terminal effect dominant for these two channels (Fig-3.11B).

The mutant channels with three serines (S3) in the C-terminus of the loop are not subjected to any type of interactions with the hydrophobic residues of the S3 helix, (Fig-3.11C). Serine residues at the N-terminal region of the loop do not have any electrostatic effect on the PD turret, showing no significant effect in stabilizing the relative open or closed state of the channel. For this reason, the V_{50} of S10 and S7QQA is statistically indifferent (p =0.13) and all the serine homo- and hetero-loop channels have V_{50} values more positive than the wild type channel.

Glutamic acid residues (E) do not participate in hydrophobic interactions. Comparing the V_{50} values of E10 and E7QQA loop channels suggest that the PD turret have small electrostatic effect on the C-terminal E trimer of the loop (Fig-3.11D). However, the highly negative V_{50} values of these two channels are mostly caused by the N-terminal 7 E residues that encounter an electrostatic repulsion caused by the PD turret (Fig-3.11D). For this reason, the V_{50} value of E10 is more negative than E7QQA, although the difference is statistically insignificant (p =0.2).

In summary, comparing the results of homo-polymeric and hetero-polymeric loops, I deduce that two parts of the loop interact differently with different parts

of the channel and differently affects the V_{50}. (i) The N-terminal region, that remains outward of the VSD in closed state possibly mediate a charge-charge interaction, with the negatively charged PD turret. (ii) The C-terminal part of the loop that is pulled downward during channel closing mediates hydrophobic interaction with the S3 helix. The effect of the C-terminal region is much smaller in setting V_{50} of the channel and is overwhelmed by the stronger effect of the N-terminal region of the loop.

Salt-bridge formation between the S2 and S4 helices is affected by both the length and composition of the S3-S4 loop

E226D mutation destabilizes the open state of mouse $K_v1.2$ possibly by forming a weaker salt-bridge with the S4 helix, compared to the wild type channel. The results of the present and past studies in mouse $K_v1.2$ indicate possible constraints on the movement of the S4 helix caused by the short S3 and E3 loops. Longer loops affect the V_{50} differently depending on their lengths and compositions (Sand et al., 2013). Here I aimed to analyze the effect of the S3-S4 loop length and composition on the interaction between the S2 and S4 helices of mouse $K_v1.2$. Among all the E226 mutations (E226D, E226N and E226Q), E226N and E226Q produced leaky channels, passing omega current through the VSD. Several double mutant channels were made by combining E226N/Q with synthetic loops and all the double mutant channels were also leaky (data not shown), indicating no significant effect of the S3-S4 loop length and composition in preventing the omega current through the VSD. Current recording without P/N subtraction and

treatment with the pore blocker show that around 75% of the total current of E226D mutant channel is passed through the canonical pore (Fig-3.5I). So, double mutant channels were made by combining E226D and all the synthetic loops to study the effect of loop length and composition on the electrostatic interaction between the S2 and S4 helices. Among the double mutations between E226D and serine loop series, EDS3 shows a V_{50} of +4.5 mV, insignificantly less positive than S3 loop channel (+6.6mV) (p = 0.51) (Fig-3.12). I reason that in the E226D single mutant, the S3-S4 loop length and composition is the same as in the wild type channel, with a length of 13aa and end-to-end distance of 16.2Å (Fig-3.2C). The loop length allows the complete transition of the S4 helix across the electric field of the membrane. The confirmation and position of the S4 helix, set by the wild-type loop length is also optimum for making a stable salt bridge between E226 and the basic residues of the S4 helix. In E226D mutant channel, D at 226, with a shorter side chain than E, creates a distance between the carboxyl group of D and R300 and R303 of the S4 helix, making the salt-bridging between the charged residues less efficient compared to the wild-type channel (Fig-3.2B and C).

In S3 loop channel, the movement of the S4 helix is constrained by the short length of S3 loop, positioning the S4 helix too far from the S2 helix to form a stable salt bridge between E226 and the basic residues (R300 and R303) of the S4 helix. When a double mutant channel EDS3 is made between E226D and S3 loop
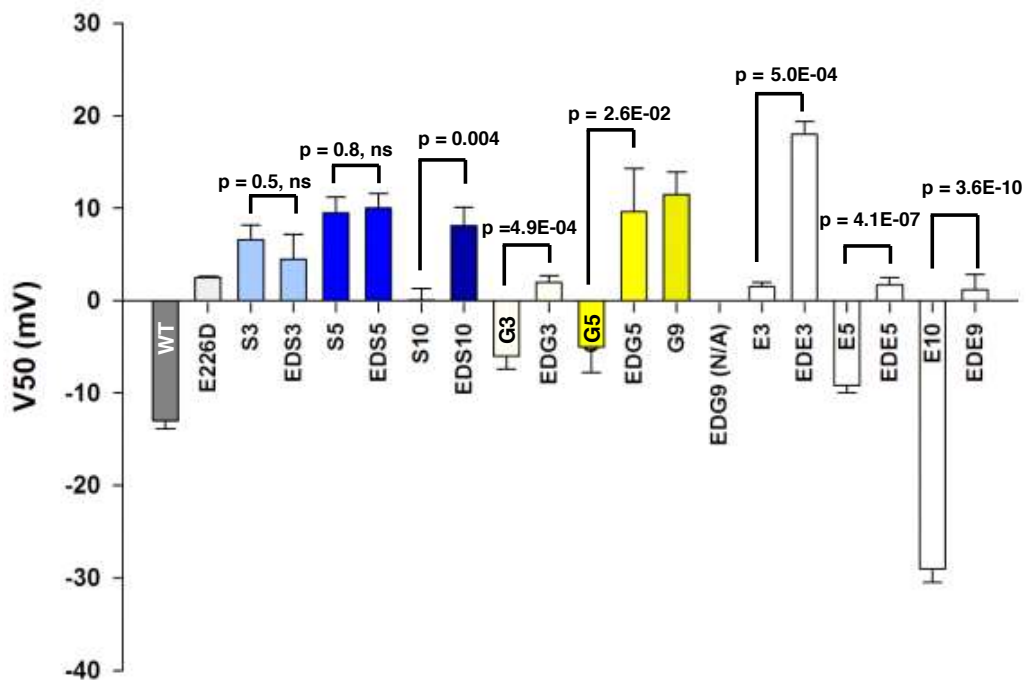
Figure 3.12: V_{50} of double mutant channels, made by combining E226D with synthetic homo-polymeric loops. The V_{50}s of the double mutants are compared with corresponding single mutants and the wild type channel. The procedure of making the double mutant channels and calculating V_{50} is described in chapter 2. Error bars represent s.e.m. p values were calculated from 2-tailed *t*-test. In this graph, p values mentioned on the bar indicate the significance of difference between the two channels compared. The significance of difference from the wild type channel is mentioned in table 3.1. 'ns' means 'not significant'. Colours of the bars have no significant meaning.

channel, the S4 helix of the mutant channel is constrained by short S3 loop, similar to homo-polymeric S3 loop mutant. As the S4 helix in both EDS3 and S3 homo-loop channel is positioned far enough to interact with the S2 helix, the presence of E (in S3 homo-loop channel) or D (in EDS3) does not make any significant difference in the V_{50} values of these two channels (S3 = +6.6mV and EDS3 = + 4.5mV) (p= 0.5, Fig-3.12) .

For the double mutant channel EDS5 (E226D + S5 loop), I suggest that the S5 loop is small enough for the S4 helix to move in sufficiently close proximity to the S2 helix and form a stable salt-bridge, as our previous study (Sand et al., 2013) showed that for serine loops, the V_{50} of the mutant channels reached a plateau at a length of S7. Thus the S5 loop constrains in the transition of the S4 helix, restricting the formation of a stable salt bridge. Consequently, no significant difference is observed in the V_{50} values of the S5 homo-loop channel with an E at 226 position (+9.5mV) and the EDS5 double mutant channel with a D at 226 position (+10mV) (p = 0.8, Fig-3.12).

The V_{50} value of the EDS10, a double mutant channel between E226D and S10 loop (+8.1mV), is more positive than the S10 homo-loop mutant channel (+0.1mV) (p = 0.004, Fig-3.12). I suggest that the length of the S10 loop, being longer than S7 allows the complete transition and the maximum movement of the S4 helix towards the S2 helix. Both the S10 homoloop channel and EDS10 double mutant channel contain identical S10 loop, but differ from each other at 226

71

position of the S2 helix. The S10 loop allows formation of a stable salt bridge between the E226 and the S4 helix in S10 homo-loop mutant. In EDS10 channel, however the energetically stable conformation of the S4 helix remains constant (as in S10 homoloop channel), but the efficiency of the salt-bridging becomes limited by the short side-chain length of D at 226, resulting a more positive V_{50} for EDS10 compared to S10 homo-loop channel.

Double mutations between E226D and glycine loops shift the V_{50} more positive compared to the respective homo-loop mutant channels. The V_{50} value of EDG3, a double mutation between E226D and G3 loop (+2mV) is more depolarized than the G3 homoloop channel (-6mV) (p = 4.9E-04). Similarly, the V_{50} value of EDG5 (+9.6mV) is more positive than G5 homo-loop mutant (-5mV) (p = 2.6E-02, Fig-3.12). Glycine, with no essential side-chain, has the least potential to interact with other amino acids. The increasing lengths of glycine in homo-loop channels tend to cause a right-ward shift the V_{50} values (Fig-3.8A). I infer that the replacement of E to D, in the context of glycine loops makes the channel opening energetically unfavourable compared to the respective glycine homo-loop channels by making less efficient salt-brides between S2 and S4 helices. Double mutant channel EDG9 could not be made.

All the double mutations between E226D and glutamic acid (E) loops shift the V_{50} more positive compared to respective E homo-loop channels (Fig-3.12). The V_{50} value of EDE3 (+18 mV), a double mutation between E226D and E3 loop, is

more positive than the E3 homo-loop channel (+1.5mV) (p = 5.0E-04). Similarly the V_{50} value of EDE5 (+1.7mV) is more right-shifted than the E5 homo-loop channel (-9.2mV) (p = 4.1E-07) and the V_{50} of EDE9 (+1.2mV) is highly depolarized than the E10 homo-loop channel (-29mV) (p = 3.6E-10) (Fig-3.12). I suggest that like all other double mutants, the efficiency of salt-bridge formation is disrupted by short side-chain of D in these sets of mutants, making the V_{50} values more positive compared to the respective E-homo-loop channels. Our previous studies showed that for the E loops, the channel V_{50} and the interaction energy between the E-loops and the channel reached a plateau at a length of 8aa (Sand et al., 2013). The E3 and E5 loops, being shorter than 8aa, contain the movement of the S4 helix, compared to the E9 loop. For this reason, the V_{50} of EDE9 is more negative compared to EDE5 and EDE3. The negatively charged PD turret has an electrostatic effect on the E-loops that destabilizes the closed state (Fig-3.11D). I infer that this charge-charge interaction between the E-loop and the PD turret is responsible of making the V_{50} values of these double mutants more negative than all other double mutant channels between E226D and homo-polymeric loops (Fig-3.12)

In summary, double mutations between the synthetic loops and E226D clearly indicate a constraint on the dynamics of the S4 helix, caused by loops of 3 aa in length. The loops of 10aa allow the S4 helix to mediate a complete transition across the membrane and form a stable salt-bridge with the S2 helix. Depending on loop sequence, a minimum length of 5 to 8aa is needed to establish this

energetically favoured confirmation of the S4 helix. For this reason, 10aa loops do not cause any additional change in the conformation of the S4 helix. Based on my findings, I suggest that when the movement of the S4 helix becomes energetically stable at a certain position, the side chain length of the acidic residue at 226 positon becomes the limiting factor in forming the stable salt-bridge between the S2 and S4 helices. However, loops of same lengths but different compositions are found to affect V_{50} differently in double mutant channels with E226D, indicating a possible effect of loop composition in regulating the interaction between the S2 and S4 helices.

Double mutations between E226D and hetero-loops show no significant effect of the C-terminus of the loop in inter-helix interactions

The results from homo-polymeric loop mutants suggest that the N-terminus and the C-terminus of the S3-S4 loop interact with different parts of the channel and affect the voltage sensitivity differently. Double mutations are made between the hetero-loops and E226D to evaluate how the interactions between the S2 and S4 helices are affected by the nature of the N and C termini of the loop in mouse $K_v1.2$. All the double mutants show a positive shift in their V_{50} values compared to the respective hetero-loop mutant channels (Table-3.1), possibly caused by the shortening of the side-chain by E226D mutation.

To study the effect of the C-terminus of the loop in the interaction between the S2 and S4 helices, the V_{50} values of the hetero-loop double mutants are compared

with respective homo-loop double mutants. Double mutant channel EDS7QQA, made by combining E226D and S7QQA loop show a V_{50} value of +12.4 mV, which is statistically invariable from the V_{50} of EDS10 (+8.1mV) (p = 0.3) (Fig-3.13). Similarly no difference is observed between the V_{50} values of EDE9 (+1.2mV) and EDE7QQA (+1.8mV) (p = 0.7). These results indicate that the C-terminus of the loop fails to make any significant effect on the inter-helix interaction in the context of serine and glutamic acids, which are the sequences of the N-terminus of the loop in the respective channels.

Based on the results from hetero-loop mutants, I have suggested an electrostatic interaction between the N-terminal region of the loop and the rest of the channel. The PD turret being negatively charged is the most potential candidate for this interaction. To identify the effect of the N-terminal region of the S3-S4 loop in the dynamics of the S4 helix, I compared the V_{50} values between EDS7QQA, EDG7QQA and EDE7QQA, all of which differ from each other only at the N-terminal region of the loop. Among the three double mutant channels, EDG7QQA (+33.4mV) show the most positive V_{50} value followed by EDS7QQA (+12.4mV) and EDE7QQA (+1.8mV) (Fig-3.13). Glycine, having no side chain, can provide the loop with structural flexibility but fails to mediate any interactions with its surrounding environment. Lack of interactions between the N-terminus of the loop and the channel might cause the positive shift in the V_{50} value of EDG7QQA channel. I suppose that unlike glycine, serine residues in the N-terminus of the
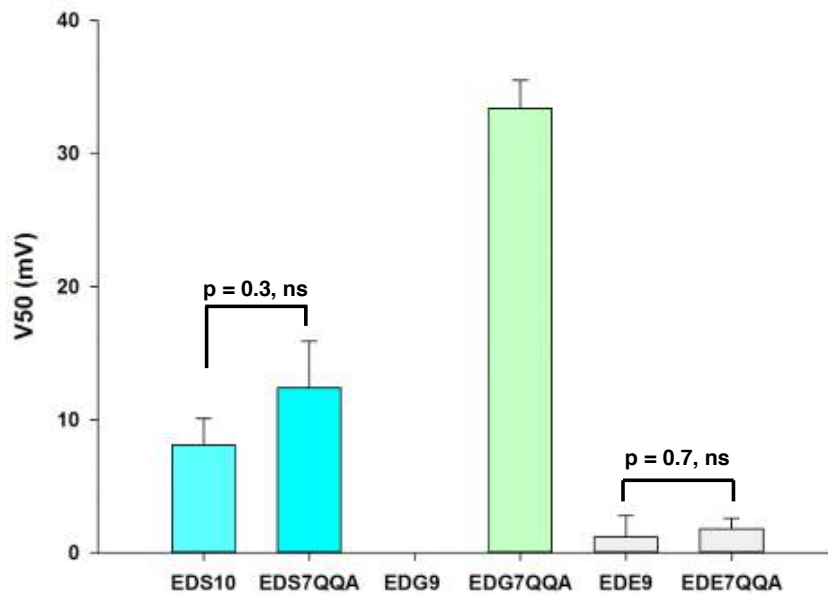
Figure 3.13: V_{50} values of double mutant channels, made by combining E226D and the synthetic hereto-polymeric loops. The V_{50} values of the hetero-polymeric double mutants were compared with respective homo-polymeric double mutants to evaluate the effect of the C-terminal region on the interaction between S2 and S4 helices. The V_{50} values were compared between EDS7QQA, EDG7QQA and EDE7QQA channels to evaluate the effect of N terminal region on the S2-S4 interaction. EDG9 mutant could not be made. Error bars represent s.e.m. p values were calculated from 2-tailed *t*-test. In this graph, p values mentioned on the bar indicate the significance of difference between the two channels compared. The significance of difference from the wild type channel is mentioned in table 3.1. 'ns' means 'not significant'. Colours of the bars have no significant meaning.

loop mediate an unknown interaction with the channel, which can stabilize the open state of EDS7QQA more compared to EDG7QQA channel. The electrostatic contribution of the channel (possibly PD turret) on E7 part of the loop of EDE7QQA destabilizes the closed state, shifting V_{50} to a negative value.

In summary, I suggest that all the double mutations between E226D and hetero-loop mutants caused a positive shift in the V_{50} values compared to the respective hetero-loop channels. This positive shift in the V_{50} is mostly caused by inefficiency in salt bridge formation, caused by the shortening of side chain length at 226 position. The N-terminal region of the loop significantly affects the V_{50} of the double mutant channels depending on its composition. The N-terminus of the E7QQA loop mediates a possible electrostatic interaction with the PD turret and destabilizes the closed state. Glycine in the N-terminus of the loop in EDG7QQA channel fails to mediate any interactions to stabilize the open state and thus shifts the V_{50} more positive compared to E7QQA and S7QQA channels. The C-terminal region of the loop, in the context of S and E in the N-terminal region, fails to show any significant effect in stabilizing either the open or the closed state of the double mutant channel.

Conclusion

The underlying mechanism of voltage-sensitivity is one of the least understood features of K_v channels. The electrostatic interaction network within the VSD stabilizes the open and the closed state of the channel. The S3-S4 loop, varying in

both length and composition within and between different families of K_v channel can also affect V_{50} significantly (Sand et al., 2013). Short loops of 3aa constrain the movement of the S4 helix in mouse $K_v1.2$ (Sand et al., 2013).The length effect of the S3-S4 linker reaches a maximum and tends to become plateau at around 5 to 8aa of length depending on channel composition (Sand et al., 2013).

I made synthetic loop mutants, varying in length and composition to evaluate the general effect of S3-S4 loop length and composition on the voltage sensitivity of mouse $K_v1.2$. Identical synthetic loops are found affect V_{50} differently in mouse $K_v1.2$ and in jellyfish channel jShak1 (study presented in chapter 4), indicating a qualitative difference in the interaction between the loop and the channel, that contributes to set the channel specific V_{50}. I also made hetero-loop mutants to evaluate the effect of N and C termini of the loop in voltage sensing mechanism in mouse $K_v1.2$. The results indicate that the N-terminal region significantly affects the channel V_{50} and also overwhelms the weak effect of C-terminal region. Based on my results, 3D models and previous studies (Jensen et al., 2012), I propose that in the closed state, the S3-S4 loop is pulled down, by the movement of the S4 helix. At this stage, most of the C-terminus of the loop passes down the PD turret, leaving the part of N-terminus in close proximity to the VSD and PD turret. The negatively charged residues of the PD turret mediate an electrostatic effect on the N-terminal region of the loop, stabilizing or destabilizing the closed state depending on the nature of the loop. I have also suggested a possible weak hydrophobic interaction between the C-terminus of the loop and the S3 helix that

weakly contributes to stabilize the open state. However, the effect of C-terminus is overwhelmed by the nature of the N-terminal region.

In this study, I focused on the negatively charged glutamic acid at 226 of the S2 helix that stabilizes the open state of the channel by forming salt-bridges with the positively charged R300 and R303 of the S4 helix. E226 mutations (E226D, E226N and E226Q) produce leak current passing through the omega pore in the VSD, which is further confirmed by using of pore blocker. The amount of omega current through the VSD is much higher in E226N and E226Q mutants, compared to E226D. From my electrophysiological studies and 3D models I propose that the formation of a stable salt-bridge is essential in mouse $K_v1.2$ to both stabilize the open state and to prevent the omega current through the VSD.

Double mutations between E226D and the homoloop show that the short (3 and 5aa) S3-S4 loop regulates the interaction between S2 and S4 helices by constraining the movement of the S4 helix. However, when the loop length is 10aa, the length of the side-chain becomes crucial for optimum salt-bridging between the S2 and S4 helices. Double mutations between the heteroloops and E226D suggest an effect of N-terminal region on the interaction between the S2 and S4 helices. However the C-terminus of the loop fails of show any significant effect on the inter-helix interaction between the S2 and S4 helices.

Chapter 4:

The effect of S3-S4 loop length and composition on the voltage sensitivity of jShak1-a K_v1 channel from jellyfish *Polyorchis penicillatus*

Background

Voltage-gated potassium ion (K_v) channels are transmembrane protein tetramers, consisting of a pore domain (PD), surrounded by 4 voltage sensing domains (VSD) (Tombola et al., 2006 and Lee et al., 2005). The pore region consists of helices S5 and S6 and the connecting P loops from each subunit. The voltage sensing regions are composed of helices S1 through S4 and their connecting loops. Three conserved acidic residues in the S2 and S3 helices are known to interact with the conserved basic residues of the S4 helix (Lee et al., 2005; Long et al., 2005 and Papazian et al., 1995). Depending on the channel type, the S4 helix contains four to seven positively charged amino acid residues. Changes in membrane potential alter the force acting on the charged residues of the S4 helix, causing a conformational rearrangement of the channel that leads to channel opening (Lee et al., 2005 and Long et al., 2005). In the *Drosophila melanogaster* Shaker channel the open conformation is stabilized by salt-bridge formation between R368 and R371 of the S4 helix with E283 of the S2 helix (Silverman et al., 2003 and Papazian et al., 1995). Although the charged residues of the VSD are conserved in most K_v channels, V_{50}, the membrane voltage at which 50% of the channels are in the open state, varies among and within the families of K_v channels in different species. This indicates that other factors contribute to determining voltage sensitivity in different members of this family.

80

Previous studies with mouse $K_v1.2$ (Sand et al., 2013) and *D. melanogaster* Shaker (Bezanilla et al., 1994) indicated a role for S3-S4 loop length and composition in setting the V_{50} of activation of the channel. The results of a mouse $K_v1.2$ study (Sand et al., 2013) implied an energetic constrain in the movement of the S4 helix caused by extremely short S3-S4 linkers. Depending on composition, the C-terminus of the mouse S3-S4 linker differentially stabilizes the equilibrium of the channel by interacting with the negatively charged turret of the PD (Sand et al., 2013), as this part of the linker is positioned in close-proximity to the negatively charged residues of the VSD and the PD turret, during channel closure (Jensen et al., 2012).

In this study I have analyzed the effect of S3-S4 linker variation on the voltage sensitivity in a completely different lineage of K_v channel. jShak1 is a K_v1 family member from the jellyfish *Polyorchis penicillatus* (Jegla et al., 1995). It is phylogenetically distant and its sequence is substantially different from mouse $K_v1.2$ and Shaker. jShak1 opens at a much higher membrane potential (V_{50} = +26.6mV) than mouse $K_v1.2$ (V_{50} = -13.3mV) or Shaker (V_{50} = -31.8mV) . In jShak1 one of the conserved acidic residues of the S2 helix (E283 *Drosophila melanogaster* and E226 in mouse $K_v1.2$) is replaced by neutral asparagine, N227. Also, jShak1 has one less positively charged motif in the S4 region and a very short S3-S4 linker, consisting of only five amino acid residues (Klassen et al., 2008 and Grigoriev et al., 1997) (Fig-4.1). Mutations of the length of the S4 helix

Figure 4.1: Homology model of jShak1 voltage sensing domain (VSD) in open state (A), showing three important candidate sites for shaping V_{50}: S3-S4 loop shown in red, N227 in green and K278 in purple. In jShak1 the negatively charged glutamate residue in the S2 helix (position 227) that is conserved in most other K_v1 channels is replaced by neutral asparagine. jShak1 also has a shorter than normal S4 helix, with one less positively charged 3 residue motif in the S4 helix than is found in most other K_v1 channels and a very short S3-S4 linker, consisting of only five amino acid residues. The model is made in SWISS MODEL using 3LUT, the crystal structure of rat $K_v1.2$ (Chen et al., 2010) as template (A). The 3-D model of mouse $K_v1.2$ VSD from 3LUT (Chen et al., 2010) (B). E226 forms salt bridge with R300 and R303 to stabilize the open state. Molecular model images are made in PyMOL. Multiple Sequence Alignment of S2 helix (C) and part of the pore domain (D). The PD of jShak1 is also different from most other K_v channels where two of the four conserved negatively charged residues are replaced by positively charged K and neutral G in jShak1.

in conjunction with mutation of N227 in jShak1 indicated that the movement of the S4 helix might be constrained by the extremely short natural S4-S5 linker (Klassen et al., 2008).

In the current study, the natural short S3-S4 linker of jShak1 is replaced with synthetic homopolymers varying both in length and composition. The C-terminal positively charged residue, K278, is mutated in both natural and synthetic loops. To evaluate the effect of the loop length and composition on the interactions within the VSD, the neutral N at 227 of jShak1 is mutated to both E and D. N227D and N227E mutations are combined with all synthetic loops to make double mutant channels. The results show that short (3aa) S3-S4 loops in jShak1 make the channel opening energetically unfavourable, similar to what was observed in mouse $K_v1.2$ (Chapter 3 and Sand et al., 2013). Synthetic loops of the same length and composition affect the V_{50} values differently in jShak1 and mouse $K_v1.2$, indicating a possible interaction between the loop and the channel that contributes to the voltage sensitivity of the channel. Mutation to a negatively charged residue at 227 in jShak1 energetically favours the opening of the channel, possibly by forming salt-bridges with the positively charged residues of the S4 helix. This electrostatic interaction between the S2 and S4 helices, caused by the negatively charged residue at 227 is significantly affected by both the length and composition of the S3-S4 linker. The results suggest that the nature of the C-terminal residue of the S3-S4 linker (K278) can significantly affect the voltage sensitivity of jshak1, but only in the presence of the wild type sequence (V274) in

the N-terminus of the loop. When combined with a negatively charged residue at 227, the C-terminus of the loop can affect both the V_{50} values and the slope factor (b) in the double mutant channels.

Based on the overall results, I infer that in jShak1 the voltage sensitivity is affected by the S3-S4 loop in following ways: (i) the short length of the S3-S4 loop restricts the movement of the S4 helix; but loops of 10 aa allow the complete transition of the S4 helix across the membrane (ii) the N-terminal region of the wild type loop (VSSS) interacts with the channel to stabilize the open state; (iii) the C-terminus of the loop (K278) interacts with the PD turret to stabilize the closed state; (iv) the N and C- termini of the S3-S4 linker is likely to mediate a coordination that is essential to set the specific V_{50} of the channel.

Results and Discussion

Synthetic loops of the same length and composition affect V_{50} differently in mouse $K_v1.2$ and jShak1

Studies with mouse $K_v1.2$ presented in chapter 3 show that 3aa long loops of serine, glycine and glutamic acid shift channel V_{50} to more positive values, compared to the wild type mouse $K_v1.2$ channel. As the loop length increases, glutamic acid (E) homo-loop channels tend to shift the V_{50} left-ward, the E5 loop approaching the wild type V_{50} and the E10 loop making the channel V_{50} even more hyperpolarized than the wild type mouse $K_v1.2$ (Fig-3.9). Glycine loops in mouse $K_v1.2$ show a positive correlation between the length and the V_{50} values,

shifting the V_{50} to more positive with increasing length of G loops (Fig-3.9). Serine loops in the same channel background show a positive shift in V_{50} with increasing length from S3 to S5 and a negative shift in V_{50} with increasing loop length from S5 to S10 (Fig-3.9).

To study the effect of loop-length and composition in jShak1, homo-polymeric loop mutants are made by replacing the natural sequence (VSSSK) with sequences varying in length (3aa, 5aa and 10aa) and composition (serine, glycine and glutamic acid). Similar to mouse $K_v1.2$, the 3aa long loops of serine and glycine in jShak1 shift V_{50} to more positive values compared to the wild-type channel (Fig-4.2A), possibly by causing a constraint on the movement of the S4 helix. The other synthetic loops are found to act differently in jShak1 and in mouse $K_v1.2$ backgrounds.

Unlike mouse $K_v1.2$, the serine loops in jShak1 tend to shift the V_{50} more negative with an increasing loop length. The V_{50} of S3 in jShak1 (+36.5mV) is significantly more positive than the wild-type channel (+26.6 mV) (p = 2.5E-09; Table-4.1). The S5 (V_{50} = +31.9mV) and the S10 (V_{50} = +26.1 mV) loops shifts the V_{50} more left-ward, compared to the S3 loop and clearly shows an effect of increasing loop length in relatively stabilizing the open state of the channel (Fig-4.2A).

Similar to mouse $K_v1.2$, the glutamic acid (E) loops in jShak1 show the most left-ward shift in V_{50} values compared to all other synthetic loop series in jShak1.

(A)

(B)
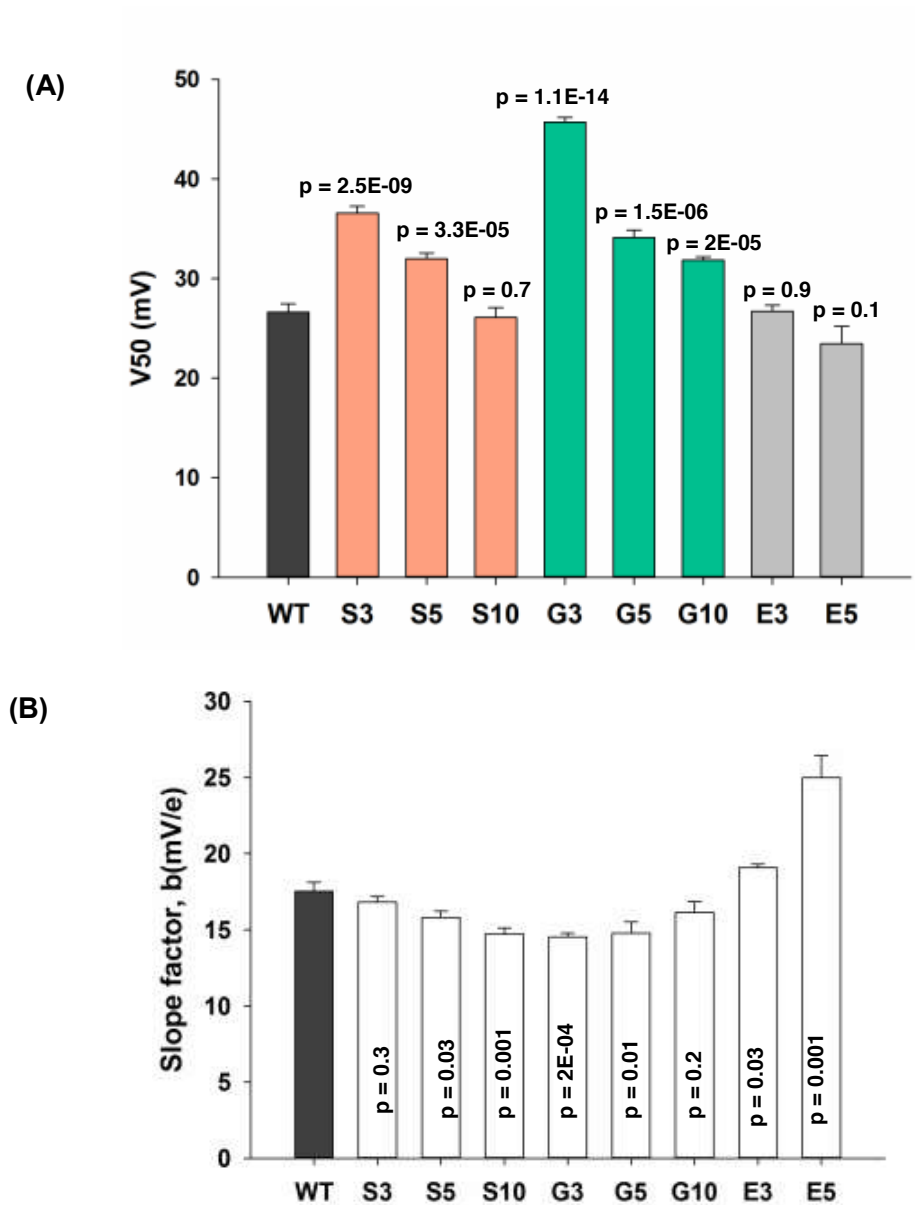
Figure 4.2: Voltage of half activation (V_{50}) (A) and Boltzmann slope factor, b (B) as a function of S3-S4 loop length and composition. The natural loop VSSSK of jshak1 was replaced with synthetic homoloops, varying in length and composition. Currents were recorded from two-electrode voltage clamp. Individual G-V curves (from -80 to + 50 mV) were normalized and fitted to the Bolzmann equation: $G/Gmax = 1/(1+exp((V-V_{50})/b)^4)$. The single subunit V_{50} obtained from the equation was used to calculate whole channel V_{50} by solving for V when G/Gmax = 0.5. Error bars represent s.e.m. p values were calculated from 2-tailed *t*-test and indicate the significance of difference from the wild-type channel. Colours of the bars have no significant meaning.

Table 4.1: Half-activation voltages (V_{50}) for wild type jShak1 and S3-S4 loop variants.
Channel conductance was calculated from the average plateau currents by using the formula $G=I/(V-V_{rev})$, where reversal potential V_{rev} was taken as -70mV. Individual G-V curves (from -80 to + 50 mV) were normalized and fitted to the Boltzmann equation: $G/G_{max} = 1/(1+\exp((V-V_{50})/b)^4)$. The single subunit V_{50} obtained from the equation was used to calculate whole channel V_{50} by solving for V when $G/G_{max} = 0.5$

Channels	Loop sequence (5'-3') / Description	n	V_{50} (mV)	S.E	p	Slope factor, b (mV/e)	SE	p
jShak1 WT	VSSSK	15	26.6	0.8		17.5	0.6	
TEV loop	VLENLYFQG	5	6.1	0.9	5.5E-09	21	0.9	0.014
TEV_K loop	VLENLYFQGK	5	8.13	0.5	1.9E-09	22	0.6	0.005
TEV long loop	VLENLYFQGVSSSKENLYFQG	6	-2.1	1.4	1.6E-10	15.3	1.3	0.17
S3	SSS	11	36.5	0.7	2.5E-09	16.8	0.4	0.3
S5	SSSSS	10	31.9	0.6	3.3E-05	15.8	0.4	0.03
S4K	SSSSK	6	26.8	0.5	0.9	16.5	0.4	0.2
S10	SSSSSSSSSS	12	26.1	1	0.7	14.7	0.4	0.001
S9K	SSSSSSSSSK	6	26.0	0.5	0.5	16.7	2.2	0.7
G3	GGG	10	45.7	0.4	1.1E-14	14.5	0.3	2.0E-04
G5	GGGGG	8	34.1	0.7	1.5E-06	14.8	0.7	0.01
G4K	GGGGK	6	34	1.6	0.005	17.1	0.8	0.7
G10	GGGGGGGGGG	8	31.8	0.3	2.0E-05	16.2	0.7	0.2
G9K	GGGGGGGGGK	6	30.6	0.5	0.001	17.1	0.7	0.7
E3	EEE	10	26.7	0.6	0.9	19.1	0.2	0.03
E5	EEEEE	7	23.4	1.7	0.136	25	1.4	0.001
E4K	EEEEK	5	29.4	1.6	0.2	15.8	1.3	0.3
E10	EEEEEEEEEE	Not expressed						
E9K	EEEEEEEEEK	Not expressed						
K278A	VSSSA	9	32.4	0.4	7.0E-06	14.2	0.8	0.004
K278D	VSSSD	9	17.5	1.2	9.2E-06	13.6	0.4	5.2E-05
K278E	VSSSE	7	16.3	2.1	1.6E-03	17.5	0.8	0.98
K278G	VSSSG	9	20	0.7	6.0E-06	10.7	0.4	5.7E-09
K278N	VSSSN	9	28.5	1.5	0.3	14.5	0.6	0.002
K278Q	VSSSQ	9	26.7	0.6	0.9	17	0.4	0.43
K278S	VSSSS	9	27.5	1.8	0.6	14	1.8	0.078
N227D	Point mutation in S2 helix	5	13.7	0.6	1.5E-09	21.1	1.2	0.02
N227E	Point mutation in S2 helix	4	-15.7	1.8	1.1E-05	20.7	0.8	0.02
NDS3	N227D + S3 loop	6	24	1.3	0.129	18.5	0.4	0.18
NDS5	N227D + S5 loop	6	16.5	1.7	4.3E-04	23.3	0.7	1.1E-05
NDS10	N227D + S10 loop	7	10.3	0.8	2.1E-11	19	0.7	0.15
NES3	N227E + S3 loop	5	-14.5	0.5	5.99E-19	19	1	0.13
NES5	N227E + S5 loop	7	-8.5	0.9	4.62E-14	20.8	1.6	0.09
NES10	N227E + S10 loop	9	-20.4	1.5	9.07E-13	22.4	1.1	0.002
NDS4K	N227D + S4K loop	9	16.5	1.1	1.7E-06	21.5	0.6	1.1E-04

Table 4.1: Continued.

Channels	Loop sequence (5'-3') / Description	n	V_{50} (mV)	S.E	p	Slope factor, b (mV/e)	SE	p
NDS9K	N227D + S9K loop	8	15	0.8	2.4E-09	23	1.5	0.005
NES4K	N227E + S4K loop	6	-10.2	0.9	1.6E-13	19.6	0.4	0.01
NES9K	N227E + S9K loop	9	-13.8	1.5	5.2E-12	17.4	1.4	0.96
NDG3	N227D + G3 loop	9	37	1.4	2.23E-05	15.7	0.9	0.12
NDG5	N227D + G5 loop	9	20.2	0.6	3.38E-06	20.1	0.4	0.001
NDG10	N227D + G10 loop	9	20.7	0.5	5.1E-06	17.6	0.7	0.9
NEG3	N227E + G3 loop	4	9.8	0.6	6.1E-11	13	1.2	2.4E-02
NEG5	N227E + G5 loop	9	-18.4	2.3	1.89E-08	20.1	0.9	0.03
NEG10	N227E + G10 loop	6	-19.7	1.1	1.15E-12	17.8	0.8	0.8
NDG4K	N227D + G4K loop	9	21.4	0.7	8.1E-05	20.4	0.5	0.002
NDG9K	N227D + G9K loop	8	24.4	0.7	0.05	18.8	0.8	0.221
NEG4K	N227E + G4K loop	9	-0.3	0.7	3.2E-17	17	0.6	0.55
NEG9K	N227E + G9K loop	Not expressed						
NDE3	N227D + E3 loop	9	20.5	1.5	2.8E-03	21.8	0.6	3.5E-05
NDE5	N227D + E5 loop	7	12.9	1.2	6.3E-07	29.8	3.4	0.011
NDE10	N227D + E10 loop	Not expressed						
NEE3	N227E + E3 loop	9	-12.4	2	1.66E-09	25.1	0.8	0.13
NEE5	N227E + E5 loop	8	-28	1.7	2.49E-11	23	0.9	0.09
NEE10	N227E + E10 loop	Not expressed						
NDE4K	N227D + E4K loop	7	19	1.4	0.001	25.1	1.1	2.0E-04
NDE9K	N227D + E9K loop	Not expressed						
NEE4K	N227E + E4K loop	4	-8.2	0.9	3.2E-09	22	0.9	0.007
NEE9K	N227E + E9K loop	Not expressed						
NDK278A	N227D + K278A loop	9	10.7	1.5	4.2E-07	21.7	0.7	0.00021
NDK278D	N227D + K278D loop	9	7.2	0.5	4.7E-15	22.1	0.2	1.1E-06
NDK278E	N227D + K278E loop	8	9.8	0.9	1.7E-10	23	1.4	0.006
NDK278G	N227D + K278G loop	9	3.5	1.5	7.5E-09	20.7	0.6	0.0006
NDK278N	N227D + K278N loop	9	15.2	0.4	1.7E-10	20.2	0.4	0.001
NDK278Q	N227D + K278Q loop	9	8.4	0.9	1.6E-11	23.2	0.6	6.3E-07
NDK278S	N227D + K278S loop	8	8.6	0.9	1.8E-10	22.3	0.4	1.2E-06
NEK278A	N227E + K278A loop	5	-29.3	1.6	2.9E-08	22.6	1.4	0.017
NEK278D	N227E + K278D loop	9	-27.5	1.4	3.2E-14	33.2	4.1	0.004
NEK278E	N227E + K278E loop	9	-26.1	3.2	5.7E-08	42.3	3.7	0.0002
NEK278G	N227E + K278G loop	9	-36.3	1.5	3.2E-14	24.4	2.3	0.03
NEK278N	N227E + K278N loop	9	-23.7	2	1.2E-10	25	1.6	0.001
NEK278Q	N227E + K278Q loop	9	-22.3	1.7	3.1E-13	27	2	0.001
NEK278S	N227E + K278S loop	9	-25.3	2.3	1.5E-08	27	1.8	0.0006

The V_{50} values of the E3 (+26.7 mV, p =0.9) and the E5 (+23.4mV, p = 0.13) loop mutants are not significantly different from the wild type jShak1, but are more negative than the other mutant channels with neutral (G and S) synthetic loops (Table-4.1). This effect of the negatively charged loops in stabilizing the relative open state over the neutral residues indicates a possible electrostatic effect on the loop, caused by the jShak1 channel that contributes to set the V_{50} of the channel. E10 homo-loops in jShak1 did not produce a functional channel.

Glycine loops in mouse $K_v1.2$ background tend to shift channel V_{50} to more positive values with increasing loop length (Fig-3.9) (Sand et al., 2013). In jShak1, the longer glycine loops show less positive V_{50} values than the shorter glycine loops. The V_{50} values of the G3 (+45.7mV), G5 (+34.1mV) and G10 (+31.8mV) loop-mutants clearly indicate the effect of increasing length of glycine loops in stabilizing the relative open state of the channel.

Unlike mouse $K_v1.2$, the synthetic loops in a jShak1 background have shown a small but clear effect of increasing loop length in shifting the V_{50} to more negative values (Fig-4.2A). Mouse $K_v1.2$ and jShak1 are evolutionarily divergent. The whole channel sequence of jShak1 possesses only 44% identity and 64% similarity with mouse $K_v1.2$. The VSDs (helices S1-S4) of these two channels share 30% identity and 59% similarity in their protein sequence. From the comparative results of homo-polymeric loops in mouse $K_v1.2$ and jShak1 background I infer that similar loop sequences interact differently with the rest of

89

the channel, leading to different effects on V_{50} in jShak1 and mouse $K_v1.2$. Our previous studies presented in Sand et al., (2013) showed that the length effect of synthetic loops in mouse $K_v1.2$ reached a maximum at around 5 to 8aa depending on the loop composition (Sand et al., 2013). In jShak1, the longer loops (S10 and G10) fail to make the V_{50} more negative than the wild-type loop, which is naturally 5 aa long. I propose that the natural S3-S4 linker of jShak1 is adapted to allow the complete transition of the S4 helix across the membrane in response to change in voltage. Short loops of 3aa constrain the movement of the S4 helix, similar to what was observed in mouse $K_v1.2$ (chapter 3). The 10aa loops being longer than the natural length of jShak1 S3-S4 loop, allow complete transition of the S4 helix. However, the additional flexibility in the movement of the S4 helix, fail to shift the V_{50} more negative to the wild type channel, as jShak1 is adapted to mediate the complete transition of the S4 helix using a short 5aa long loop. The Boltzmann slope factor of the fitted G-V curves, b, a rough measure of the steepness of the voltage dependence, do not differ greatly between wild type and loop variants, except for E5 (Fig-4.2B).

In summary, the overall results of the synthetic homo-polymeric loops suggest that the extremely short 3 aa long loops make the channel opening energetically unfavourable in both mouse $K_v1.2$ and jShak1, probably by causing an energetic constraint on the movement of the S4 helix. The longer homo-polymeric loops of the same length and composition affect V_{50} differently in mouse $K_v1.2$ and jShak1, indicating possible interactions between the loop and the channel.

K278 mutations in a WT background significantly affect V_{50}

Homo-polymeric loops affect the voltage sensitivity differently in jShak1 and in mouse $K_v1.2$. One possible explanation for this difference is that the interactions between the loop and the rest of the channel that affect the voltage sensitivity are qualitatively different in the two channels. The results from the negatively charged E3 and E5 loops in jShak1 suggest involvement of charged residues in this interaction. The natural loop sequence of jShak1 (VSSSK) is serine rich, having a neutral valine in the N-terminus and a positively charged lysine in the C-terminus of the loop. The C-terminus of the S3-S4 linker is proposed to interact with the negatively charged residue of the VSD and the PD turret during channel closing in $K_v1.2$ (Jensen et al., 2012). In our previous study, changing the C-terminal segment of the loop is shown to affect the V_{50} in mouse $K_v1.2$ (Sand et al., 2013). The C-terminal residue of the S3-S4 linker of jShak1 is lysine (K), whereas in mouse $K_v1.2$ it is a neutral alanine (A). The PD turret of jShak1 is also different from that of mouse $K_v1.2$, where two of the four negatively charged residues in mouse $K_v1.2$ are replaced by positively charged K and neutral G in jShak1 (Fig-4.1C).

The results from the homo-polymeric loop mutants in jShak1 suggest a possible interaction between the C-terminal lysine (K278) of jShak1 and the PD turret in the closed state, similar to what was observed in mouse $K_v1.2$ (Chapter 3 and Sand et al., 2013). To test this assumption, K278 mutants are made by replacing the C-terminal K of the jShak1 loop by S, G, A, N, Q, D and E. The negatively

charged residues (D, E) at the C-terminus of the loop significantly shift the V_{50} to less positive values (Fig-4.3A). The largest left shift in the V_{50} value is caused by the K278E mutant (V_{50} = +16.3mV, p = 1.6E-03). The K278D (V_{50} = +17.5mV, p = 9.2E-06) and the K278G (V_{50} = + 20mV, p = 6E-06) mutants also shift the V_{50} to significantly less positive values compared to the wild type channel (Fig-4.3A, Table-1). The K278A (V_{50} = +32.4 mV, p = 7E-06) loop on the other hand significantly shifts the V_{50} of the channel to a more positive value (Fig-4.3A). Other K278 mutants fail to show any substantial difference in the V_{50} values compared to the wild-type channel. Changes in slope factors are found for K278A, K278G, K278N and K278D (Fig-4.3B).

I have made a homology model of the closed state of jShak1 showing the relative position of K278 from one subunit and the PD turret (E338, K340, E341, G343) from the adjacent subunit (Fig-4.4A). Compared to the open state model of the channel (Fig-4.4B), K278 is located closer to the negatively charged PD turret in closed state. According to Jensen et al. when the C-terminus is pulled in between VSD and PD turret, it becomes exposed to interaction with both the VSD and the PD turret. From the homology model (Fig-4.4A) two residues that appear to have the most potential to interact with the C-terminus of jShak1 are D260 of the S3 helix and E338 of the PD turret (Fig4.4A). However, E338 is found closer to K278 (distance measured 9.4Å) compared to D260 (distance from K278 is 14.3Å).
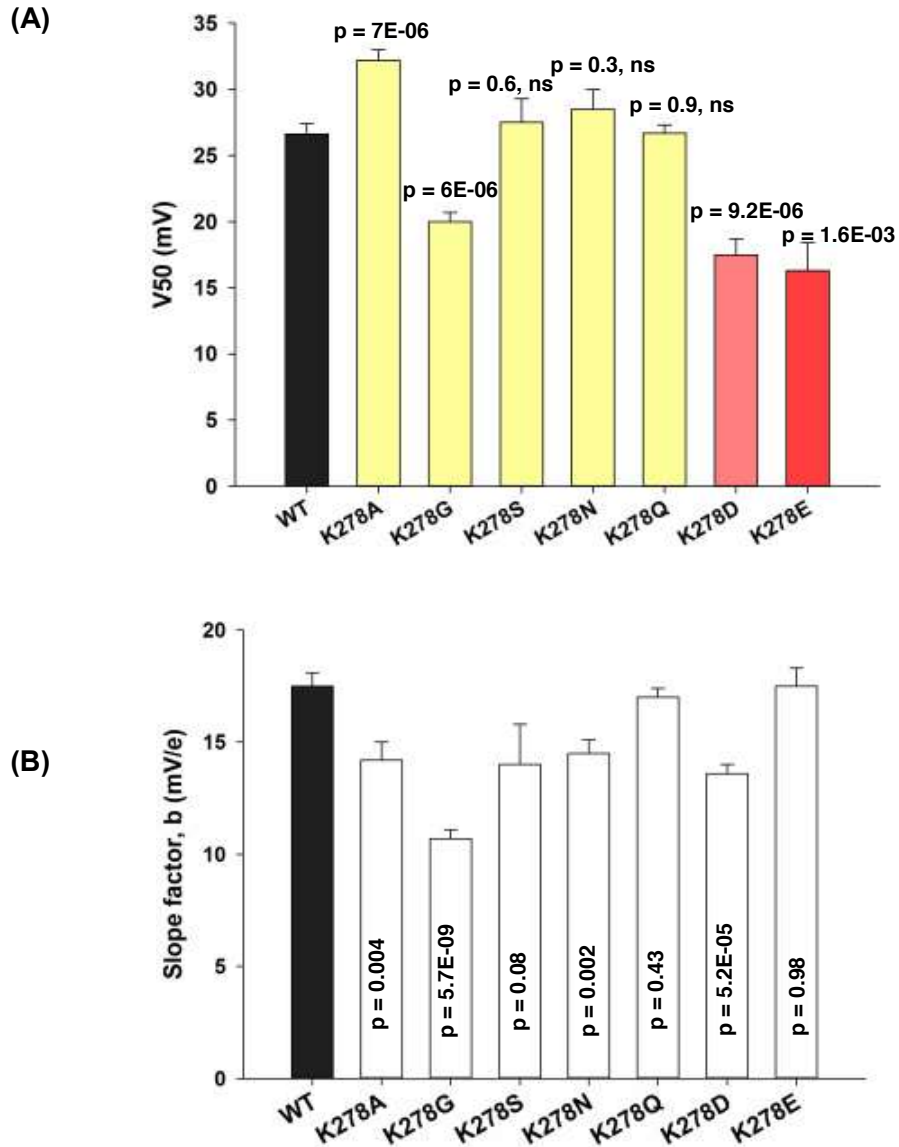
Figure 4.3: Voltage of half activation (V_{50}) (A) and Boltzmann slope factor, b (B) of K278 single mutants. Single mutations were made by replacing the C-terminus residue, K278 of S3-S4 loop. Current recording and data analysis procedure is same as described in Fig-4.2. Error bars represent s.e.m. p values were calculated from 2-tailed *t*-test and indicate the significance of difference from the wild-type channel. 'ns' stands for 'not significant.' Colours of the bars have no significant meaning.
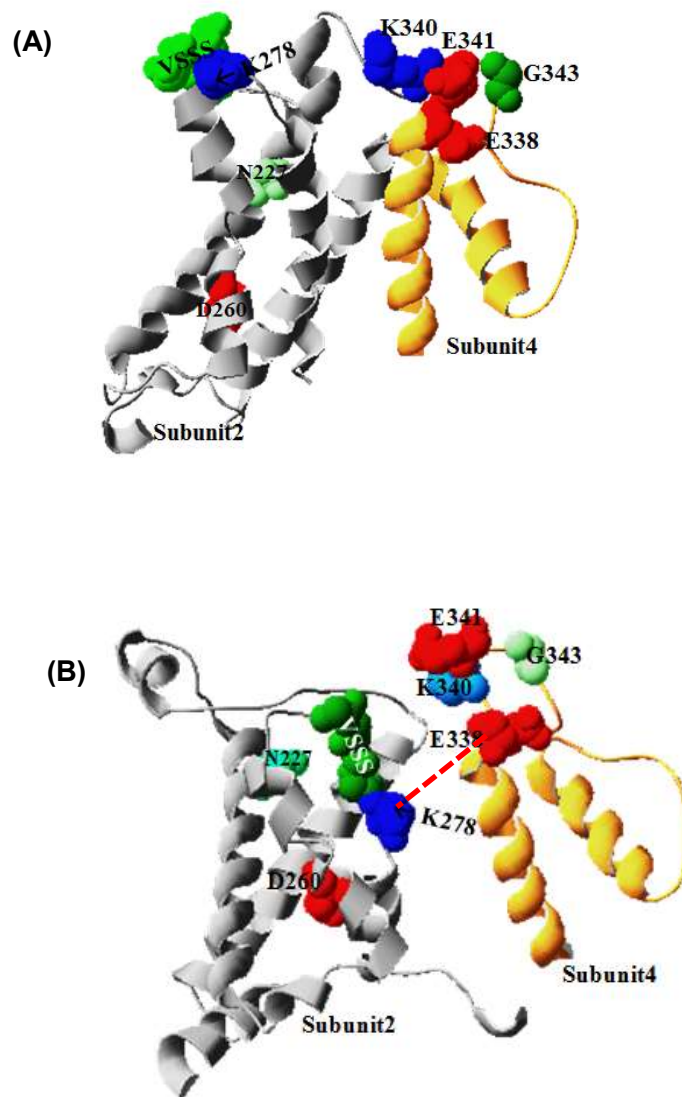
Figure 4.4: Homology model of jShak1 in open (A) and closed state (B). The open state model is made in SWISS MODEL using 3LUT, the crystal structure of rat $K_v1.2$ (Chen et al., 2010) as template. The close state model is made using the inferred closed state model of Jensen et al., (2012) as template. In the closed state model (B), the C terminal K278 is pulled closer to the negatively charged residues of the PD turret and the D260 of the S3 helix. The distance between K278 and E338 of the PD turret is measured as 9.4Å and the distance between D260 and K278 is found as14.3 Å. Possible electrostatic interaction between K278 and E338 in the wild type channel is shown in red dots.

I infer from the electrophysiology data and the homology model that K278 of the S3-S4 linker interacts with E338 of the PD turret, making an electrostatic contribution to stabilize the closed state of jShak1. For the K278E and K278D mutants, the presence of E and D at position 278 repels E338 and destabilizes the closed state. The destabilization of the closed state ultimately leads to an ease of channel opening and shifts the V_{50} more negative than the wild-type channel.

In K278G, the glycine residue with no side chain can shift the V_{50} more negative compared to the wild type channel either (i) by providing with more structural flexibility to the C-terminal region, allowing it to interact with some region of the channel, otherwise inaccessible by the loop; or (ii) by avoiding electrostatic interactions with E338 of the PD turret, making the channel opening easier than the wild-type channel.

The K278A mutant channel with a small neutral residue at 278 position shifts the V_{50} value more positive than the wild-type channel (Fig-4.3A). Since the alanine side chain is unlikely to interact significantly with an environment that interacts with acidic side-chains, I propose that the effect of alanine may be mediated through effects on backbone conformation rather than inter-residue interactions.

The C-terminal residue is a neutral alanine in mouse $K_v1.2$, but a positively charged lysine in jShak1. Two of the negatively charged residues of the PD turret

of mouse $K_v1.2$ are replaced by lysine and glycine in jShak1 (Fig-4.1). Besides these sequence variations, my results indicate an electrostatic effect on the C-terminal region of the jShak1 S3-S4 loop, similar to what was observed in mouse $K_v1.2$ in our previous study (Sand et al., 2013). The results suggest that jShak1, with a positively charged lysine at 278, stabilizes the closed state, probably by interacting with E338 of the PD turret. Glycine at 278 (K278G mutant) either fails to mediate interactions with the PD turret, or interacts with some region of the channel, not accessible by larger amino acids causing a left-ward shift of the V_{50} compared to the wild-type channel. The K278D and K278E mutants mediate repulsive interaction between D/E at 278 and the negatively charged E338 of the PD turret. This repulsive interaction destabilizes the closed state and makes the V_{50} of K278D/E more negative than both wild-type and K278G.

Hetero-polymeric loops illustrate two possible interactions between the S3-S4 linker and the channel that contributes to set the V_{50} of jShak1

Hetero-polymeric loops are made by replacing the C-terminal residue of the homo-loops with lysine (K), the natural sequence at the C-terminus of jShak1 S3-S4 linker. To evaluate the effect of the N-terminal region of the jShak1 S3-S4 loop in voltage sensitivity of the channel, I have compared the V_{50} values between S4K, G4K and E4K hetero-loop channels, which varied from each other only in the N-terminal regions (Fig-4.5A). The V_{50} value of G4K is more positive than the V_{50} value of S4K (p = 0.007), suggesting that serine residues in the N-

terminus of the loop can stabilize the open state (or destabilize the closed state) compared to glycine in that region.

Comparison between the homo-polymeric and hetero-polymeric loops show no significant differences between the V_{50} values of the G4K and G5 (p = 0.8); G9K and G10 (p = 0.07); E4K and E5 (p = 0.03) and S9K and S10 (p = 0.9) mutant channels (Fig-4.5A).   From this comparison the charge-charge interaction between the C-terminal region of the loop and the rest of the channel appears to have no significant contribution in setting the V_{50} in jShak1. This finding conflicts with my previous results with jShak1 K278 (C-terminal region) mutants. Whereas the K278 mutations on the wild type jShak1 background show significant effect of the C-terminal region in voltages sensitivity, the hetero-polymeric loops with a C-terminal K in homo-loop background fail to show any significant effect on V_{50} values of G4K, G9K and S9K, compared to the respective homo-loop channels. For example a K to G mutation in the wild type loop context shows a significant left shift (p = 6E-06) in the V_{50} of K278G mutant compared to the wild type channel. However, the same K to G change in glycine loop context fails of show any significant change in the V_{50} values of G4K and G5 loop mutants (Fig-4.5A). To understand the varying role of the C-terminal lysine in different loop context, I compared the V_{50} values of the homo- and hetero-polymeric loop channels with the respective K278 mutants (mutations made at the C-terminus of the wild type jShak1 channel) and wild type jShak1(Fig-4.5A).
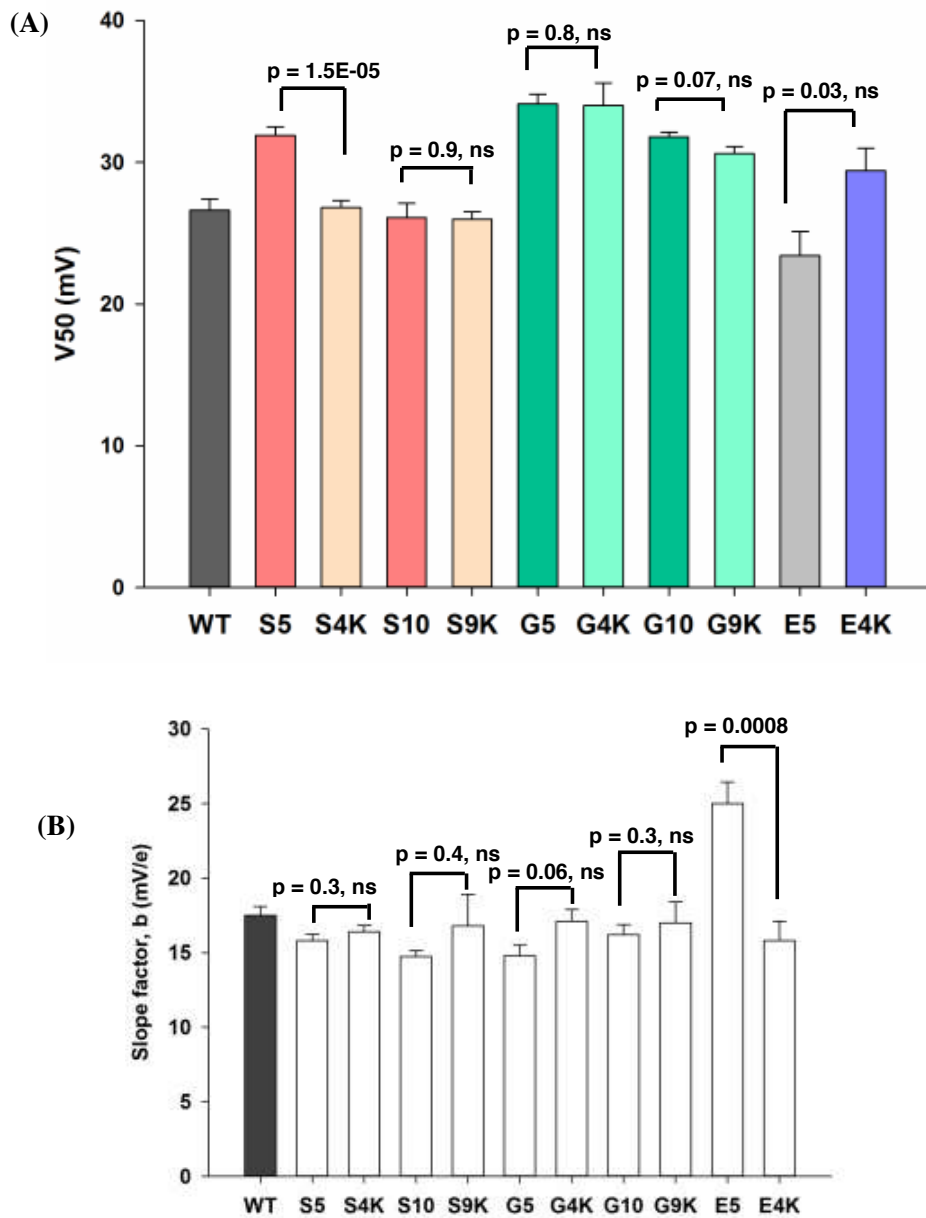
Figure 4.5: V_{50} values (A) and slope factor (B) are compared between the homo and hetero-loops. Hetero-loop mutants are made by replacing the C-terminus of the homoloops with K, which is the naturally occurring sequence in jShak1. Current recording and data analysis procedure is same as described in Fig-4.2 and also in chapter 2. Error bars represent s.e.m. p values were calculated from 2-tailed *t*-test. In this graph, p values mentioned on the bar indicate the significance of difference between the two channels compared. The significances of difference from the wild type channel are mentioned in table 4.1. 'ns' means 'not significant'. Colours of the bars have no significant meaning.

The wild type channel (loop = VSSSK, V_{50} = + 26.6mV) and S4K loop channel (SSSSK, V_{50} = +26.8mV), differ from each other only at the N-terminal valine (V274) of the loop, showing no difference in the V_{50} values. This indicates no significant difference in the effect of S and V at the N-terminus of the loop. The S9K loop (SSSSSSSSSK, V_{50} = +26 mV), with a longer length, does not have any additional effect in V_{50} of the channel (Table-4.1). The K278S mutant (VSSSS,V_{50} = +27.5mV), with only K to S changed from the wild type also fails to show any significant change in the V_{50}, from the wild type channel (p = 0.6). The S5 homoloop channel (SSSSS, V_{50} = + 31.9mV), with serine at both N and C-termini of the loop showed a large positive shift in V_{50} (p = 3.3E-05). Based on the above stated results, I speculate that the N-terminal valine (V274) acts in a co-ordinating fashion with the C-terminal region to set the V_{50} of jShak1. For this reason, the effect of the C-terminus becomes dominant only in the presence of a valine in the N-terminus of the loop. In the K278S channel the N terminal V274 co-ordinates with the C-terminal serine, contributing to set the V_{50} at +27.5mV. In the S5 loop mutant the mutation at both N and C termini of the loop disrupts the co-ordination, which in turn shifts the V_{50} more positive compared to the wild type channel. The middle region of the S3-S4 linker, which is 'SSS' remains constant in all the channels discussed above.

Comparison between the G5 (loop = GGGGG, V_{50} = +34.1mV) and G4K (GGGGK, V_{50} = +34mV) loop channels shows no difference in the V_{50} values (Fig-4.5A). I propose that, unlike wild type jShak1, the N-terminal glycine residue

of the loop either fails to mediate any interaction with the channel to stabilize the open state, or it mediates some other types of interactions to either destabilize the open state or stabilize the closed state of the channel, showing a positive shift in the V_{50} value compared to the wild type jshak1. G9K (GGGGGGGGGK, V_{50} = +30.6mV) with a longer glycine loop might help the loop to better mediate some unknown interactions to stabilizing the open state compared to G4K channel. In G5 and G4K mutants, I propose that the C-terminal effect is suppressed by the N-terminal glycine residue that fails to mediate the co-ordination with the C-terminal region as is found in wild type channel. For this, a change in K to G does not show any effect in G4K and G5 loop mutants, whereas, the same K to G change in wild type background shows significant left shift in V_{50} of K278G mutant. K278G also differs from G5 and G4K in the middle region of the loop: G5 and G4K having glycine in place of serine in the wild type channel. The three serine residues in the middle region of the wild type loop might also have a contribution in setting the V_{50} of the channel.

The homo-polymeric loop mutant channel E5 (loop = EEEEE, V_{50} = +23.4mV) shift the V_{50} more negative compared to the E4K channel (EEEEK, V_{50} = +29.4mV) (Fig-4.5A), which further indicates an electrostatic effect on the C-terminus of the loop, possibly caused by the PD turret (Fig-4.4B). The N-terminal regions of both E4K and E5 channels are negatively charged E. However, the homology model shows that the N-terminal region of the jShak1 S3-S4 linker is exposed to an area with least possibility of having an electrostatic interaction in

the open state (Fig-4.4). I propose that replacement of N-terminal V274 with E in E5 and E4K mutants disrupts the co-ordination between the N and C-termini of the loop. The middle region of the loop (EEE) also fails to mediate any significant interaction with the rest of the channel, for which reason, E4K and E5 do not show any significant difference in V_{50} values compared to the wild type jShak1. Comparing E5 with K278E channel (VSSSE, V_{50} = +16mV), I suggest that in K278E, the N terminal V mediates a coordination with the C-terminus, expressing the electrostatic effect of E in the C-terminal region. The absence of V274 in the E5 loop disrupts the coordination, suppressing the effect of C-terminal E and in turn resulting a V_{50} more positive than K278E. No significant change is observed in the slope factor (b) values of the hetero-loop mutants (Fig-4.5B).

I summarize that the S3-S4 linker in jShak1 can mediate at least two types of interactions with the channel that contribute to set the V_{50} value: (i) The C-terminal region (K278) mediates a charge-charge interaction with the PD turret, stabilizing the closed state in the wild type channel. (ii) Either the complete N-terminal region (VSSS) or only the middle region (SSS) of the wild type loop mediates an interaction with the channel to stabilize the open state. Based on the results I suggest a possible coordination between the N-terminal valine (V274) and the C-terminal region of the S3-S4 loop that is necessary for the expression of the C-terminal effect. For this reason, although the C-terminal mutations show dominant effects in wild type background in K278 mutants, they fail to cause any significant change in V_{50} in the hetero-loop mutants, where the N-terminal valine

(V274) is mutated. In the hetero-loop channels the change in the N-terminal region changes the natural co-ordination between the N and C termini of the loop, suppressing the effect of the C-terminal region.

N227 and homo-loop Double mutants showed a strong effect of salt-bridge between S2 and S4 helix in setting the V_{50} of jShak1

The negatively charged residues of the S2 and S3 helices form salt-bridges with positively charged residues of the S4 helix to stabilize the open state (Lee et al., 2005; Long et al., 2005 and Papazian et al., 1995). Mutagenesis studies with jShak1 by Klassen et al., (2008) have shown that both N227D and N227E mutations in the S2 helix can stabilize the open state. I have made double mutant channels by combining N227D/E with homo polymeric loops to analyse how the interaction between S2 and S4 helices in jShak1 is affected by the S3-S4 loop length and composition.

Both N227D (V_{50} = +13.7mV, p = 1.5E-09) and N227E (V_{50} = -15.7mV, p = 1.1E-05) single mutants stabilize the open state compared to the wild-type channel, with N227E being more effective than N227D (Fig-4.6), similar to what was reported by Klassen et al., (2008). The negatively charged residue in the S2 helix is thought to form a salt bridge with the positively charged residues of the S4 helix (Klassen et al., 2008). Glutamic acid (E) has a longer side chain than
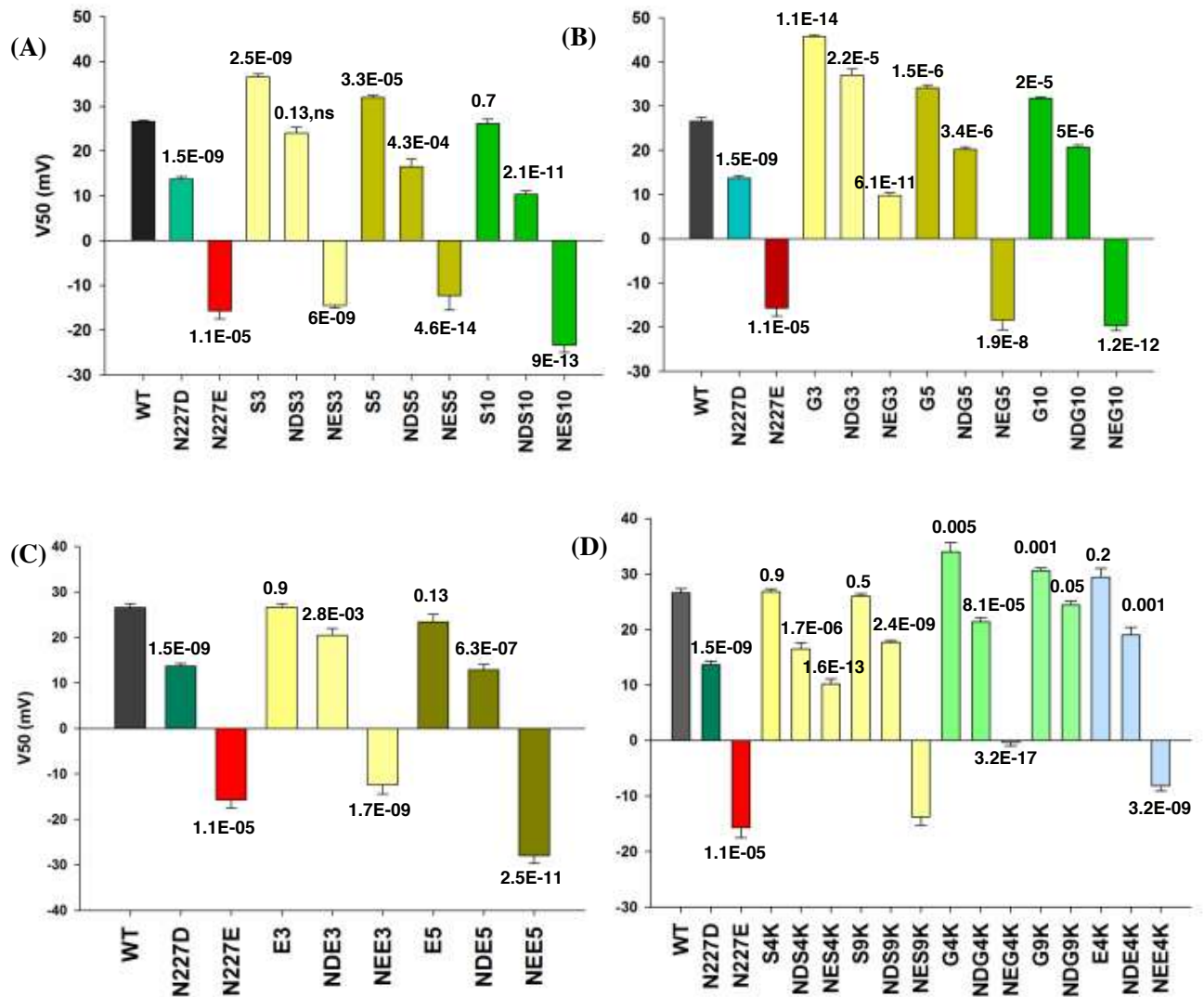
Figure 4.6: V_{50} values of double mutant channels made by combining N227D/E with S-series (A), G-series (B), E-series (C) and hetero-loops (D). jShak1 WT is shown in black bar.N227D and N227E single mutants are represented by blue and red bars respectively. The method used to calculate V_{50} in described in Fig-4.2 and also in chapter 2. Error bars represent s.e.m. p values were calculated from 2-tailed *t*-test and indicate the significance of difference from the wild-type channel. Colours of the bars have no significant meaning.

103

aspartic acid (D). If the S2 and S4 helices are constrained in position, then the longer side chain of E can arguably stabilize the open state more compared to D, if the distance between the E and R side chains is closer to the minimum energy distance than the D and R side chains can be.

The double mutation between N227D and the S3 loop, NDS3, shows a V_{50} (+24mV) somewhat in the middle of N227D (+13mV) and S3 loop (+36.5mV) mutants (Fig-4.6A, Table-4.1). Similarly the V_{50} of NDS5 (V_{50} = +16.5mV) is less positive (p = 3.7E-05) compared to the S5 loop (V_{50} = +31.9mV) but is not significantly different (p = 0.2) from the N227D single mutant. However, double mutation of the longest synthetic loop S10 and N227D, NDS10, shifts the V_{50} significantly left-ward compared to both S10 and N227D single mutant (Fig-4.6A). The results indicate that D at 227 can stabilize the open state more when combined with longer serine-homoloops compared to when combined with shorter serine-homoloops. I interpret that the V_{50} values observed in these double mutants are a combined effect of (i) a possible salt-bridge formation between the S2 and S4 helix at open state, (ii) the length effect of the synthetic serine loops and (iii) the effect of loop composition, including the C-terminal effect, the N-terminal effect and a coordination between the N and C termini of the S3-S4 loop.

The short S3 loop constrains the movement of the S4 helix, which results in a more positive V_{50} value for NDS3 compared to NDS5 and NDS10 (Fig-4.6A). In NDS5 and NDS10 channels the movement of the S4 helix becomes less restricted

with a longer S3-S4 linker, allowing the charged residues to come closer to each other, which leads to a more stable salt-bridge formation in the open state. The different interactions of the N and C-termini of the loop with the channel also contribute in setting the V_{50} values of these double mutant channels.

Similar to N227D and serine loop double mutants, double mutations between N227E and serine loops tend to stabilize the open state more with increasing loop length. The double mutant channels NES3 (-14.5 mV), NES5 (-8.5 mV) and NES10 (-20.4 mV) show an effect of increasing loop length in relatively stabilizing the open state (Fig-4.6A). The V_{50} values of NES3, NES5 and NES10 are significantly less positive compared to NDS3 (+24mV), NDS5 (+16.5mV) and NDS10 (+10.3 mV) respectively (Fig-4.6A). This indicates that besides the effect of the S3-S4 loop length and composition, the side-chain length of the negatively charged residue at 227 is also important for the proper interaction between the S2 and S4 helices and thus stabilizing the open state of jShak1. Glutamic acid (E) with a side chain longer than aspartic acid (D), allows the carboxylate group to be closer to the positively charged residues of the S4 helix, forming a more stable salt bridge and thus stabilizing the open state more, compared to D.

The results of the double mutations of N227D/E with glycine loops differ from the results of the double mutants with serine loop series showing no significant differences in 5aa and 10aa long loops in double mutant channels (Fig-4.6B). Although NDG5 (V_{50} = +20.2 mV), a double mutation between N227D and G5

loop, shifted the V_{50} more negative (p = 3.8E-07) than NDG3 (V_{50} = +37 mV), there is no significant difference (p = 0.6) between the V_{50} values of NDG5 (V_{50} = +20.2 mV) and NDG10 (V_{50} = +20.7 mV) (Fig-4.6B). This observation is also true for double mutations between N227E and glycine-loops (Fig-4.6B).

From the results of N227D/E and glycine loop double mutants I suggest that glycine, having no side chain, fails to meditate any significant interactions with the channel. So, for glycine loops, the length effect is the only governing factor. In double mutants with short 3aa loops (NDG3 and NEG3), the interaction between N227D/E and the S4 helix is restricted by the loop length. In the double mutant channels with 5 and 10aa long loops, the energetic constraints in interaction between the S2 and S4 helices are removed. Based on my previous results of homo-polymeric loops, I proposed that the 5aa long natural loop in jShak1 is adapted to allow the complete transition of the S4 helix across the membrane electric field in response to voltage change. In NDG5 and NEG5 channels, I suppose that the complete transition of the S4 helix is achieved by the G5 loop. For NDG10 and NEG10 mutants, the G10 loop fails to mediate any interaction with the channel to affect V_{50} and cannot affect the stability of the salt-bridge, as the complete transition is attained by the G5 loop. For this reason, no significant differences are observed between the V_{50} values of NDG5 and NDG10 (p = 0.6) and also between NEG5 and NEG10 (p = 0.7).

A dramatic negative shift in V_{50} values are found for N227D/E double mutants with E3 and E5 (Fig-4.6C, Table-4.1). The V_{50} value of the NDE3 (+20.5 mV) is more depolarized than NDE5 (+12.9mV) and the V_{50} value of NEE3 (-12.4mV) is more right-shifted than NEE5 (-28mV) (Fig-4.6C). Similar to all other double mutants, the V_{50} values of these double mutants are affected by salt-bridging between the S2 and S4 helices and the length and composition of the S3-S4 loop. In NDE3 mutant, the interaction between N227D and the positively charged residues of the S4 helix is constrained by the short E3 loop. However the C-terminus of the E3 loop mediates a repulsive interaction with the negatively charged PD turret to destabilize the closed state, which makes the V_{50} of NDE3 more negative than both NDS3 and NDG3. In NEE3 channel, E3 loop mediates similar interaction with the channel as in NDE3. However, in NEE3, the presence of E at 227 position of S2 helix makes a more stable salt-bridge between the S2 and S4 helices compared to D at 227. In NDE5 and NEE5 mutants E5 loop allows a complete transition of the S4 helix that is optimum for stable salt-bridge formation between the S2 and S4 helices. The C-terminus of the E5 loop also mediates repulsive interactions with PD turret, destabilizing the closed state. All these interactions in turn help to shift the V_{50} values of NDE5 and NEE5 more negative compared to NDE3 and NEE3 respectively. As the E10 loop mutants failed to produced functional channels, comparison between 5 aa long and 10 aa long E chains were not possible.

In order to understand the effect of the N-terminal region of the loop in the electrostatic interaction between the S2 and S4 helices, I have compared the V_{50} values between NDS4K (+16mV), NDG4K (+21.4mV) and NDE4K (+19mV), which differ from each other only in the N-terminus of the loop. Serine residues in the N-terminus are found to stabilize the relative open state of the channel compared to glycine and glutamic acid. Similarly, the V_{50} values of NES4K (-10.2mV), NEG4K (-0.3mV) and NEE4K (-8.2mV) suggest that serine at the N-terminus of the loop has a more stabilizing effect on the relative open state of the channel compared to E and G. Longer S9K loop fail to show any major shift in V_{50} values compared to the shorter S4K hetero loops. Both the serine and glutamic acid heteroloops show a change in slope factor, b (Table-4.1).

The overall results of the double mutants indicate that the presence of a negatively charged residue at 227 position can stabilize the open state by interacting with the positively charged residues of the S4 helix as was previously shown by Klassen et al., (2008). The longer side chain of E at 227 position allows the carboxyl group reach closer to the basic residues of the S4 helix, which causes more negative V_{50} values for N227E double mutants compared to N227D double mutants. I propose that in the double mutant channels, where N227D/E are combined with the synthetic loops, the following factors contribute in setting the voltage sensitivity of the channel: (i) the stability of the salt-bridge formed between the S2 and S4 helices, (ii) the length of the S3-S4 loop (iii) the composition effect of the S3-S4 loop, which includes different interactions of the N and C-termini of the loop with

the channel (iv) the hypothetical coordination between the N and C termini of the loop. Besides having the composition effect, the short (3aa) synthetic loops affect the V_{50} of the double mutant channels by restricting the movement of the S4 helix. Based on the results I suggest that 10aa long loops fail to cause any additional transition of the S4 helix to stabilize the open state, as the jShak1 is naturally adapted to meditate the complete transition of the S4 helix using a 5aa long natural loop. I propose that when a negatively charged residue is present at 227 position of the S2 helix, jShak1 can efficiently form a salt bridge to stabilize the open state. However the stability of the open state is limited by the side chain length of the charged residue at 227 and constrained by the short S3-S4 linker. The S3-S4 loop composition can also affect the V_{50} significantly even in the presence of a negatively charged residue at 227 position.

Double mutants of N227D/E with K278 loop affect both the V_{50} and the slope factor of the channel

I have made double mutations between the K278 mutant loops (point mutations made only at the C-terminus of the wild type loop) and N227D/E to evaluate how the nature of the C-terminus of the S3-S4 loop in jShak1 affects the electrostatic interaction between the S2 and S4 helices.

In my previous experiment with K278 single mutants, K278E (V_{50} = +16.3 mV) and K278D (V_{50} = +17.5mV) showed the most left-shift in the V_{50} values, followed by K278G (V_{50} = +20 mV) (Fig-4.3A). Interestingly, when combined

with a negatively charged residue (E and/or D) at 227 position, K278G loop shows the most negative shift in V_{50} value (e.g. NEK278G = -36.3mV, p = 3.2E-14) among all the double mutants (Fig-4.7A). The second most negative V_{50} values are from K278D and K278E loops when combined with N227E in the double mutant channels NEK278D (V_{50} = -27.5 mV, P = 3.2E-14) and NEK278E (V_{50} = -26.1mV, p = 5.7E-08) respectively (Fig-4.7A). This trend is also true for the double mutations between K278 loops and N227D (Fig-4.7A).

All the double mutant channels between the K278 loops and N227D/E show a large change in slope factor, b, compared to the wild type and the respective single mutant channels (Fig-4.7B, Table-4.1). As the slope factor is calculated from RT/zF, where z is the apparent gating charge, a change in slope factor indicates changes in the underlying mechanism of the voltage sensitivity, possibly caused by a change in gating charge (Fernández et al., 2011 and Latorre et al., 2007). The largest change in slope factor is caused by the double mutant channels made by combining N227D/E with the K278D/E loops. The slope factor (b) values tend to increase with an increase in side chain length at both C-terminus of the loop and the N227 position of the S2 helix. The previous results suggest that in jShak1, the strong effect of the C-terminus of the loop becomes dominant only with wild type loop sequence in the N-terminus. Here, the results of the double mutant channels suggest that the strong electrostatic effect of the C-terminus,

(A)

(B)
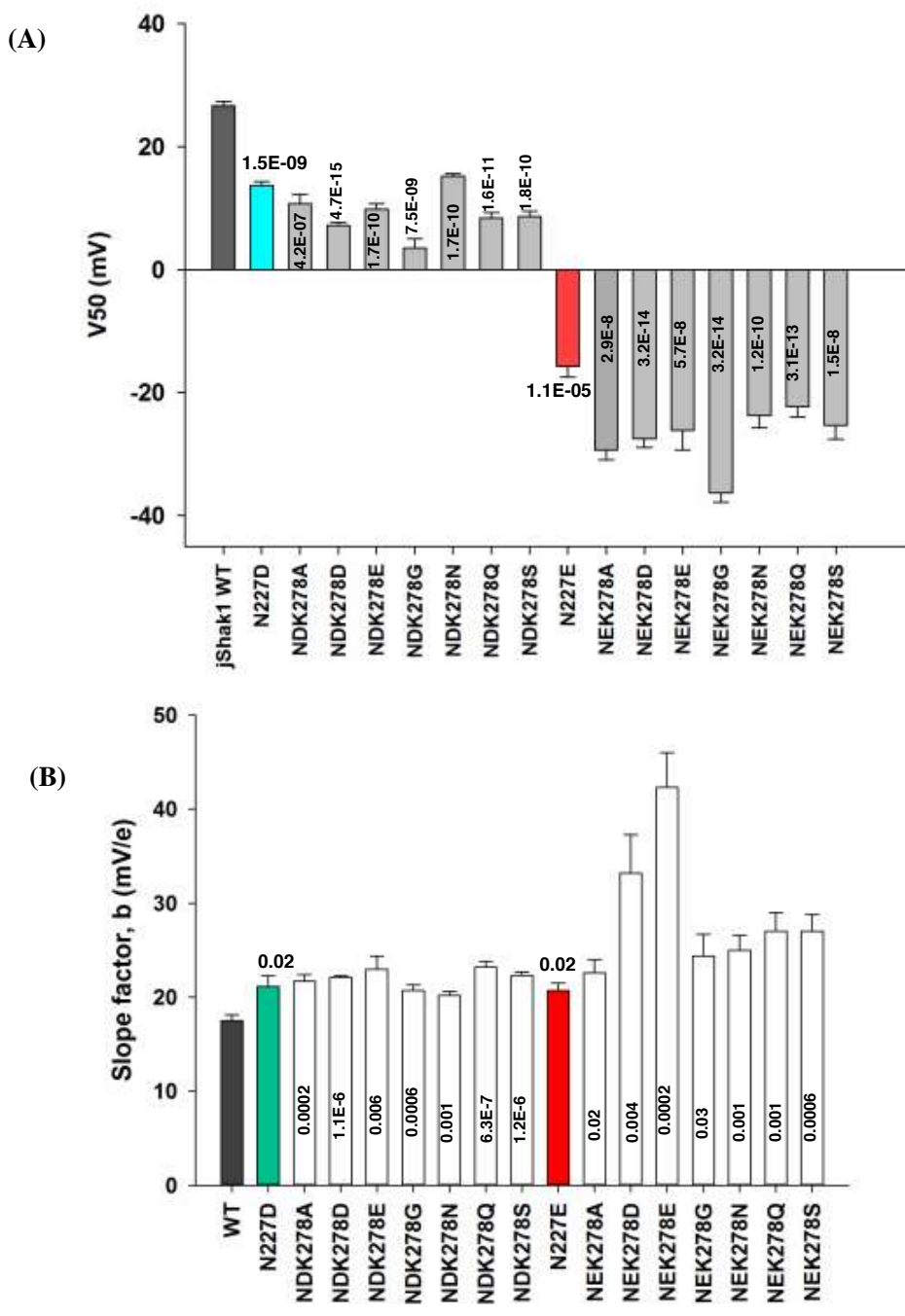
Figure 4.7: V_{50} values (A) and slope factor, b (B) of double mutant channels made by combining N227D and N227E with K278 mutant loops. jShak1 WT is shown in black bar. N227D and N227E single mutants are represented by blue and red bars respectively. The method used to calculate V_{50} in described in Fig-4.2 and also in chapter 2. Error bars represent s.e.m. p values were calculated from 2-tailed *t*-test and indicate the significance of difference from the wild-type channel. Colours of the bars have no significant meaning.

111

combined with the electrostatic effect from the N227/E can cause a change in the transition of the S4 helix (gating charge), which is evident from the large change in slope factor, b. Further studies are necessary to identify the combined electrostatic effects of the loop and the VSD. However, based on the homology model, I propose the following hypothetical model to explain the possible interactions occurring in the double mutant channels (Fig-4.8).

In the wild type jShak1 and all the other synthetic loop mutant channels, I suggest that the complete transition of the S4 helix across the membrane in response to voltage change (represented by the gating charge) is achieved by the natural S3-S4 loop. However, the double mutant channels between K278 loops and N227D/E indicate a possible change in gating charge that is represented by a change in slope factor, b. I suppose that for these double mutant channels, the combined effect of the C-terminal mutations in the loop and the D / E mutations at position 227 might cause a change in the overall transition of the S4 helix, allowing S4 helix to move closer towards the S2 helix and in turn stabilizing the relative open state of the channel (evident from the negative shift in V_{50} values).

For double mutant channels like NDK278D (D at S2 helix and D at C-terminus of the loop, $V_{50} = +7.2$ mV), the E338 of PD turret repeal the D at the C-terminus of the K278D loop, causing a destabilization of the closed state (Fig-4.8 A, C). The salt-bridge between the D227 and the S4 helix stabilizes the open state. These two
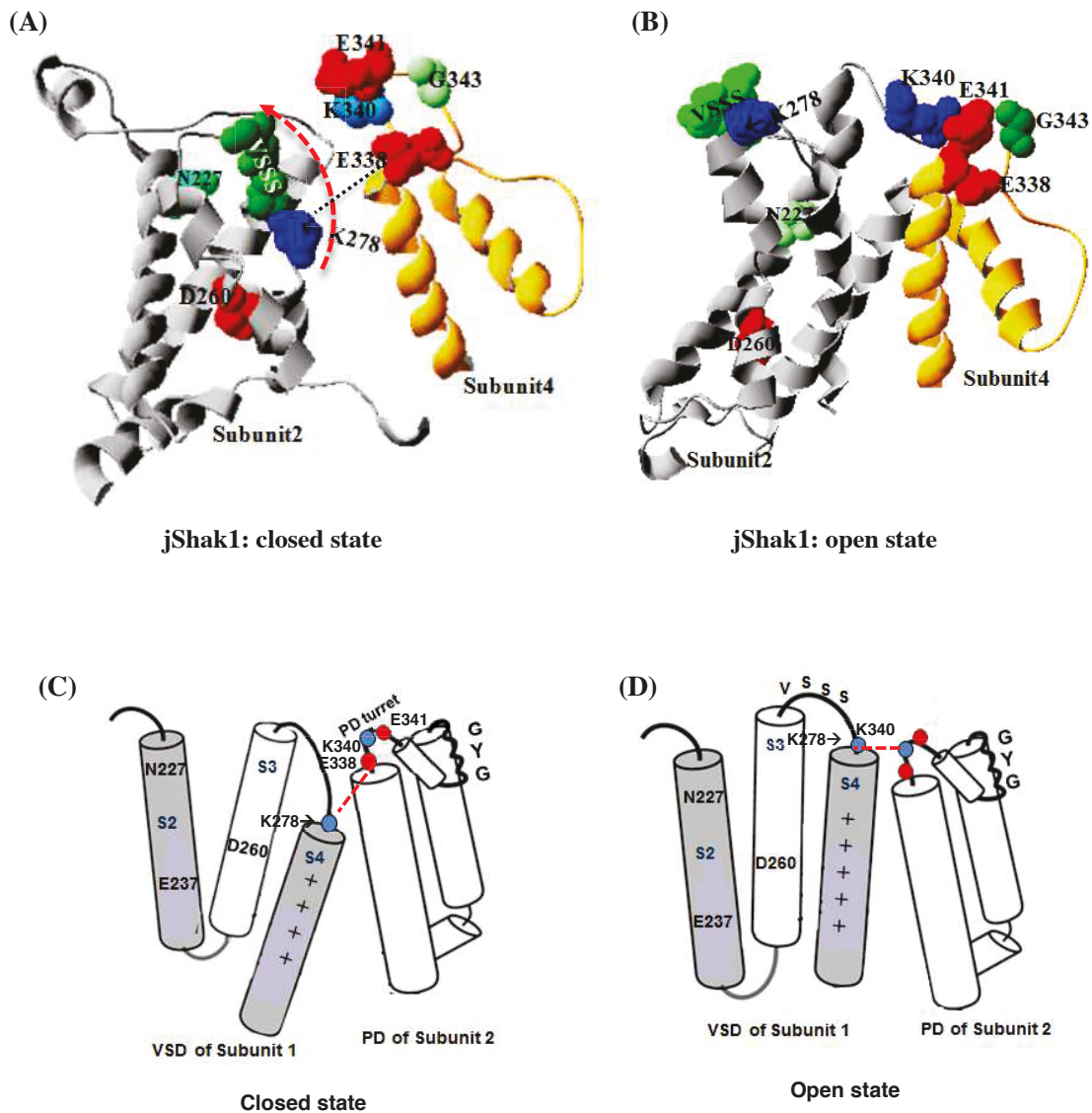
Figure 4.8: Homology model of jShak1 in closed (A) and open (B) states. Interaction between the S3-S4 loop of subunit 2 (grey) and the charged residues of the PD turret of subunit 4 (yellow) is shown here. During closed state, K278 might interact with negatively charged E338 to stabilize the closed state. The possible electrostatic interaction is shown with black dotted line (A). When the channel opens, the loop, especially K278 is moved outward with the movement of S4 helix (the possible pathway is shown in red arrow (B). In the open state K278 is found to locate away from the PD turret (B). A simpler model of the interaction is presented in (D) and (E) for closed and open state respectively.

113

combined effects drive the S4 helix more towards the S2 helix, compared to the wild type and the single mutant channels. The extensive movement of the S4 helix (change in gating charge) pulls the S3-S4 linker outward, making the C-terminus of the loop (D278) to pass by the K340 of the PD turret (Fig-4.8 B,D). During this process, D278, the C-terminal D of the loop encounters an electrostatic affect by K340, which might tend to destabilize the open state (or stabilize the closed state). Similar phenomenon is true for the double mutant channels NEK278E, NDK278E and NEK278E. Glutamic acid E has a longer side chain than D. I suppose that E at the C-terminus of the loop would mediate stronger electrostatic interaction with K340 during the channel opening process and E at 227 would mediate stronger interaction with the S4 helix. The combination between the electrostatic interactions in the VSD and the C-terminus of the loop contribute to set the V_{50} and the slope factor (b) observed in the above stated double mutant channels.

Mouse $K_v 1.2$ and most other K_v channels stabilize the open state by forming a salt bridge between the S2 and S4 helices. jShak1 is naturally evolved with a neutral N227 in the S2 helix and is adapted to stabilize the open state without forming a salt-bridge between the helices. My previous results from the homo and hetero-polymeric loops in jShak1 indicate that the N-terminal region of the wild type S3-S4 linker might interact with the channel to stabilize the open state. N227D and N227E mutagenesis show that jShak1 can efficiently form salt-bridges between the S2 and S4 helices to stabilize the open state, when a negatively charged residue is present at 227 position. The double mutations between the C-terminus-

mutated loops and N227D/E show that the electrostatic effect between the PD turret and the C-terminal region of the loop can cause a change in the slope factor, b, when combined with a negatively charged residue at 227 position. Change in slope factor, b indicates a possible change in underlying mechanism (gating charge) caused by the combined effect of the charged residue at 227 and the nature of C-terminus of the S3-S4 loop.

TEV loop mutants further illustrate a possible interaction between the loop sequence and rest of the channel

The previous results clearly indicate a possible interaction between the N-terminal region of the S3-S4 loop and the channel that affects the V_{50} significantly. Based on the results, I have also suggested that the 5aa long natural S3-S4 loop in jShak1 is adapted to allow the complete transition of the S4 helix across the membrane in response to voltage change. To further test the possible constraints caused by the loop length and the effect of loop length in the voltage sensitivity of jShak1, I have made synthetic loops by inserting single and double TEV protease cut sites (ENLYFQG) with and without C-terminal K in jShak1(Table-4.1). I cut the loops with TEV protease to remove the energetic constraint caused by the loop length. The results show that all the uncut TEV loops shift the V_{50} much more negative ($\sim$ +6 mV) than both the wild type and all the synthetic homo-loop channels (Fig-4.9). The V_{50} value of uncut long TEV loop (with 2 cut sites) are

(A)

(B)

(C)

(D)

(E)
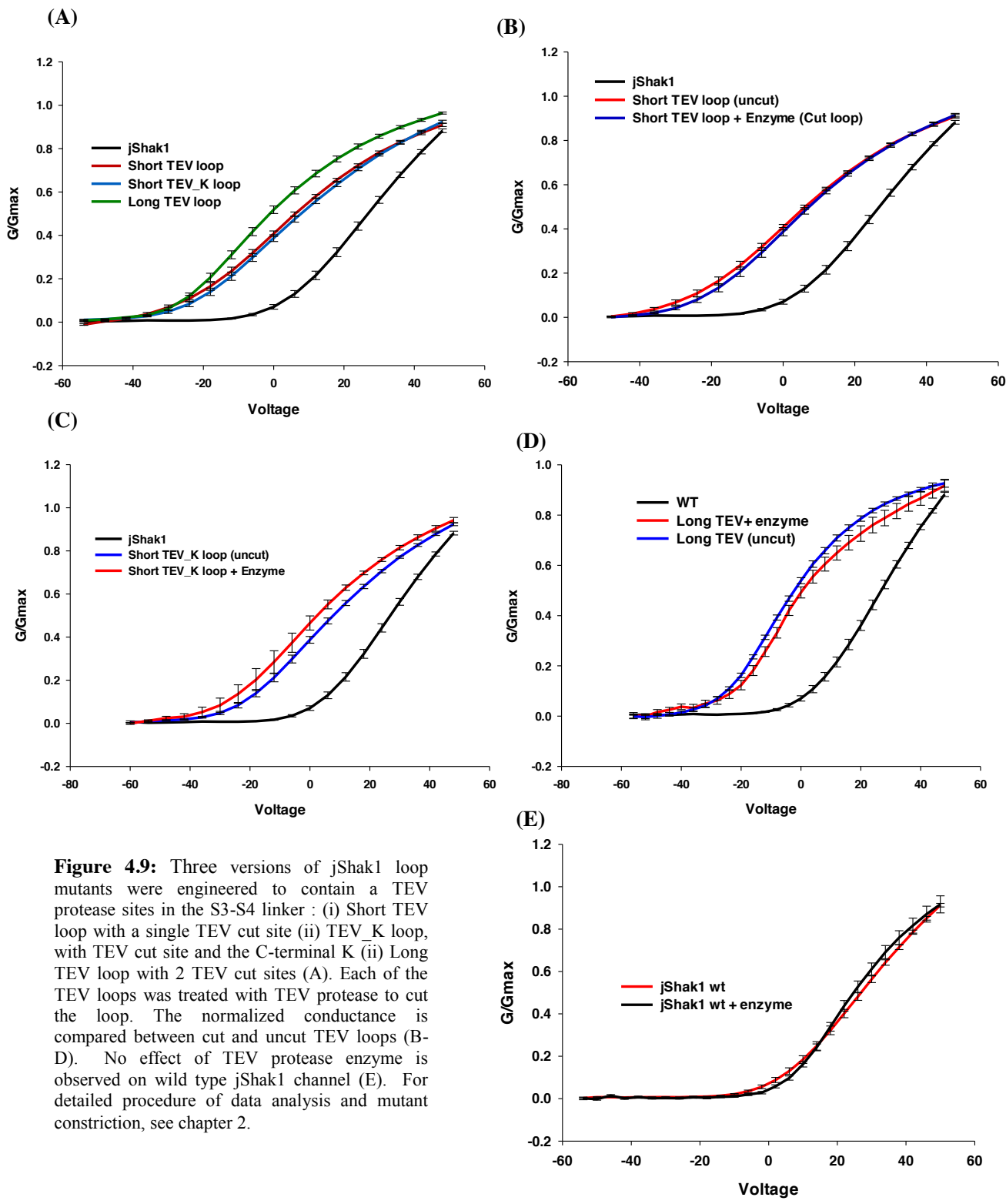
Figure 4.9: Three versions of jShak1 loop mutants were engineered to contain a TEV protease sites in the S3-S4 linker : (i) Short TEV loop with a single TEV cut site (ii) TEV_K loop, with TEV cut site and the C-terminal K (ii) Long TEV loop with 2 TEV cut sites (A). Each of the TEV loops was treated with TEV protease to cut the loop. The normalized conductance is compared between cut and uncut TEV loops (B-D). No effect of TEV protease enzyme is observed on wild type jShak1 channel (E). For detailed procedure of data analysis and mutant constriction, see chapter 2.

more negative (-2.1mV) than the uncut short TEV loops (1 cut site) (Fig-4.9A). No significant differences are found between the TEV and TEV_K loops and between the cut and uncut loops (Fig-4.9, Table-4.1). TEV loops with a single cut site (ENLYFQG, ENLYFQGK) are 7 and 8 aa long, which is longer than the natural length of S3-S4 linker of jShak1, proposed to be adapted to allow the complete transition of the S4 helix across the membrane. For this reason, I suggest that the TEV loops do not cause any energetic constraint on the movement of the S4 helix and thus cutting of the loop fails to show any effect on the V_{50} value of the channel.

The uncut TEV loops show a large negative shift in V_{50} compared to the wild type and all other loop mutant channels. I propose that the sequence of TEV cut site (ENLYFQG) in the N-terminus of the loop mediate a strong interaction with a yet to identify region of jShak1 and stabilize the relative open state of the channel. The TEV loop with double cut sites (V_{50} = - 2.1 mV) being longer in length mediates stronger interactions with the channel and shifts the V_{50} more negative compared to the short TEV loops (V_{50} = +6 mV) (Fig-4.9A). The presence and absence of C-terminal K in TEV loop mutants does not make any significant difference in the V_{50} values (Fig-4.9A, Table-4.1). My previous results suggest that the effect of the C-terminus of the S3-S4 loop in jShak1 becomes apparent only with the wild type loop sequence in the N-terminal region. In TEV loops, the

117

N-terminal sequence is also replaced, which, suppress the effect of the C-terminal K in these TEV loop mutants.

The overall results of the TEV loops in jShak1 background are different from what was observed in mouse $K_v1.2$ (Sand et al., 2013). In mouse $K_v1.2$, the TEV loop did not show any significant difference in V_{50} compared to the wild type mouse $K_v1.2$; cutting the TEV loop shifted the V_{50} more positive compared to the uncut loop (Sand et al., 2013). I suggest that unlike mouse $K_v1.2$, the S3-S4 loop of jShak1 is adapted to interact with the channel, which is a significant factor in setting the V_{50} of channel.

Conclusion

The structural basis of the voltage sensing mechanism of K_v channel is unclear. An electrostatic interaction network between the conserved acidic and basic residues of the VSD affects the V_{50} in most K_v channels. However, a wide variation in the V_{50} values within and between the K_v channel families with high sequence similarity indicates the involvement of less conserved regions in amendment of the voltage sensitivity of the channel. The S3-S4 linker is one of the regions that are highly variable in channels and is found to affect the V_{50} by constraining the movement of S4 helix (Sand et al., 2013 and Klassen et al., 2008).

With an aim to evaluate the effect of S3-S4 loop length and composition on the voltage sensitivity of jShak1, the natural 5aa long loops of jShak1 was replaced with synthetic loops, varying both in length (3, 5 and 10 aa) and composition (S, E, G). Point mutations changing the C-terminal region in both natural and homo-polymeric loop channels are also made. To study how the interaction between the S2 and the S4 helices is affected by loop length and composition, double mutants are made by combining N227D/E with all the synthetic loops. A summary of the all the mutant channels is presented in figure 4.10. I have also compared my results with mouse $K_v1.2$, which is evolutionarily divergent from jShak1.

Results from the homo-polymeric loop channels, where the length and composition of the entire loop is varied (Fig-4.10A) reveal that loops of the same length and composition affect the V_{50} differently in mouse $K_v1.2$ and in jShak1(detailed in page-80). To evaluate the effect of the C-terminal region of the loop in voltage sensitivity, K278 mutant loop channels are made, where only the C terminal K278 residue is mutated (Fig-4.10B). The results of the C-terminal mutations indicate a possible electrostatic interaction between the C-terminus and the PD turret in jShak1 (detailed in page- 87). To understand the possible contribution of the N-terminus of the S3-S4 loop, hetero-polymeric loops are made where the N-terminal region is varied, keeping the natural lysine (K278) constant at the C-terminus (Fig-4.10C). Comparison between the homo- and hetero- loops shows that the effect of the C-terminus of the loop becomes dominant only in the presence of wild type sequence (V274) at the N-terminus

(A) Homo- loop channels

Length and composition of the entire loop is varied
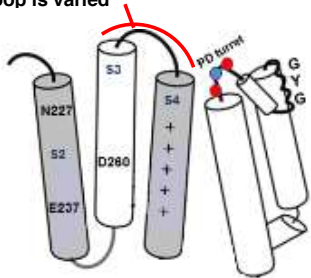
The entire loop sequence (VSSSK) is replaced with S3, S5, S10, G3, G5, G10, E3 and E5 sequence. Interaction between the C-terminus of the loop with PD turret is affected. Interaction between the N-terminal region of the loop and rest of the channel is affected. Length of the loop is changed. N at 227 of the S2 helix remains unchanged.

(B) K278 mutant channels (mutation is the C-terminus of the loop.

Point mutation at K278
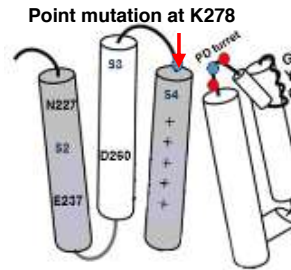
Only C-terminal K is replaced with A, N, D, E, G, S and Q. Interaction between the C-terminus of the loop with PD turret affected. Interaction between the N-terminal region of the loop and rest of the channel remains unchanged. Length of the loop is same as wild type channel. N at 227of the S2 helix remains unchanged.

(C) Hetero-loop channels

Length and composition of the N-terminus of the loop are varied
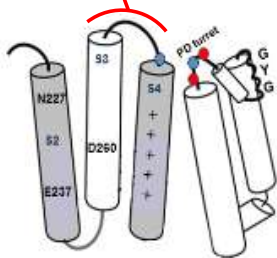
The N-terminal part of the loop sequence (VSSS) is mutated. Interaction between the C-terminus of the loop with PD turret is unaffected. Interaction between the remaining loop and rest of the channel is changed. Length of the loop is varied. N at 227of the S2 helix remains unchanged.

(D) Homo- loop double mutant channels
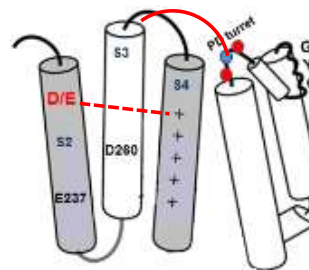
The entire loop sequence (VSSSK) is replaced with S3, S5, S10, G3, G5, G10, E3 and E5 sequence. Interaction between the C-terminus of the loop with PD turret is affected. Interaction between the N-terminus of the loop and rest of the channel is affected. N at 227 of the S2 helix is replaced with D or E, which interacts with the basic residues of the S4 helix to stabilize the open state.

(E) K278 loop double mutant channels
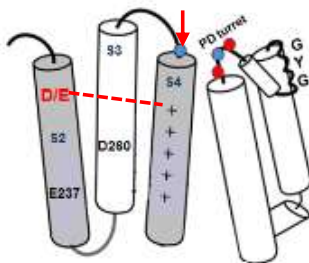
The C-terminal K is replaced with A, N, D, E, G, S and Q. Interaction between the C-terminus of the loop with PD turret is affected. Interaction between the N-terminus of the loop and rest of the channel remains unchanged. Length of the loop is same as wild type channel. N at 227of the S2 helix is replaced with D or E, which interacts with the basic residues of the S4 helix to stabilize the open state. .

(F) Hetero-loop double mutant channels
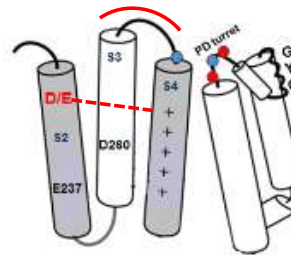
The N-terminal part of the loop sequence (VSSS) is mutated. Interaction between the C-terminus of the loop with PD turret is unaffected. Interaction between the N-terminus of the loop and the rest of the channel is changed. Length of the loop varied. N at 227of the S2 helix is replaced with D or E, which interacts with the positively charge residues of the S4 helix to stabilize the open state.

Figure 4.10: Schematic diagram of the types of mutant channels made for the study presented in chapter 4. The mutated regions are shown in red. The possible alterations caused by the mutations are summarized below each diagram.

120

(detailed in page- 92). Similar to Klassen et al., (2008), the N227D and N227E mutant channels in jShak1 shift the V_{50} values to more negative than the wild type channel, possibly by forming salt-bridge with the basic residues of the S4 helix. E at 227 can stabilize the open state more compared to D at that position. The results from the double mutant channels, made by combining N227D/E with homo- and hetero-loops (Fig-4.10D,F) indicate two possible limitations on the stable salt bridge formation: (i) the side chain length of the acidic residue at 227 and (ii) the length of the S3-S4 linker. The results from the double mutation channels between N227D/E and K278 loop (Fig-4.10E) shows that the nature of the C-terminus of the loop can affect both the V_{50} and the slope factor, when combined with a negatively charged residue at 227 position (detailed in page-105). Unlike mouse $K_v1.2$, a large negative shift in V_{50} value of the TEV loop further indicates a possible interaction between the loop and the jShak1 channel that can stabilize the relative open state and significantly contribute in setting the V_{50} of the channel.

In previous studies, the S3-S4 linker has been shown to affect the V_{50} simply by restricting the movement of the helices of the voltage sensing domain during activation (Klassen et al., 2008 and Gonzalez et al., 2000). My results from jShak1 and its comparison with mouse $K_v1.2$ clearly indicate that the loop sequence interacts with the rest of the channel and is not only a passive tether restricting the dynamics of the S4 helix. Based on my studies presented in chapter 4, I propose that the S3-S4 loop in jShak1 affects the V_{50} in the following ways:

(i) the loop length constrains the transition of the S4 helix across the membrane and its interaction with the S2 helix; (ii) the N-terminal region of the wild type loop (VSSS) interacts with the channel to stabilize the relative open state; (iii) the C-terminus mediates an electrostatic interaction with the PD turret to stabilize the closed state in the wild type channel (iv) the N and C- termini of the loop mediates a hypothetical coordination, necessary to set the V_{50} of the channel. All the proposed interactions are summarized in Fig-4.11.

Comparing the results from jShak1 and mouse $K_v1.2$ (chapter 3) I suggest that these two channels have evolved a voltage sensing mechanism that is highly divergent from each other. Mouse $K_v1.2$ carries an acidic glutamic acid at 226 position of S2 helix. Shortening the length of E by E226D mutation or neutralizing the change by E226N and E226Q mutation in mouse $K_v1.2$ produced omega current through the VSD. jShak1, on the other hand contains a naturally occurring asparagine at the respective position, with no omega current through the VSD. I suggest that the helices in the VSD of jShak1 are are more compactly packed together than the helices in mouse $K_v1.2$. For this reason, shortening and neutralizing the side-chain at position 226 in mouse $K_v1.2$ create an omega pore, whereas lengthening and adding negative charge to the side-chain at position 227 in jShak1 shift the voltage sensitivity of the channel to more negative values without changing the nature of the current.
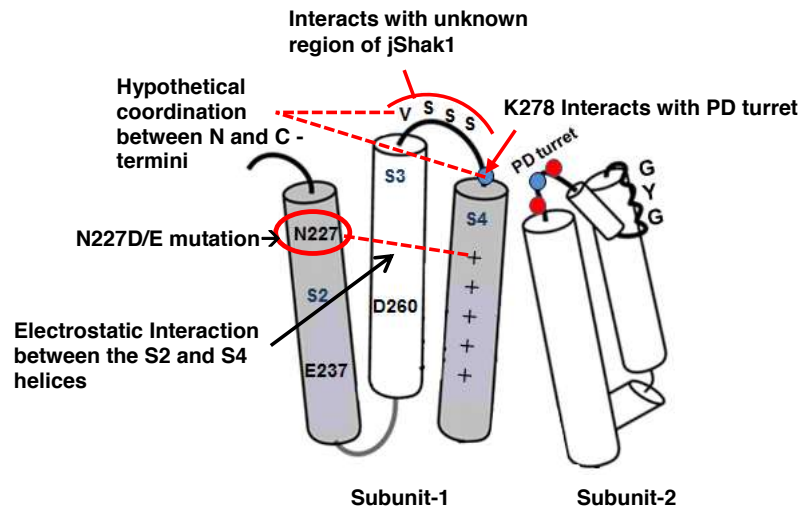
Figure 4.11: Summary of interactions in jShak1, proposed to contribute in setting the V_{50} of the channel. N-terminal region of the S3-S4 loop (VSSS) interact with the unknown part of the channel to stabilize the open state. The C-terminal region of the loop interacts with the PD turret to stabilize the closed state. The N and C-termini of the loop mediate a hypothetical coordination. In the presence of an acidic residue at 227 position, the S2 helix of jShak1 can form salt-bridges with the basic residues of the S4 helix.

Change in slope factor, b indicates change in the underlying mechanism of voltage sensitivity. Unlike mouse Kv1.2, the C-terminus-mutated (K278) loops affected the slope factor, when combined with an acidic residue at 227 position. The TEV sequence in mouse Kv1.2 background did not show any effect in V_{50} values, where as in jShak1, the TEV loop sequence shifted the V_{50} much more negative than the wild type channel. I propose that jShak1 has adapted a mechanism of stabilizing the relative open state of the channel without forming a salt-bridge between the S2 and S4 helices. However, given an acidic residue at 227 position, jShak1 can efficiently form stable salt bridge between S2 and S4 helices. The interaction between the charged residues of the S2 and S4 helices are also affected by the length and composition of the S3-S4 linker.

Chapter 5: Conclusion and General Discussion

The work presented in this thesis is focused on one of the most complex yet important aspects of K_v channels-the mechanism of voltage sensitivity. Although the charged residues that interact within the VSD to stabilize the open and the closed state are conserved in most K_v channels, the half activation voltage, V_{50} is widely varied between K_v channels with high sequence similarity. Previous studies indicated a possible role of S3-S4 linker in voltage sensitivity of K_v channels (Sand et al., 2013 and Gonzalez et al., 2001). Inter-helix loops are one of the highly variable regions of the channel. Contribution of such variable regions in setting the V_{50} of a channel indicates a possible mechanism of fine-tuning of voltage sensitivity that can vary between channel types. In this thesis the effect of S3-S4 loop length and composition on the voltage sensing mechanisms of mouse $K_v1.2$ and jellyfish K_v1 channel jShak1are compared. jShak1 and mouse $K_v1.2$ are evolutionarily highly divergent from each other and possess some differences, interesting and important for the study. In jShak1 the residue at postion 227, within the S2 helix, that is conserved as glutamate in most other K_v1 channels is replaced by neutral asparagine. jShak1 also has a S4 helix with one less positively charged motif compared to mouse $K_v1.2$ and most other K_v1 channels and a very short S3-S4 linker, consisting of only five amino acid residues. Previous studies indicated a possible constraint on the movement of the S4 helix, caused by the extremely short natural S3-S4 loop of jShak1 (Klassen et al., 2008).

125

In this study, the natural S3-S4 loop of both jShak1 and mouse $K_v1.2$ were replaced with synthetic homo-polymeric loops varying in length (3aa, 5aa, 10aa) and composition (glycine, serine, glutamic acid). To study the effect of the C-terminal region of the loop, hetero-polymeric loops were made by mutating only the C-terminal regions in both mouse and jShak1. I also mutated the E226 and N227 in the S2 helix of mouse $K_v1.2$ and jShak1 respectively to study the nature of interaction between the S2 and S4 helices. Double mutations were made in both mouse $K_v1.2$ and jShak1 by combining mutations in S2 helix with the synthetic homo and hetero-polymeric loops to evaluate how the interaction between S2 and S4 helices are affected by S3-S4 loop length and compositions in two different channel backgrounds.

From the comparative studies on two different K_v1 family members, I have found that in mouse $K_v1.2$ the 3aa long loops of serine, glycine and glutamic acid shift channel V_{50} to more positive, compared to the wild type channel. As the loop length increases, glutamic acid (E) homo-loop channels tend to shift the V_{50} leftward, the E5 loop approaching the wild type V_{50} and the E10 loop making the channel V_{50} even more hyperpolarized than the wild type mouse $K_v1.2$ (Fig-3.9). Glycine loops in mouse $K_v1.2$ show a positive correlation between the length and the V_{50} values, shifting the V_{50} to more positive with increasing length of glycine loops (Fig-3.9). Serine loops, on the other hand, show a positive shift in V_{50} with increasing length from S3 to S5 and a negative shift in V_{50} with increasing loop length from S5 to S10 (Fig-3.9). Unlike mouse $K_v1.2$, all the synthetic loops in a

126

jShak1 background have shown a clear effect of increasing loop length in shifting the channel V_{50} to more negative, i.e. longer synthetic loops shifted channel V_{50} more negative compared to respective shorter loops in jShak1 (Fig-4.2A).

Besides the length effect, I have also found that the synthetic loop of same composition affects V_{50} differently in mouse $K_v1.2$ and jShak1, indicating a possible qualitative difference in interactions between the S3-S4 loop and the two different channels. To describe the interaction pattern between the S3-S4 loop and the channel, the loop is divided in two functional regions: (i) the C-terminal part of the S3-S4 loop that is pulled downward in between the VSD and the PD turret in the closed state (Jensen et al., 2012) and (ii) the N-terminal region that remains outside of the VSD vestibule in the closed state. The C-terminal residue is a positively charged lysine (K278) in jShak1, but a neutral alanine (A) in mouse $K_v1.2$. The sequence of the PD turret is also different between mouse $K_v1.2$ and jShak1.

To evaluate the effect of the N-terminal region of the S3-S4 loop in the voltage-sensitivity of mouse $K_v1.2$, I have compared the V_{50} values within the hetero-loop mutants (S7QQA, G7QQA, E7QQA) and with the wild type channel. Both the wild type channel and the hetero loop mutants contain QQA in their C-terminal regions. The N terminal parts of the loop are the only variable regions among these channels. No significant difference are observed between the V_{50} values of S7QQA and G7QQA, indicating no major difference in interactions between the

S7 and G7 part of the loop with the rest of the channel. The V_{50} values of wild type mouse $K_v1.2$ and E7QQA are highly negative compared to S7QQA and G7QQA, E7QQA being more negative than the wild –type channel. This indicates a possible interaction of the channel with the wild-type loop (**AEKPED**AQQG) and the E7 loop that either stabilizes the open state or destabilizes the closed state. I suspect a possible charge-charge interaction between the N-terminal region of the loop and the rest of the channel. The E7 loop being completely negatively charged could mediate an interaction with the channel stronger than the wild type loop, which has three negatively charged residues in the N-terminal region. The G7 and the S7 loops having no charges, fail to mediate any significant interaction with the channel. From the homology model of the closed state mouse $K_v1.2$, the negatively charged PD turret appears to have the most potential to interact with the N-terminal region of the loop. However more studies are needed to confirm this supposition.

To evaluate the effect of the C-terminal region of the S3-S4 linker in the V_{50} of mouse $K_v1.2$, I have compared the longest synthetic homo-loops (S10, G9 and E10) with respective hetero-loop mutants (S7QQA, G7QQA and E7QQA). The comparison indicates that when the 3 C-terminal residues of the loop are glycine (G3), the closed state is significantly stabilized over the natural QQA sequence with G7 sequence in the N-terminus of the loop. Three residues of serine (S3) and glutamic acids (E3) in the C-terminal region of the loop apparently make no difference compared to QQA, in the context of S7 and E7 in the N-terminal

regions respectively. Comparison of several combinations of N and C terminal mutations suggest that the C-terminus of the S3-S4 loop affects the channel V_{50} differently depending on the nature of its side chain. However, the C-terminal effect is overwhelmed by the effect of possible electrostatic interactions between the N-terminus of the loop and the rest of the channel (Sand et al., 2013).

In the closed state, the C-terminal end of the S3-S4 loop is pulled downward, closer to the VSD and PD turret, which makes the C-terminal QQA exposed to interaction with both the PD turret and the S3 helix (Jensen et al., 2012). While comparing between the homo and hetero loop mutants, no significant differences are observed in the V_{50} values of the E10 loop channel and the E7QQA, indicating that in the context of E7 N-terminal region, the C terminus do not make a significant contribution in setting the V_{50} of the channel. An interaction between the negatively charged PD turret and the trimer of glutamic acid (E3) in the C-terminus of the E10 loop is expected to cause a repulsive force to destabilize the closed state compared to QQA sequence, which is not true for the results. From the results of our past (Sand et al., 2013) and current studies (chapter 3 and 4), I suggest that in the closed state, the C-terminus of the S3-S4 loop of mouse $K_v1.2$ is pulled down-ward, passing most of the charged residues of the PD turret, placing the C-terminus of the loop near the hydrophobic residues of the S3 helix. During this process, I suppose that part of the N-terminus of the loop becomes exposed to the negatively charged region of the PD turret (Fig-3.10 and 3.11). However, the PD turret might still have smaller effect on the C-terminal region. In

mouse $K_v1.2$, the conserved D259 of the S3 helix is surrounded by a cluster of hydrophobic residues (I227, I226, I229, V230, A231), which appear to have potentials to make weak hydrophobic interactions with the C-terminal region of the S3-S4 loop in the closed state. I propose that in wild type channel, the C-terminal alanine (A) makes a weak hydrophobic interaction with I229, V230 and A231, stabilizing the closed state of the channel (Fig-3.11A). Mutant channels with three glycine residues (G3) in C-terminus make stronger hydrophobic interactions with the hydrophobic residues of the S3 helix, stabilizing the closed state more compared to the wild-type QQA sequence (Fig-3.11B). Trimers of serine (S3) and glutamic acid (E3) in the C-terminus of the loop fail to interact with the hydrophobic residues of the S3 helix, which result in showing no significant differences between the V_{50} values of S10 and S7QQA and between E10 and E7QQA channels (Fig-3.11, Table-3.1). However, this C-terminal effect is overwhelmed by the stronger electrostatic interaction between the negatively charged residues of the N-terminal region of the wild type loop and the negatively charged residues of the PD turret (Fig-3.11). Similarly I suppose that the highly negative V_{50} values of both the E10 and the E7QQA channels are mostly caused by the first seven E residues (N-terminal E7) of the channel, overwhelming the C-terminal effect and in turn showing no significant differences in the V_{50} values of the E10 and the E7QQA channel.

According to my results the C-terminus of the S3-S4 linker of jShak1 is likely involved in an electrostatic interaction with the negatively charged residues of the

PD turret. The results from K278 point mutations in jShak1 show the most negative shift in the channel V_{50} by negatively charged E and D at the C-terminal position, followed by the neutral G (Fig-4.3A). K278A mutation shifts the V_{50} of the channel to a more positive value (Fig-4.3A). The homology model of jShak1 at closed state shows that the C-terminus of the S3-S4 loop is positioned in close-proximity to the negatively charged PD turret of the adjacent subunit (Fig-4.4). The S3-S4 loop of jShak1 being extremely short appears more stretched by the downward transition of the S4 helix in the closed state compared to mouse $K_v1.2$. I suggest that the negatively charged E338 of the PD turret interacts with positively charged K278 to stabilize the closed state of jShak1 (Fig-4.4). In K278E and K278D mutants, the E and D at position 278 repeal E338 and destabilize the closed state, shifting the V_{50} more negative compared to the wild type channel. In K278G, glycine with no side chain shifts the V_{50} value more negative compared the wild type channel possibly by allowing more structural flexibility to the C-terminal region or by avoiding electrostatic interactions with E338 of the PD turret, making the channel opening easier than the wild-type channel. The positive shift in V_{50} of K278A mutant may be mediated through effects on backbone conformation rather than inter-residues interaction, since there are no apparent side-chain interactions.

To evaluate the effect of the N-terminal region of the jShak1 S3-S4 loop in voltage sensitivity of the channel, I have compared the V_{50} values between S4K, G4K and E4K hetero-loop channels, which varied from each other only in their

N-terminal regions (Fig-4.5A). The V_{50} values of E4K and G4K are more positive than the V_{50} value of S4K; this result suggests that charge-charge interactions between the N-terminal region of the loop and the rest of the jShak1 channel are not a significant factor in the V_{50} shifts, unlike what I proposed for mouse $K_v1.2$. This comparison also indicates that serine residues in the N-terminal region of the loop can stabilize the open state (or destabilize the closed state) compared to glycine and glutamic acids in that region.

I have further compared the V_{50} values of the homo-polymeric (S5, S10, G5, G10, E5) loop channels with the respective hetero-polymeric loop (S4K, S9K, G4K, G9K, E4K) channels (Fig-4.5). Whereas the K278 mutations in wild type jShak1 background showed significant effect of the C-terminal region in voltages sensitivity, the hetero-polymeric loops with a C-terminal K in homo-loop background failed to show any significant effect on V_{50} values for G4K, G9K and S9K compared to the respective homo-loop channels (Fig-4.3 and 4.5). This suggests that the effect of the C-terminal regions become dominant only in the context of wild type N-terminal sequence, as observed with the C-terminal loop mutations in jShak1 background (K278 mutants). Comparing the V_{50} values between the S5, S4K, K278S and the wild type channel, I suggest that the N and C-termini of the S3-S4 loop mediates a coordination that is necessary for the expression of the C-terminal effect (detailed in page-95). Mutations in the N-terminal region change the natural co-ordination between the N and C termini of the loop, suppressing the effect of the C-terminal region. For example, in G5 and

G4K mutants, the effects of C-terminal regions are suppressed by the N-terminal glycine residues that fail to mediate the hypothetical co-ordination with the C-terminal region as is found in wild type channel. For this reason, a change in K to G does not show any effect in G4K and G5 loop mutants, whereas, the same K to G change in wild type background shows significant left shift in the V_{50} value of K278G mutant (Fig-4.3 and 4.5).

Mouse $K_v1.2$, like most other K_v1 channels, has evolved with a negatively charged residue, E at 226 position, which forms a salt-bridge with the positively charged R residues of the S4 helix in the open state. Replacement of E with D (which has a shorter side chain than E) shows a positive shift in the V_{50} value, indicating possible inefficiency in forming the salt bridge compared to the wild type mouse $K_v1.2$. I reason that the natural absence of E in the S2 helix of jShak1 is one of the reasons for which the longer homo-polymeric loops fail to make the V_{50} of the channel any more negative than the wild type jShak1. Point mutations N227D and N227E in jShak1 were previously shown to shift the V_{50} highly negatively compared to the wild type channel (Klassen et al., 2008), indicating possible salt-bridge formation between the negatively charged D/E with the R residues of the S4 helix to stabilize the open state, similar to mouse $K_v1.2$. The N227E mutation in jShak1 shift the channel V_{50} more negative compared to N227D, similar to what was observed in mouse $K_v1.2$, further illustrating the importance of side-chain length in stable salt-bridge formation.

The TEV loop mutants with single and double cut sites in jShak1 background show a large shift in V_{50} value, significantly more negative than the wild type and any of the homo-polymeric synthetic loops (Fig-4.9). Similar TEV loop in mouse $K_v1.2$ showed no significant difference in V_{50} value compared to the wild type mouse $K_v1.2$ (Sand et al., 2013). This further indicates a channel specific interaction between the loop and the rest of the channel that stabilizes the relative open state in jShak1. I propose that in jShak1 the S3-S4 loop is adapted to mediate an interaction with the channel that helps to stabilize the relative open state without forming a salt-bridge between the S2 and S4 helices. However, when a negatively charged residue is present at 227 position of S2 helix, jShak1 can efficiently form a salt bridge to stabilize the open state. Unlike mouse $K_v1.2$, The nature of the C-terminal region of the jShak1 loop affects the mechanistic cooperativity of the channel (slope, b) when combined with a negatively charged residue in the S2 helix (Fig-4.7B), indicating a possible change in the underlying mechanism caused by such double mutants.

E226D, E226N and E226Q mutations in mouse $K_v1.2$ produce leak current passing through the omega pore in the VSD. Use of pore blocker agitoxinI confirms the nature of the non-canonical omega current (Fig-3.5). The amount of omega current passing through the VSD is much higher in E226N and E226Q mutants, compared to E226D. From my electrophysiological studies and 3D models I propose that a stable salt-bridge formation is essential in mouse $K_v1.2$ to both stabilize the open state and to prevent the omega current through the VSD.

134

The conformation of the VSD (specially the S4 helix), attained at the open state of this channel by stable salt-bridge formation can make a constriction in the water crevices of the VSD that prevents omega current through this region. In E226D mutant D contains a shorter side chain than E, which widens the omega pore compared to the wild type channel and allows some current through the VSD at hyperpolarized potential. At depolarized potential, the S4 helix moves towards the S2 helix and forms an inefficient salt-bridge with D226 that blocks the omega current. But for E226N and E226Q mutants, no salt-bridges are formed between neutral N or Q at 226 with the positively charged R residues of the S4 helix. This results in omega current both at hyperpolarized and depolarized potentials. jShak1, on the other hand is naturally adapted with a neutral N at position 227 of the S2 helix, showing no omega currents. The 3D homology model also shows no trace of omega pore through the VSD (Fig-3.6K). I propose that the helices in the VSD of jShak1 are more compactly packed together than are the helices in mouse $K_v1.2$. For this reason, shortening and neutralizing the side-chain at position 226 in mouse $K_v1.2$ creates an omega pore, whereas lengthening and adding negative charge to the side-chain at position 227 in jShak1 shifts the voltage sensitivity of the channel to more negative values without changing the nature of the current.

This study extends our knowledge in understanding channel specific mechanisms that have evolved to fine-tune the voltage sensitivity. The study was performed in K_v1 family channels from two species: mouse and jellyfish that are both physiologically and evolutionarily different from each other (detail in chapter 1).

135

Comparison between two such divergent members of K_v1 family reveals the importance of the S3-S4 loop length and composition in setting the specific V_{50} of the channel. Results from the same synthetic loops in two different channel backgrounds have helped to evaluate channel-specific interactions between the S3-S4 loop and the rest of the channel that are important for the dynamics and stability of the VSD. Based on the electrophysiological results several possible interactions have been proposed in this study, which needs to be verified by future experiments. Several approaches are available to confirm possible interactions between amino acid residues. One possible experiment that could be done to identify interacting residues in our available laboratory facilities was to replace the potential residues by cysteine and then break the cys-cys bond by treating the channel with reducing agents like Dithiothreitol (DTT) or 2-Mercaptoethanol (BME). Another approach to identify the possible interactions between charged residues could be to replace the candidate residues with histidine and analyze the channel behaviour at different pH, as the net charge of His varies at different pH. Both the above mentioned approaches were attempted in this study, but neither of them could be used as the jellyfish channel jShak1 was sensitive to DTT, BME and high pH. In this context, a possible approach for further studies would be to mutate the potential candidate charged residues with neutral or oppositely charged residues to identify the specific residues in the loop and the channel that are interacting differently in mouse $K_v1.2$ and jShak1. Such an approach would help to better understand the channel specific fine-tuning mechanism of voltage sensitivity.

REFERENCE

Aggarwal SK and MacKinnon R. (1996). Contribution of the S4 segment to gating charge in the Shaker K$^+$ channel. *Neuron* **16**, 1169-1177.

Augustine GJ (1990*)* Regulation of transmitter release at the squid giant synapse by presynaptic delayed rectifier potassium current. *Journal of Physiology (London)* **431**, 343-364.

Bhalla T, Rosenthal JJ, Holmgren M, Reenan R. (2004). Control of human potassium channel inactivation by editing of a small mRNA hairpin. *Nature Structural & Molecular Biology* **11**, 950-956.

Chen XR, Wang QH, Ni FY and Ma JP. (2010). Structure of the full-length Shaker potassium channel $K_v1.2$ by normal-mode-based X-ray crystallographic refinement. *Proceedings of the National Academy of Sciences of the United States of America* **107**, 11352-11357.

Cole KS and Curtis HJ (1939). Electrical impedance of the squid giant axon during activity. *Journal of General Physiology* **22**, 649–670.

Czempinski K, Zimmermann S, Ehrhardt T and Muller-Rober B. (1997). New structure and function in plant K$^+$ channels: KCO1, an outward rectifier with a steep Ca^{2+} dependency. *EMBO Journal* **16**, 2565–2575.

Dominguez I, Itoh K and Sokol SY. (1995). Role of glycogen synthase kinase 3 beta as a negative regulator of dorsoventral axis formation in *Xenopus* embryos. *Proceedings of the National Academy of Sciences of the United States of America* **92**, 8498-502.

Doyle DA, Morais Cabral J, Pfuetzner RA, Kuo A, Gulbis JM, Cohen SL, Chait BT, MacKinnon R. (1998). The structure of the potassium channel: Molecular basis of K$^+$ conduction and selectivity. *Science* **280**, 69-77.

Durell SR, Shrivastava IH and Guy HR. (2004). Models of the structure and voltage-gating mechanism of the shaker K$^+$ channel. *Biophysical Journal* **87,** 2116-2130.

Enyedi P, Czirják G. (2010). Molecular background of leak K$^+$ currents: two-pore domain potassium channels. *Physiological Reviews* **90**, 559-605.

Fenn W, Cobb D. (1936) Electrolyte changes in muscle during activity. *American Journal of Physiology* **115**, 345–356.

Fernández JA, Skryma R, Bidaux G, Magleby KL, Scholfield CN, McGeown JG, Prevarskaya N, Zholos AV.(2011). Voltage- and cold-dependent gating of single TRPM8 ion channels. *Journal of General Physiology* **137**, 173-95.

Freites JA, Tobias DJ and White SH. (2006). A voltage-sensor water pore. *Biophysical Journal* **91**, L90–L92.

Garcia ML, Garcia-Calvo M, Hidalgo P, Lee A, MacKinnon R. (1994). Purification and characterization of three inhibitors of voltage-dependent K$^+$ channels from *Leiurus quinquestriatus* var. *hebraeus* venom. *Biochemistry* **33**, 6834-9.

Goldin AL (2006). Expression and Analysis of Recombinant Ion Channels. WILEY-VCH Verlag GmbH & Co. KGaA,Weinheim.

Goldstein SA, Price LA, Rosenthal DN, Pausch MH. (1996). ORK1, a potassium-selective leak channel with two pore domains cloned from *Drosophila melanogaster* by expression in *Saccharomyces cerevisiae*. *Proceedings of the National Academy of Sciences USA* **93**, 13256–13261.

Gonzalez C, Baez-Nieto D, Valencia I, Oyarzún I, Rojas P, Naranjo D, Latorre R. (2012). K($^+$) channels: function-structural overview. *Comprehensive Physiology* **3**, 2087-149.

Gonzalez C, Rosenman E, Bezanilla F, Alvarez O, Latorre R. (2001). Periodic perturbations in Shaker K$^+$ channel gating kinetics by deletions in the S3-S4 linker.

Proceedings of the National Academy of Sciences of the United States of America **98**, 9617-23.

Gonzalez C, Rosenman E, Bezanilla F, Alvarez O, Latorre R.(2000). Modulation of the Shaker K$^+$ channel gating kinetics by the S3-S4 linker. *Journal of General Physiolog*. **115**, 193-208.

Gordon CJ. (1993). Temperature regulation in laboratory rodents. Cambridge University Press, New York.

Grigoriev NG, Spafford JD, Gallin WJ and Spencer AN. (1997). Voltage sensing in jellyfish Shaker K$^+$ channels. *Journal of Experimental Biology* **200**, 2919-26.

Grosse G, Draguhn A, Höhne L, Tapp R, Veh RW and Ahnert-Hilger G. (2000). Expression of K$_v$1 potassium channels in mouse hippocampal primary cultures: development and activity-dependent regulation. *Journal of Neuroscience* **20**, 1869-82.

Gutman GA, Chandy KG, Grissmer S, Lazdunski M, McKinnon D, Pardo LA, Robertson GA, Rudy B, Sanguinetti MC, Stuhmer W, Wang X. (2005). International Union of Pharmacology. LIII. Nomenclature and molecular relationships of voltage-gated potassium channels. *Pharmacological Reviews* **57**, 473-508.

Hattan D, Nesti E, Cachero T.G, Morielli A.D. (2002). Tyrosine phosphorylation of K$_v$1.2 modulates its interaction with the actin-binding protein cortactin. *Journal of Biological Chemistry* **277**, 38596–38606.

Heinemann SH, Rettig J, Graack HR, Pongs O. (1996). Functional characterization of K$_v$ channel beta-subunits from rat brain. *Journal of Physiology* **493**, 625-633.

Hille B. (2001). *Ionic Channels of Excitable Membranes*. (3rd edition). Sunderland, Massachusetts: Sinauer Associates Inc.

Ho SN, Hunt HD, Horton RM, Pullen JK, Pease LR. (1989).Site-directed mutagenesis by overlap extension using the polymerase chain reaction. *Gene* **77**, 51-9.

Hodgkin AL and Huxley AF (1952). A quantitative description of membrane current and its application to conduction and excitation in nerve. *Journal of Physiology-London* **117**, 500-544.

Hodgkin AL, Katz B (1949). The effect of sodium ions on the electrical activity of the giant axon of the squid. *Journal of Physiology* **108**, 37–77.

Jegla T and Salkoff L. (1997). A novel subunit for Shal K^+ channels radically alters activation and inactivation. *Journal of Neuroscience* **17**, 32-44.

Jegla T, Grigoriev N, Gallin WJ, Salkoff L and Spencer AN. (1995). Multiple Shaker potassium channels in a primitive metazoan. *Journal of Neuroscience* **15**, 7989-99.

Jensen MØ, Jogini V, Borhani DW, Leffler AE, Dror RO and Shaw DE. (2012). Mechanism of voltage gating in potassium channels. *Science* **336**, 229-33.

Jogini V and Roux B. (2007). Dynamics of the K_v1. 2 voltage-gated K^+ channel in a membrane environment. *Biophysical Journal*. **93**, 3070–3082.

Katz B, Miledi R (1969) Tetrodotoxin-resistant electric activity in presynaptic terminals. *Journal of Physiology (London)* **203**, 459-487.

Klassen TL, Spencer AN and Gallin WJ. (2008). A naturally occurring omega current in a Kv3 family potassium channel from a platyhelminth. *BMC Neuroscience* **9**, 52.

Klassen, TL, O'Mara ML, Redstone M, Spencer AN and Gallin WJ. (2008). Non-linear intramolecular interactions and voltage sensitivity of a K_v1 family potassium channel from *Polyorchis penicillatus* (Eschscholtz 1829). *Journal of Experimental Biology* **211**, 3442-53.

Krepkiy D, Mihailescu M, Freites JA, Schow EV, Worcester DL, Gawrisch K, Tobias DJ, White SH and Swartz KJ. (2009). Structure and hydration of membranes embedded with voltage-sensing domains. *Nature*. **462**, 473–479.

Latorre R, Vargas G, Orta G, Brauchi S. (2007). Voltage and Temperature Gating of ThermoTRP Channels. In: Liedtke WB, Heller S, editors. Boca Raton (FL): CRC Press; Chapter 21.

Leao RM, Li S, Doiron B, Tzounopoulos T. (2012). Diverse levels of an inwardly rectifying potassiumconductance generate heterogeneous neuronal behavior in a population of dorsal cochlear nucleuspyramidal neurons. *Journal of Neurophysiology* **107**, 3008–3019.

Lee SY, Lee A, Chen JY and MacKinnon R. (2005). Structure of the KvAP voltage-dependent K+ channel and its dependence on the lipid membrane. *Proceedings of the National Academy of Sciences of the United States of America* **102**, 15441-15446.

Li J, Blankenship ML and Baccei ML. (2013). Inward-rectifying potassium (K_{ir}) channels regulate pacemaker activity in spinal nociceptive circuits during early life. *Journal of Neuroscience* **33,** 3352-62.

Lin Y-C and Spencer AN. (2001). Calcium currents from jellyfish striated muscle cells: preservation of phenotype, characterisation of currents and channel localisation. *The Journal of Experimental Biology* **204**, 3717–3726.

Lin Y-C, Gallin WJ and Spencer AN. (2001). The anatomy of the nervous system of the hydrozoan jellyfish, Polyorchis penicillatus, as revealed by a monoclonal antibody. *Invertebrate Neuroscience* **4**, 65-75.

Li-Smerin Y, Hackos DH and Swartz KJ. (2000). alpha-helical structural elements within the voltage-sensing domains of a K^{+} channel. *Journal of General Physiology* **115**, 33-50.

Long SB, Campbell EB and Mackinnon R. (2005). Crystal structure of a mammalian voltage-dependent Shaker family K$^+$ channel. *Science* **309**, 897-903.

Macholán, M. (1999). Mus spretus. The Atlas of European Mammals, Academic Press, London, UK. 290-291.

Miledi R and Parker I. (1984). Chloride current induced by injection of calcium into *Xenopus* oocytes. *Journal of Physiology* **357**, 173-83.

Miller C. (2000). An overview of the potassium channel family. *Genome Biology* **1**, reviews0004-reviews0004.5

Moshelion M, Becker D, Czempinski K, Mueller-Roeber B, Attali B, Hedrich R, Moran N. (2012). Diurnal and circadian regulation of putative potassium channels in a leaf moving organ. *Plant Physiology* **128**, 634–642.

Musser GG and Carleton MD. (2005). Superfamily Muroidea. *Mammal Species of the World a Taxonomic and Geographic Reference*. D. E. Wilson and D. M. Reeder eds. Johns Hopkins University Press, Baltimore.

Papazian DM, Shao XM, Seoh SA, Mock AF, Huang Y, Wainstock DH. (1995). Electrostatic interactions of S4 voltage sensor in Shaker K$^+$ channel. *Neuron* **14**, 1293-301.

Papazian DM, Timpe LC, Jan YN, Jan LY. (1991). Alteration of voltage-dependence of Shaker potassium channel by mutations in the S4 sequence. *Nature* **349**, 305-10.

Patel AJ, Honore E, Maingret F, Lesage F, Fink M, Duprat F, Lazdunski M. (1998).A mammalian two pore domain mechano-gated S-like K$^+$ channel. *EMBO Journal* **17**, 4283–4290.

Perney TM, Marshall J, Martin KA, Hockfield S, Kaczmarek LK. (1992).Expression of the mRNAs for the Kv3.1 potassium channel gene in the adult and developing rat brain. *Journal of Neurophysiology* **68**, 756-66.

Perozo E, Santacruz-Toloza L, Stefani E, Bezanilla F, Papazian DM. (1994). S4 mutations alter gating currents of Shaker K channels. *Biophysical Journal* **66,** 345-54.

Pongs O. (1999). Voltage-gated potassium channels: from hyperexcitability to excitement. *FEBS Letters* **452,** 31-5.

Sand R, Sharmin N, Morgan C, Gallin WJ. (2013) Fine-tuning of voltage sensitivity of the $K_v1.2$ potassium channel by inter-helix loop dynamics. *Journal of Biological Chemistry* **288**, 9686-95

Sand RM, Atherton DM, Spencer AN and Gallin WJ. (2011). jShaw1, a low-threshold, fast-activating K_v3 from the hydrozoan jellyfish *Polyorchis penicillatus*. *The Journal of Experimental Biology* **214**, 3124-3137.

Schoppa NE, Sigworth FJ. (1998). Activation of Shaker potassium channels.III. An activation gating model for wild-type and V2 mutant channels. *Journal of General Physiology* **111**, 313-342.

Schwarz TL, Tempel BL, Papazian DM, Jan YN, Jan LY. (1988). Multiple potassium-channel components are produced by alternative splicing at the Shaker locus in *Drosophila*. *Nature* **331**, 137-42.

Silverman, W. R, Roux, B. and Papazian, D. M. (2003). Structural basis of two-stage voltage-dependent activation in K^+ channels. *Proceedings of the National Academy of Sciences USA* **100**, 2935-2940.

Sokolov S, Scheuer T, Catterall WA. (2007). Gating pore current in an inherited ion channelopathy. *Nature*. **446**, 76-8.

Spencer AN. (1978). Neurobiology of Polyorchis I. Function of effector systems. *Journal of Neurobiology* **9**, 143-157.

Spencer AN. (1979). Neurobiology of Polyorchis II. Structure of effector systems. *Journal of Neurobiology* **10**, 95-117.

Spencer AN. and Arkett SA. (1984). Radial symmetry and the organization of central neurons in a hydrozoan jellyfish. *Journal of Experimental Biology* **110**, 69-90.

Starace DM and Bezanilla F. (2001).Histidine scanning mutagenesis of basic residues of the S4 segment of the shaker potassium channel. *Journal of General Physiology* **117**, 469–490.

Takeuchi K, Yokogawa M, Matsuda T, Sugai M, Kawano S, Kohno T, Nakamura H, Takahashi H, Shimada I. (2003). Structural basis of the KcsA K($^+$) channel and agitoxin2 pore-blocking toxin interaction by using the transferred cross-saturation method. *Structure* **11**, 1381-92.

Tarek M and Delemotte L. (2013). Omega currents in voltage-gated ion channels: what can we learn from uncovering the voltage-sensing mechanism using MD simulations? *Accounts of Chemical Research* **46**, 2755-62.

Theilig F, Goranova I, Hirsch JR, Wieske M, Unsal S, Bachmann S, Veh RW, Derst C.(2008). Cellular localization of THIK-1 (K(2P)13.1) and THIK-2 (K(2P)121) K channels in the mammalian kidney. *Cellular Physiology and Biochemistry* **21**, 63–74.

Thomas D, Karle CA and Kiehn J. (2006) The cardiac hERG/IKr potassium channel as pharmacological target: structure, function, regulation, and clinical applications. *Current Pharmaceutical Design* **12,** 2271-83.

Tiwari-Woodruff SK, Lin MA, Schulteis CT and Papazian DM. (2000).Voltage-dependent structural interactions in the Shaker K($^+$) channel. *Journal of General Physiology* **115**, 123-138.

Tombola F, Pathak MM and Isacoff EY. (2005) Voltage-sensing arginines in a potassium channel permeate and occlude cation-selective pores. *Neuron* **45**, 379-88.

Tombola F, Pathak MM, Gorostiza P and Isacoff EY.(2007) The twisted ion-permeation pathway of a resting voltage-sensing domain. *Nature* **445**, 546-9.

Treptow W and Tarek M. (2006). Environment of the gating charges in the $K_v1.2$ Shaker potassium channel. *Biophysical Journal* **90**, L64–L66.

Widmaier EP, Raff H and Strang KT (2014). Vander's Human Physiology: The Mechanisms of Body Function (13th Edition). McGraw-Hill Science/Engineering/Math.

Wilson DE and Reeder DM. (2005). Mammal Species of the World. Johns Hopkins University Press, Baltimore, MD, USA.

Zhong Y, Wang J, Liu W and Zhu Y (2013). Potassium ion channels in retinal ganglion cells (Review). *Molecular Medicine Reports* **8**, 311-319.

APPENDIX

Fine-tuning of Voltage Sensitivity of the K$_v$1.2 Potassium Channel by Interhelix Loop Dynamics*

Rheanna Sand[‡1], **Nazlee Sharmin**[‡], **Carla Morgan**[‡], and **Warren J. Gallin**[‡§2]

From the ‡Department of Biological Sciences, University of Alberta, Edmonton, Alberta T6G 2E9, Canada and §Department of Cell Biology, University of Alberta, Edmonton, Alberta T6G 2H7, Canada

Background: Potassium channels change conformation in response to transmembrane voltage.
Results: The loop connecting the voltage sensing helix to an adjacent helix affects the voltage sensitivity.
Conclusion: Loop length and charge distribution on the interacting surfaces of the voltage sensor and pore domain are responsible for this effect.
Significance: Variation in loop length and composition is a factor in determining the voltage sensitivity of voltage-gated channels.

Many proteins function by changing conformation in response to ligand binding or changes in other factors in their environment. Any change in the sequence of a protein, for example during evolution, which alters the relative free energies of the different functional conformations changes the conditions under which the protein will function. Voltage-gated ion channels are membrane proteins that open and close an ion-selective pore in response to changes in transmembrane voltage. The charged S4 transmembrane helix transduces changes in transmembrane voltage into a change in protein internal energy by interacting with the rest of the channel protein through a combination of non-covalent interactions between adjacent helices and covalent interactions along the peptide backbone. However, the structural basis for the wide variation in the V_{50} value between different voltage-gated potassium channels is not well defined. To test the role of the loop linking the S3 helix and the S4 helix in voltage sensitivity, we have constructed a set of mutants of the rat K$_v$1.2 channel that vary solely in the length and composition of the extracellular loop that connects S4 to S3. We evaluated the effect of these different loop substitutions on the voltage sensitivity of the channel and compared these experimental results with molecular dynamics simulations of the loop structures. Here, we show that this loop has a significant role in setting the precise V_{50} of activation in K$_v$1 family channels.

Voltage-gated potassium (K$_v$)[3] channels are transmembrane proteins essential for the electrical activity of excitable cells (1). K$_v$ proteins, similar to other voltage-gated ion channels, convert changes in membrane potential into useful work (2) open-ing and closing the ion permeation pathway (3). Four α subunits assemble to form a functional channel, with the pore domain (PD) regions interlocking in the center to form the ion pathway and potassium selectivity filter (4, 5). The surrounding voltage-sensing domains (VSDs) contact the PD from an adjacent sub-unit (6) but are otherwise largely surrounded by membrane lipids (4, 7, 8).

Each K$_v$ channel subunit consists of six transmembrane helices, the linker sequences that connect them, and N- and C-terminal modulatory domains. Helices S1 through S4 constitute the VSD, and helices S5, S6, and the intervening re-entrant pore loop make up the PD. The VSD response to changes in membrane potential originates from the S4 helix, which contains four to seven positive amino acids (depending on the channel type) and translocates through the changing electric field of the membrane to drive the opening and closing of the channel (9–11). Under depolarizing conditions, each VSD traverses a number of pre-opening conformations before the channel undergoes a final, cooperative step that opens the pore (12–14).

A combination of three-dimensional crystal structures (5, 8) and molecular dynamics simulations (15–19) support a "sliding helix" model of K$_v$ activation. The predominant feature of this model is a significant translation and rotation of the S4 helix relative to the rest of the VSD. The movement of S4 is constrained by and acts on the rest of the channel by non-covalent interactions with adjacent helices in the VSD and by covalent interactions with the extracellular loop that links the S3 and S4 helices as well as the intracellular loop that links the S4 and S5 helices. Thus, when the force on the S4 helix changes with membrane potential, the overall conformation of the channel protein changes. The sum of these energetic interactions within the protein and between the protein and the lipid bilayer is ultimately responsible for setting the V_{50} of the channel, the voltage at which half of the channels are in an open state and half are in a closed state.

Although there is a growing consensus regarding the structure of K$_v$ channels in the open and closed states, the mechanisms by which voltage sensitivity is modulated remain unclear. Even within the same subfamily, V_{50} can vary widely between K$_v$ channels. In the K$_v$1 group, for example, published V_{50} val-

[3] The abbreviations used are: K$_v$, voltage-gated potassium; V_{50}, voltage at which conductance is activated to 50% of maximum; VSD, voltage-sensing domain; PD, pore domain.

ues range from -46 mV in a lobster channel (20) to $+22$ mV in a jellyfish channel (21). Human channels K$_v$1.1 and K$_v$1.2 share 80% sequence identity and yet differ in voltage sensitivity by 25 mV, with V_{50} values of -30 mV and -5 mV, respectively (22). These differences in V_{50} despite sequence conservation indicate that precise control of V_{50} ultimately resides in the more variable, and generally less studied, regions such as interhelical loops.

Besides the membrane lipid head groups (23, 24) and acidic residues in adjacent helices (25, 26), the S3/S4 linker has been implicated in the regulation of voltage sensitivity in K$_v$1 channels. In a cnidarian K$_v$1 channel, the role of one of the S2 acidic residues in setting the V_{50} can be modified by the constraints of a short S3/S4 loop (27). Sequential truncation of the S3/S4 loop in the Shaker channel also changes voltage sensitivity and gating kinetics (28, 29); however, this simple reduction of the wild type loop length could have several confounding effects that cannot be distinguished in a single truncation mutagenesis series.

In this study, we have varied both the length and composition of the S3/S4 loop in the K$_v$1.2 channel to evaluate their contributions to the overall voltage sensitivity of the channel. The experimental results from the mutant channels were combined with molecular dynamics simulations of the same loops constrained by models of open and closed states of the channel. We found that both the length and the composition of the loop are responsible for an energetic constraint on the transition between the opened and closed states. We conclude that the highly variable range of lengths and compositions of S3/S4 linkers found in nature is one factor in the quantitative evolution of voltage sensitivity in the K$_v$1 family of voltage-gated cation channels.

EXPERIMENTAL PROCEDURES

Channel Construction and Expression—Full-length mouse K$_v$1.2 was purchased (OpenBiosystems, Huntsville, AL) and subcloned into the *Xenopus laevis* oocyte expression vector pXT7 (30); note that mouse and rat K$_v$1.2 have identical amino acid sequences. To create loop variants, two opposing BbsI sites were introduced into the S3/S4 loop by overlapping PCR mutagenesis to create a construction vector. Annealed oligonucleotides with the correct sequence and overhangs were ligated into the BbsI-digested K$_v$1.2 vector. Sequences of all plasmids were confirmed by Sanger sequencing. Plasmids were linearized with XbaI (Promega, Fitchburg, WI) for *in vitro* mRNA transcription with T7 RNA polymerase (Ambion, Austin, TX). Injection volumes of the *in vitro*-transcribed mRNA were optimized to produce between 4 and 18 μA maximal current, as currents larger than $\sim$20 μA cause local distortions in membrane potential (31) and because some channels have been shown to be sensitive to high extracellular [K$^+$] (32). Oocytes were incubated at 18 °C in modified Barth's medium (33) prior to experiments. During experiments, oocytes were bathed in a solution containing 96 mM NaCl, 2 mM KCl 2, 1.8 mM CaCl$_2$, 1 mM MgCl$_2$, 5 mM HEPES, 1 mM diisothiocyanatostilbene-2,2′-disulfonic acid to block native chloride currents (34), pH 7.4.

Electrophysiology—Ionic currents were recorded 24–48 h post-injection from *X. laevis* oocytes at room temperature using two-electrode voltage clamp as described previously (35). Traces were filtered at 1 kHz and sampled at 10 kHz with P/4 leak subtraction. Cells were held at a potential of -90 mV and test pulses were 50-ms in duration. Conductance was derived from tail current amplitudes fitted with double exponential decay functions. Individual *G-V* curves were normalized and fitted to a Boltzmann equation of the form (36).

$$G/G_{\mathrm{max}} = 1/(1 + \exp((V_m - V_{50})/b)^4) \qquad \text{(Eq. 1)}$$

The V_{50} in this equation is of one subunit; channel V_{50} values were calculated by solving for V_m when $G/G_{\mathrm{max}} = 0.5$. Data were collected and analyzed using pClamp (version 9; Molecular Devices, Sunnyvale, CA) and SigmaPlot (version 12; Systat Software, Inc., Point Richmond, CA).

Molecular Models—The open state models for rat K$_v$1.2 are based on the Protein Data Bank code 3LUT refinement (37) of the crystal structure (5). The closed state models are based a structure inferred by Jensen *et al.* (16), based on the structure of a K$_v$1.2/K$_v$2.1 chimera; the K$_v$2.1 segment from that chimera was replaced with the homologous K$_v$1.2 sequence using SWISS-MODEL (38). The structures of the various sequence variants were obtained by using SWISS-MODEL for homology modeling and PyMOL (39) for simple mutagenesis; as such, these models should be considered as heuristic.

Molecular Dynamics Simulations—Peptide structures were constructed in Protein Data Bank format using PyMOL (39), with the N terminus capped with an acetyl group and the C terminus capped with an amine group. Protein Data Bank files were processed using the GROMACS suite of programs (40), using the AMBER99-SB force field to produce a peptide in an aqueous environment with a NaCl concentration of 96 mM. An initial ensemble of conformations was generated by performing simulation under constant pressure and temperature (NPT) conditions (after appropriate pre-equilibration) for 100 ns. 10 conformations at 10-ns intervals were then selected and used as starting points for independent free energy simulations. For free energy calculations, each selected conformation was reprocessed into an aqueous environment with NaCl concentration of 96 mM, energy minimized, equilibrated under a constant volume and temperature regime followed by an NPT regime, and simulated under NPT conditions for 2 ns under an end-to-end distance constraint ranging from 0.5 to 2.5 nm in 20 equal increments, collecting data necessary for free energy calculations. The results of the simulations were processed to obtain estimates of the free energy differences between adjacent distance increments using the Bennett Acceptance Ratio (41) as implemented in the g_bar program from the GROMACS suite.

RESULTS

Design and Construction of Mutant Channels—The structure of the S3 and S4 helices in the closed (Fig. 1*A*) (16) and open (Fig. 1*B*) (37) state models show that the extracellular ends of the helices are translocated away from each other during channel closing. We wanted to determine whether the distance between the ends of the helices, and therefore the length of the linker, was the only constraint on the Gibbs free energy of activation (ΔG_{open}) or if the loop was interacting with the rest of the channel to modulate V_{50}.
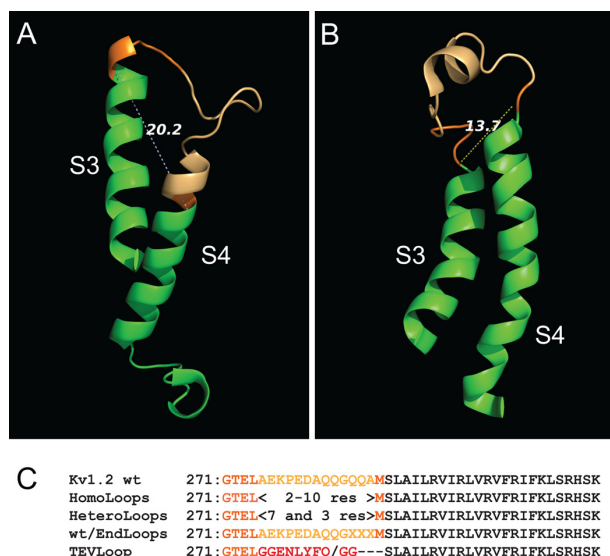
FIGURE 1. **Sequence and structure of the S3/S4 loop of K$_v$1.2.** Illustration of the relationship between the S3 and S4 helices and the loop connecting them in the closed state structure of rat K$_v$1.2 (*A*), as modeled onto a closed state structure from Jensen *et al.* (16), using SWISS-MODEL (38), and S3, S4, and connecting loop in the open state (*B*), from the Protein Data Bank code 3LUT refined crystal structure of rat K$_v$1.2 (37). S3 and S4 are colored in *green*; the connecting loop is colored in *orange* with a lighter hue for the section that is replaced in the synthetic mutants. The distance lines indicate the 2.02 nm (20.2 Å) distance between the nitrogen atom in the N terminus of the loop and the carbon atom at the C terminus of the loop in the closed state and the 1.37 nm (13.7 Å) distance between the same atoms in the open state. *C*, illustration of the wild type loop sequence (Gly-271 through Met-288) and the S4 helix, the sequence into which were inserted the various homopolymeric and mixed loop sequences (same color key as in *A* and *B*) and the mutation that was created to introduce the site of cleavage by TEV protease (*red text*). The letter *X* represents any of the amino acid residues (Glu, Gly, or Ser) that were used in the WT/endloop constructs.

We prepared 39 mutants of the mouse K$_v$1.2 channel (accession no. NM_008417), which is identical in amino acid sequence to the rat K$_v$1.2 channel (hereafter we will refer to this as a rat channel for consistency with other published results using the same amino acid sequence). Fig. 1*C* illustrates the mutagenesis where the 13 amino acids from the middle of the 18-amino-acid-long S3/S4 loop were replaced with the following: (i) homoloops, homopolymers of glutamate (Glu), glycine (Gly), and serine (Ser) ranging in length from 2 to 10 amino acids (except for Gly, where G$_9$ was the longest loop); (ii) heteroloops, E$_7$, G$_7$, and S$_7$ loops combined with three C-terminal residues consisting of E$_3$, G$_3$, S$_3$, or glutamine-glutamine-alanine (QQA, the wild type C-terminal three amino acids) in all combinations; (iii) WT/endloops - wild type K$_v$1.2 linker with the C-terminal QQA replaced with E$_3$, G$_3$, or S$_3$; or (iv) TEV-loop, with a sequence that contained the target site for TEV protease. The mutants expressed in *X. laevis* oocytes all mediated delayed rectifier currents, with distinct V_{50} values and rates of activation and deactivation.

ΔG_{open} of Loopless Channel (ΔG_{core}) Reveals S3/S4 Loop Stabilizes the Open State—The Gibbs free energy of activation (ΔG_{open}) of an intact channel can be decomposed into the free energy of the conformational change in the S3/S4 loops (ΔG_{loops}) plus the free energy of the conformational change of the rest of the channel (ΔG_{core}) plus an unknown interaction

energy (ΔG_{inter}) that represents the difference in non-covalent interaction energy between the loop and the rest of the channel in the open and closed states.

$$\Delta G_{open} = \Delta G_{core} + \Delta G_{loops} + \Delta G_{inter} \qquad \text{(Eq. 2)}$$

To characterize the unknown interaction energy for the various mutant constructs, we first determined ΔG_{core} experimentally by cleaving the S3/S4 loops with TEV protease (*i.e.* by making $\Delta G_{loops} + \Delta G_{inter}$ equal to zero) and determining the V_{50} of this modified channel (Fig. 2*A*).

The V_{50} for the TEV digested loop mutant was -7.5 ± 0.9 mV, which was significantly different from the wild type channel (-13.3 ± 1.7 mV) and from the TEV mutant channel that was not digested with the TEV enzyme (-14.7 ± 1.4 mV) (Fig. 2*A*).

The free energy of opening was calculated as shown in Equation 3,

$$\Delta G_{open} = 13 V_{50} F \qquad \text{(Eq. 3)}$$

where F is Faraday's constant and 13 represents the total gating charge that translocates during channel opening in rat K$_v$1.2 (42).

This calculation yielded a ΔG_{core} of -9.4 ± 1.1 kJ/mol for the TEV-digested TEVloop mutant. Subtraction of ΔG_{core} from the ΔG_{open} of the wild type channel yields a net difference on ΔG of -7.3 ± 2.5 kJ/mol (Table 1), implying that each of the four wild type loops in the K$_v$1.2 channel stabilizes the open state to the extent of ~1.8 ± 0.6 kJ/mol.

Length and Composition Modulate ΔG_{open} in Loop Mutants—Changing the length and character of the S3/S4 loop shifted the midpoint of steady-state activation left or right on the voltage axis but did not greatly affect the slope in the linear portion of the sigmoid curve (Fig. 2, *B–F*).

The effects of loop length and composition on V_{50} were pronounced among the homoloop mutants (Fig. 2, *B–D*). Loops with inserts consisting of only two residues (E$_2$, G$_2$, and S$_2$) had extremely positive V_{50} values, showing shifts of approximately $+40$ to $+55$ mV compared with wild type. As the loop inserts were lengthened V_{50} values for all homoloop channels became more negative, approaching and sometimes becoming more hyperpolarized than that of the wild type channel. Glutamate loops produced the most negatively shifted V_{50} values; E$_6$ through E$_{10}$ had significantly more negative V_{50} values (-19 ± 2 mV for E$_6$ and -28.3 ± 1.5 mV for E$_{10}$) than wild type K$_v$1.2 (-13.3 ± 1.8 mV). Interestingly, G$_4$ and S$_4$ also manifested significantly hyperpolarized V_{50} values compared with wild type, approximately -24 and -22 mV, respectively.

Because current models of the closing process involve the S4 helix moving a substantial distance in the intracellular direction relative to the rest of the VSD, thus pulling the C terminus of the S3/S4 loop into the extracellular vestibule of the VSD, we also constructed loop mutants in which the last three residues of the loops were swapped between all of E$_{10}$, G$_{10}$, S$_{10}$, and wild type, to test whether changing the C-terminal end of the loop would alter ΔG_{open} by virtue of being pulled into a position in which it would directly interact with other VSD residues. The relative effects of varying just the C-terminal three amino acids in the
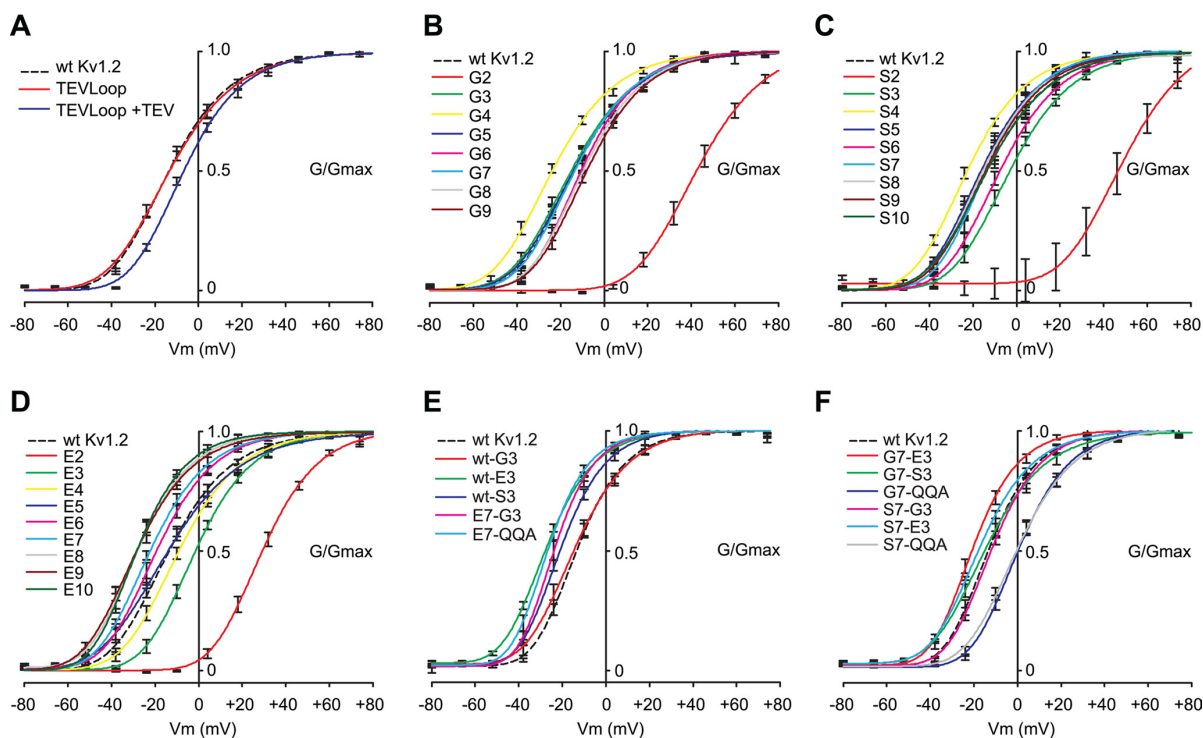
FIGURE 2. **Conductance *versus* voltage curves for the channels used in this study.** *A*, comparison of wild type, TEVloop, and TEVloop with digestion. *B*, the series of glycine homoloop mutants. *C*, the series of serine homoloop mutants. *D*, the series of glutamate homoloop mutants. *E*, the WT/endloop mutants and glutamate series of heteroloop mutants. *F*, the glycine and serine series of heteroloop mutants. For all panels, *error bars* represent S.E. and *n* values range from 5–12 (see Table 1).

loop insert on the conductance-voltage curve are shown in Fig. 2, *E* and *F*. Clearly, the composition of the C-terminal segment of the loop sequence has a significant effect on the channel V_{50} and thus the energy difference between open and closed states.

Overall, the loop variants produced ΔG_{open} values ranging from -35.7 kJ/mol in E_8 channels to $+53.8$ kJ/mol in S_2 channels (Table 1). Subtracting ΔG_{core} from ΔG_{open} produced values ranging from -26.3 to $+63.2$ kJ/mol per channel. Thus, replacing each wild type S3/S4 linker with eight glutamate residues stabilized the open state by ~6.5 kJ/mol/loop, while replacing it with two serine residues destabilized the open state by ~15.8 kJ/mol/loop. Recalling Equation 2, these energies represent the sum of ΔG_{loop} and ΔG_{inter}. To find ΔG_{inter}, we estimated ΔG_{loop} through molecular dynamics simulations.

Molecular Dynamics Simulations of Loops—The first step in estimating ΔG_{loop} was to simulate untethered individual loop peptides in water and determine the Gibbs free energy as a function of loop end-to-end distance (Fig. 3). We then assumed the closed (2.02 nm) and open (1.37 nm) state distances predicted by recent models (Fig. 1, *A* and *B*) and found the free energy difference between those points on each curve. This difference represented ΔG_{loop} in all subsequent energetic calculations.

In addition, each curve had a single minimum corresponding to the most energetically favored end-to-end distance for that loop. We compared these favored end-to-end distances to the V_{50} values for each loop type to see whether these minima correlated with voltage sensitivity. Surprisingly, the loops with

energy minima at end-to-end distances close to that observed in the three-dimensional crystal structure, which is considered typical of the open state ensemble of conformations, did not correspond to the most negative V_{50} value. In fact, these loops yielded channels with some of the most positive V_{50} values. Among all loop mutants, there was no significant correlation of V_{50} with the end-to-end distance of minimum energy ($R^2 = 0.165$ on linear regression of the data in Table 1).

ΔG_{inter} *of Loop Mutants Demonstrates Collateral Loop Interactions*—The difference between ΔG_{open} and the sum of ΔG_{core} and ΔG_{loop} is attributable to collateral interactions between the loop and the rest of the channel ($\Delta \underline{G}_{inter}$). Thus, a non-zero ΔG_{inter} value indicates that the energy difference between open and closed states is not simply the sum of the internal energy of the channel core and the end-to-end energy difference of the loops.

Fig. 4*A* shows the ΔG_{inter} values as a function of loop length for the homoloops series. Loop insertions of two and three have large positive values of ΔG_{inter} for all three amino acids tested, which is a reflection of the extremely positive V_{50} values (and thus ΔG_{open}) in these channels. Glycine loop inserts of lengths 5 through 9 have ΔG_{inter} values essentially equal to zero, whereas glutamate loop inserts of lengths 5 through 10 have monotonically increasingly negative ΔG_{inter} values that plateau at approximately -47 kJ/mol. This implies a strong interaction between glutamate loops and the rest of the channel. Serine inserts, on the other hand, tend to have small ΔG_{inter} values

TABLE 1

ΔG values for mutant channels

Calculated values for free energy of loop stretching (ΔG$_{loops}$ calculated from data in Fig. 3, multiplied by four to account for the presence of four loops in each functional channel) and free energy of collateral interaction (ΔG$_{inter}$ calculated according to Equation 2) for the wild type and all mutant channels. ND, not determined.

Loop	n	V$_{50}$	S.E.	ΔG$_{loops}$ + ΔG$_{inter}$	S.E.	ΔG$_{loops}$	S.E.	ΔG$_{inter}$	S.E.
TEV uncut	9	−14.7	1.4	−9.0	2.1	−9.1	2.1	0.1	3.0
WT	8	−13.3	1.8	−7.3	2.5	3.9	1.1	−11.2	2.8
G$_2$	11	42	2.7	62.1	3.6	−19.7	1.3	81.7	3.8
G$_3$	7	−15.2	1.5	−9.7	2.2	−12.1	0.9	2.5	2.4
G$_4$	8	−23.8	1.2	−20.4	1.9	−1.0	0.5	−19.5	2.0
G$_5$	9	−13.9	1.5	−8.0	2.2	−4.2	0.9	−3.9	2.4
G$_6$	9	−10.7	1.3	−4.0	2.0	−2.8	0.4	−1.2	2.0
G$_7$	9	−10.7	1.2	−4.0	1.9	−0.7	0.6	−3.3	2.0
G$_8$	9	−9.6	1.2	−2.6	1.9	−1.3	0.3	−1.3	1.9
G$_9$	9	−9.2	0.8	−2.1	1.5	−1.2	0.6	−1.0	1.6
S$_2$	9	42.9	7.4	63.2	9.4	−27.4	1.9	90.6	9.5
S$_3$	8	−3.3	1.5	5.3	2.2	−35.6	1.5	40.9	2.7
S$_4$	11	−22.5	1.1	−18.8	1.8	−11.7	1.9	−7.1	2.6
S$_5$	11	−16.1	1.7	−10.8	2.4	−14.4	1.2	3.6	2.7
S$_6$	9	−7.7	1.4	−0.3	2.1	−9.3	1.2	9.1	2.4
S$_7$	9	−14.3	2.7	−8.5	3.6	1.9	0.8	−10.4	3.7
S$_8$	9	−14.6	2.7	−8.9	3.6	8.8	0.5	−17.7	3.6
S$_9$	9	−14.2	1.9	−8.4	2.6	−8.2	1.0	−0.2	2.8
S$_{10}$	10	−13.7	2.1	−7.8	2.9	1.9	0.8	−9.7	3.0
E$_2$	12	29.1	1.5	45.9	2.2	−25.2	2.6	71.1	3.4
E$_3$	9	−1.6	1.4	7.4	2.1	−24.9	2.1	32.3	2.9
E$_4$	8	−9.2	1.5	−2.1	2.2	8.8	1.7	−10.9	2.8
E$_5$	7	−13.9	1.5	−8.0	2.2	9.2	1.5	−17.2	2.7
E$_6$	9	−19.8	2	−15.4	2.8	13.8	0.7	−29.2	2.8
E$_7$	9	−22.1	1.2	−18.3	1.9	19.2	1.1	−37.5	2.2
E$_8$	9	−28.5	2.1	−26.3	2.8	20.9	0.8	−47.3	3.0
E$_9$	5	−28.3	1.8	−26.1	2.5	20.6	0.9	−46.6	2.7
E$_{10}$	7	−28.3	1.5	−26.1	2.2	20.6	0.6	−46.7	2.3
WT-G$_3$	9	−16.4	1.6	−11.2	2.3	5.7	0.6	−16.8	2.4
WT-S$_3$	11	−21.6	1.1	−17.7	1.8	12.5	0.5	−30.2	1.9
WT-E$_3$	9	−22.9	0.6	−19.3	1.4	−2.8	1.6	−16.6	2.1
G$_7$-QQA	10	1.8	1.2	11.7	1.9	−8.0	1.0	19.7	2.1
G$_7$-S$_3$	9	−13.6	1.6	−7.7	2.3	−6.2	0.8	−1.5	2.4
G$_7$-E$_3$	10	−19.9	0.9	−15.6	1.6	1.9	0.7	−17.5	1.7
E$_7$-QQA	10	−23.3	1.4	−19.8	2.1	20.9	0.5	−40.7	2.2
E$_7$-G$_3$	8	−24.5	1.7	−21.3	2.4	16.7	0.5	−38.0	2.5
E$_7$-S$_3$	ND	ND	ND	ND	ND	ND	ND	ND	ND
S-$_7$-QQA	10	0.1	1.2	9.5	1.9	2.1	1.0	7.4	2.1
S$_7$-G$_3$	12	−12.9	0.9	−6.8	1.6	−2.3	0.8	−4.4	1.8
S-$_7$-E$_3$	9	−17.3	1	−12.3	1.7	−2.0	1.2	−10.3	2.1

with a periodic variation in effect that decreases in amplitude as the length of the insert increases.

To determine the contributions of two parts of the S3/S4 loop, that which is pulled into the VSD vestibule upon channel closing and that which remains in a relatively unordered conformation outside the core of the VSD in the closed state, to the energetics of channel opening and closing, we evaluated the heteroloops and WT/endloops series of mutants (Fig. 4B). The range in ΔG$_{inter}$ values among the mutants indicates that both the C-terminal end of the loop, which translocates into the VSD (Fig. 1A), and the N-terminal end interact with the channel to modulate voltage sensitivity.

The negative value of ΔG$_{inter}$ for wild type (Fig. 4B, WT, *blue bar*) indicates that the native loops interact with the rest of the channel to destabilize the closed state (or stabilize the open state, but for simplicity from this point we will refer only to the effects on the closed state). Altering the three C-terminal residues to glycine, serine, or glutamate increases the interaction energy and further destabilizes the closed state, suggesting that the wild type C-terminal sequence is stabilizing the closed state relative to the other C-terminal tripeptide sequences.

The importance of the three C-terminal residues is also apparent in the glycine series of heteroloops. The G$_9$ loop (G$_6$ loop plus G$_3$ C terminus) has essentially no energetic interactions outside of the constraints imposed by the change in end-to-end distance between the open and closed state (Fig. 4A). However, when the C-terminal three glycine residues are replaced by the corresponding residues from the wild type loop sequence (QQA), there is an approximately +20 kJ/mol positive interaction energy, stabilizing the closed state (Fig. 4B). Substituting three glutamate residues in the same location yields an approximately −18 kJ/mol ΔG$_{inter}$, destabilizing the closed state. A similar trend can be observed in the serine series of heteroloops. Thus, the interaction of the portion of the S3/S4 loop that translocates into the VSD on channel closing can stabilize or destabilize the closed state depending on the identity of the side chains.

Analysis of ΔG$_{inter}$ also shows that the N-terminal end of the loop has a significant energetic interaction with the rest of the channel (Fig. 4B). For example, when the three C-terminal residues are the wild type QQA (Fig. 4B, *blue bars*), changing the N-terminal seven residues has a large effect on ΔG$_{inter}$. Replacing the N-terminal residues with glycine or serine strongly stabilizes the closed state, whereas replacing them with glutamate strongly destabilizes the closed state. In fact, all loops with seven glutamate residues at the N terminus have highly negative ΔG$_{inter}$ values (ranging from −38 to −47 kJ/mol), virtually independent of the C-terminal three residues, further supporting an interaction of the amino-terminal of the S3/S4 linker with the rest of the channel.
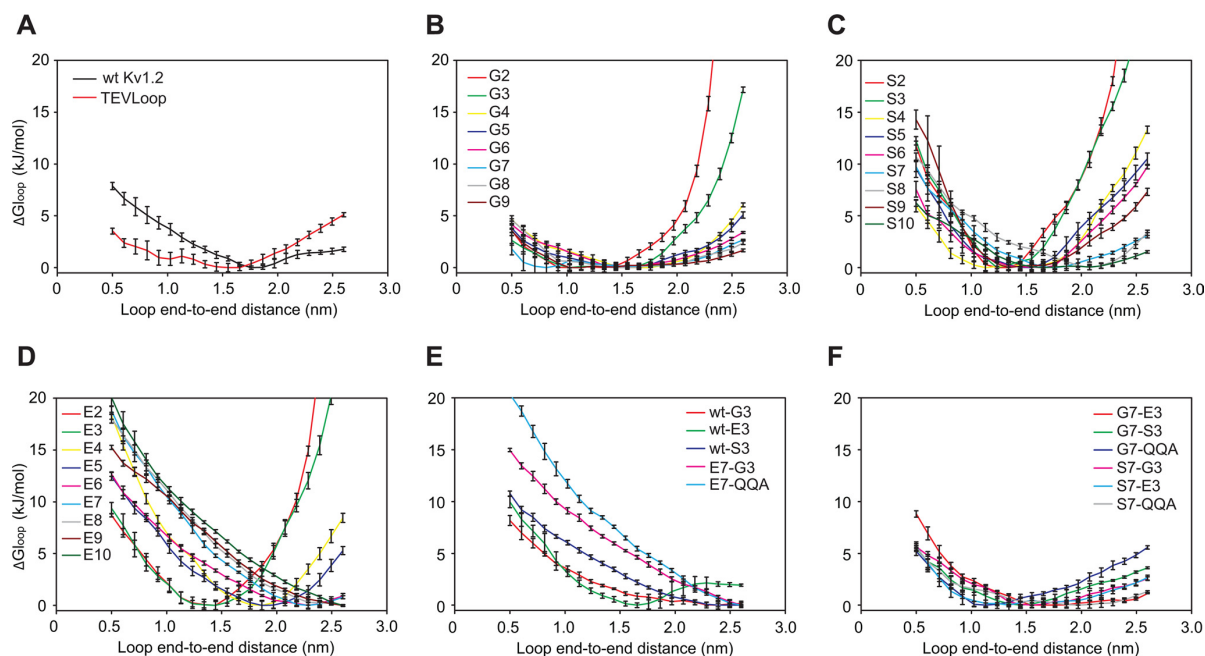
FIGURE 3. **Graphs of free energy differences as a function of end-to-end distance for simulated loop peptides.** The graphs have all been normalized such that the minimum for each graph is 0 kJ/mol. *A*, the wild type loop and the loop mutation containing the TEV cleavage site (sequences shown in Fig. 1*C*). *B*, the glycine series of homoloop mutants. *C*, the serine series of homoloop mutants. *D*, the glutamate series of homoloop mutants. *E*, the WT/endloop mutants and glutamate series of heteroloop mutants. *F*, the glycine and serine series of heteroloop mutants. For all panels, *error bars* represent S.E. ($n = 10$).

Moreover, the value of ΔG_{inter} is not simply a sum of effects of the two parts. For example, the C-terminal S_3 (Fig. 4*B*, *green bars*) has little or no effect when compared with G_3 (Fig. 4*B*, *red bars*) when placed with the G_7 N-terminal sequence, whereas in the context of the wild type and S_7 N-terminal sequences, C-terminal S_3 causes a substantially more negative ΔG_{inter} (*i.e.* destabilizes the closed state) than the G_3 sequence. This further supports the idea that the S3/S4 loop interacts with the rest of the channel via pathways other than the peptide bonds connecting the loop to the S3 and S4 helices, and these interactions and their impact on V_{50} are a function of the channel-specific loop residue side chains.

Electrostatic Properties near the S3/S4 Loop Influence Voltage Sensitivity—As the glutamate loops series manifested by far the largest negative ΔG_{inter}, we sought to understand the variation in ΔG_{inter} by examining the electrostatic properties near the loop in the open and closed state models. Fig. 5 illustrates the relative positions of the loop residues in the open and closed states to the nearest (within 1 nm) negatively charged residues in the rest of the channel. There are five acidic residues that are within 1 nm of at least one of the S3/S4 loop residues in the closed state but not in the open state.

Glu-226 in the S2 helix and Asp-259 in the S3 helix have both been shown to interact with and stabilize basic residues of S4 in the open state (10, 26). Because they are also near the residues from the loop that are translocated into the VSD when the channel closes, it appears that they also play a role in destabilizing the closed state, if the C-terminal end of the S3/S4 loop contains acidic residues.

Residues Glu-350, Asp-352, and Glu-353 are present in the extracellular vestibular loop of the PD. These residues are all

within 1 nm of at least one of the fourth, fifth, and eighth residues in the E_{10} loop in the closed state (Fig. 5, *A* and *C*) but are much farther from these residues in the open state (Fig. 5, *B* and *D*). This suggests that residues in the S3/S4 loop that are not interacting with the core of the VSD may be contributing to the overall energetics of activation by interacting with residues in the adjacent PD vestibule.

Given these results, the ΔG_{inter} values presented in Fig. 4 are consistent with the most recent closed state structural model of $K_v1.2$ (18). Glycine has no side chains and polyglycine has a low tendency to form stable secondary structures, so the interactions of the glycine series loop inserts would be the least likely to mediate non-backbone interactions with the rest of the channel. Once the polyglycine loop reaches a length of five or more and is capable of stretching across the S3/S4 gap in both open and closed conformations, the gating energy can be accounted for as the simple sum of the energy change in four loops (ΔG_{loop}) plus the energy change in the loopless channel (ΔG_{core}), *i.e.* $\Delta G_{inter} = 0$ (Fig. 4*A*).

The polyglutamate loops show a substantial non-backbone interaction effect on gating energy. Polyglutamate inserts of five and longer have a strong bias toward the open state reflected in their hyperpolarized V_{50} values. This was unexpected for two reasons, first because the polyglutamate loops monotonically favor longer end-to-end distances over the lengths range tested (Fig. 3), and yet the most current structural models predict that the open state has a shorter end-to-end distance than the closed state. Second, if the C-terminal end of the polyglutamate chain translocates into the membrane voltage field in the closed state, depolarization would be expected to stabilize the closed state because the force of the membrane potential acting on the neg-
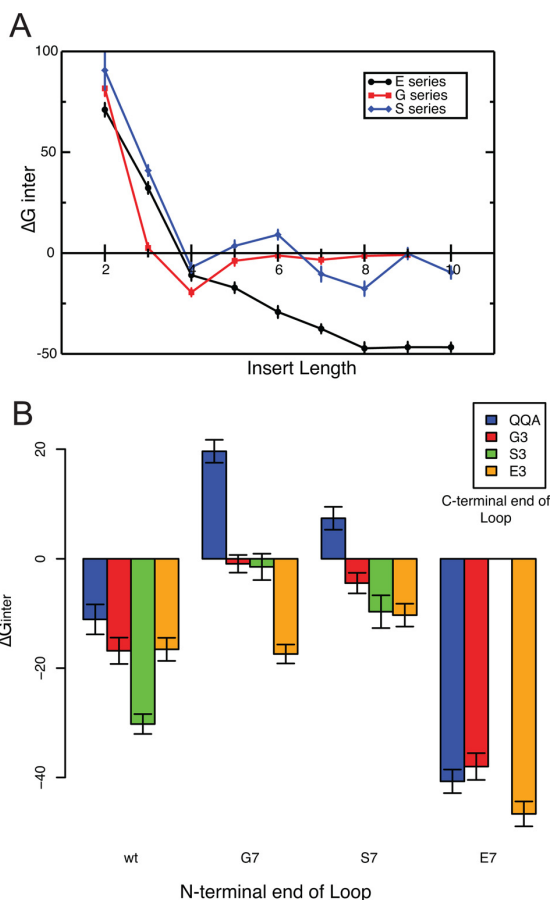
FIGURE 4. **Comparison of the ΔG_{inter} values (the effect of the loop that is not due to simple end-to-end distance constraints) for the different loop mutants.** *A*, ΔG_{inter} as a function of loop length for the three homoloop series of *insets*. *Error bars* represent S.E. *n* values range from 5–12 (see Table 1). *B*, comparison of the effects of changing the last three residues of the loop sequence in the heteroloop and WT/endloop mutants on ΔG_{inter}. The identity of the N-terminal part of the loop is indicated along the *horizontal axis*; the identities of the C-terminal three amino acid residues in the loop are indicated by the color coding of the *bars*, as per the key panel in the *upper right corner* of the *panel*. *Error bars* represent S.E. (*n* = 10). All energies are expressed as kJ/mol.

FIGURE 5. **Illustration of proximities of S3/S4 loop residues and acidic, negatively charged residues in the rest of the channel in open and closed state models.** For clarity, only the VSD from one subunit and the PD from the adjacent subunit are shown. *A* and *C* are open state conformations of the wild type channel, *B* and *D* are closed state conformations of the E$_{10}$ mutant channel. *A* and *B* are side views from within the plane of the membrane, and *C* and *D* are views from the extracellular aspect. Atoms in residues in the S3/S4 loop are rendered as *green spheres*, with the three C-terminal residues rendered as a *lighter green* than the rest of the loop. Atoms in acidic residues in the rest of the channel are rendered as *red spheres*. The remainder of the channel protein is rendered in *white*, ribbon format. The two acidic residues in the VSD that are within 1 nm of the loop in the closed state (Glu-226 and Asp-259) are labeled, except in *D*, where Asp-259 is hidden by the rendering of the extracellular loop. The other three acidic residues (Glu-350, Asp-352, and Glu-353, unlabeled) are in the vestibule loop of the immediately adjacent subunit.

atively charged glutamate side chains would be opposing the force exerted by the potential on the positively charged residues in S4. However, if the transmembrane electric field is focused below this vestibule, the glutamate homopolymer would be unaffected by that potential field.

Both of the effects discussed above appear to be overwhelmed by other interactions of the polyglutamate loop with the channel. Although repulsion of glutamate side chains by residues within the VSD in the closed state appears to be part of the effect, the fact that E$_7$G$_3$ and E$_7$QQA inserts are as negatively shifted as the E$_{10}$ insert indicates that a major part of the effect is due to the negative charge in the first seven amino acids of the loop insert. A plausible mechanism is illustrated in Fig. 5. The closed model indicates that when the channel closes, the S3/S4 loop region rotates into close proximity to the turret of the PD (16). Thus, in the case of the glutamate loop inserts, two protein regions with high negative surface potential are

brought into apposition when the channel subunit moves into the closed state. Such electrostatic repulsion in the closed state would destabilize the closed state, causing the channel to open at more hyperpolarized transmembrane potentials.

DISCUSSION

Although loops connecting core secondary structural elements of folded protein domains, as opposed to those connecting discrete domains, are often thought of as disordered and under relatively low selective pressure, they can play a significant role in the folding and functioning of proteins (43, 44). The length of the loop or more precisely, the relative differences in free energy between ensembles of different end-to-end distances, constrain the relative motion of structural elements within domains.

The lengths of loops connecting S3 and S4 in a collection of 239 members of the K$_v$1 family of voltage-gated ion channels vary in length from six amino acids up to 34 amino acids in

length, with the average length being 17. In the rat K$_v$1.2 channel, the length is 18. Thus, the range of lengths that we have tested in these experiments, seven to 18 amino acids in length, falls within the length range that has arisen naturally during evolution.

We have used the fact that varying the loop sequence causes variation in the relative energy of the loop in the open and closed channel conformations to interrogate the energetics of the VSD of the K$_v$1.2 channel and explore how these loops contribute to the overall voltage sensitivity of these channels. We have combined electrophysiological data with free energies calculated from molecular dynamics simulations in a novel way that avoids some limitations inherent to protein crystallography of dynamic transmembrane proteins and those functional experiments that introduce bulky probes or other non-native, tethered molecules.

The difference between the energetics of the negatively charged loops (based on polyglutamate and wild type amino acid sequence) and the neutral loops (based on polyglycine and polyserine homopolymers) suggests an electrostatic interaction between the S3/S4 loop and other parts of the channel. The closed state model derived from unrestrained molecular dynamics simulation (16) involves two major conformational changes that affect interactions with the S3/S4 loop. 1) The S4 helix translocates ~1.5 nm in the inward direction, drawing the C-terminal end of the loop into the interior of the VSD, and 2) the VSD rotates toward the PD, such that the S4 helix is pushed into close proximity with the negative field produced by the turret of the PD.

The translocation of the C-terminal end of the S3/S4 loop into a vestibule that stabilizes the positively charged residues of S4 in the open state can explain a significant part of the deviation of the experimental channel energetics from those predicted based solely on end-to-end distance constraints. In the case of the E$_3$ C-terminal segment electrostatic repulsion between this segment and acidic residues within the VSD would destabilize the closed state, leading to a shift to more negative V_{50} values. On the other hand, the QQA sequence at the C-terminal end of the wild type loop appears to stabilize the closed state, contributing to a more positive V_{50} value.

Electrostatic interaction between the S3/S4 loop and the PD in the closed state but not the open state also has a role in modulation of channel activity. The wild type loops have a ΔG_{inter} value of -11.2 ± 2.8 kJ/mol, but the C-terminal QQA sequence of the wild type loop tends to stabilize the closed state, *i.e.* contributes a positive term to G_{inter} (see above). Because the remainder of the wild type loop contains three acidic residues and one basic residue, it appears that repulsion between the loop and the turret of the PD is acting to destabilize the closed state, leading to the observed value for ΔG_{inter}.

Interestingly, steady-state activation of channels with loop inserts of only two or three residues is extremely right-shifted (Fig. 2) and manifests the largest positive values of ΔG_{inter} (Table 1). Yet, the most energetically stable end-to-end distance of these loop peptides in MD simulations was similar to that of the open state in the K$_v$1.2 crystal structure. How can these results be reconciled? Previous mutations made on the jellyfish channel jShak1, which has an extremely short S3/S4

loop, suggested that reducing the freedom of motion between S3 and S4 by lengthening the S4 helix caused steric clashing between helices in the VSD (27); this may be what is occurring in the shortest loops tested here. Because these loops are expected to exert significant force on the ends of S3 and S4 at the distances characteristic of the native closed state (2.02 nm), it appears that the shortest loop mutants in this study are forcing the channels into a different functional conformational ensemble, one that is dissimilar to the conformations identified in the experimentally determined structural models of the wild type K$_v$1.2 channel. These short loop constructs are similar to some of the deletion mutants constructed in the *Drosophila melanogaster* Shaker channel by Xu *et al.* (45) and by Gonzalez *et al.* (28), which also caused large rightward shifts in the *G-V* curves. In the case of these extremely short loops, however, Gonzalez *et al.* showed that the gating charge was reduced from 12 to ~5. It is possible that the effect of the short loops on V_{50} is due to restriction of S4 motion during opening and that the ΔG_{open} values that we have calculated for channels with extremely short loops could be significantly overestimated.

The opening and closing of voltage-gated ion channels is an allosteric process (46, 47). A change in the environmental conditions of the protein (*i.e.* membrane potential) leads to concerted molecular rearrangements of the protein between an inactive, ion-impermeant conformational ensemble and an active, ion permeant conformational ensemble. Opening of the channel is caused by a change in outward force on the S4 voltage-sensing helix due to depolarization of the membrane potential. This initial force is transduced into internal forces that rearrange the VSD. The rearranged VSD in turn causes channel opening by pulling on the S4/S5 intracellular loop, which in turn pulls the cytoplasmic ends of the S5 and S6 helices away from the central axis of the PD, opening a path into the cytoplasm for ions that have passed through the ion selective pore. We have delineated two mechanistic elements that affect the allosteric response within the VSD (loop length and interactions of the C terminus of the S3/S4 with charged residues within the VSD) and one mechanistic element that affects the allosteric interaction between the VSD and the PD (interaction of S3/S4 loop charged residues with charged residues in the turret of the PD).

In summary, a number of factors are responsible for the effect of varying the S3/S4 loop on the voltage sensitivity of the K$_v$1.2 channel. The length of the loop sequence is important, with very short loops (an insert of two amino acids with five additional residues flanking the insertion site, for a total length of seven residues) of any type causing an extreme positive shift in voltage sensitivity. Longer loops (of the order of five or more residues inserted with five additional residues flanking for a total of 10 or more residues) can impose subtle energetic constraints by virtue of the difference in free energy between the closed and open state conformational ensembles. However, with the exception of glycine homopolymer inserts, the loops do not solely act in this simple manner because the nature of their side chains affects the interaction energy of the loop with the rest of the channel, and this energy varies significantly between the open and closed states. A major factor in the interaction energy appears to be interactions between the S3/S4 loop

and the negatively charged turret of the pore domain, which intensifies on channel deactivation when the movement of the majority of the VSD away from the PD rotates the S3/S4 loop into closer proximity with the PD turret. In addition, residues near the C terminus of the loop, which are part of the unordered loop in the open state, are translocated into the core VSD structure in the closed state, bringing them into proximity with acidic residues within the VSD core. The combination of these two kinds of interaction is ultimately responsible for shifting the voltage sensitivity of the channel.

REFERENCES

1. Hille, B. (2001) *Ionic Channels of Excitable Membranes*, 3rd Ed., pp. 131–149, Sinauer Associates, Inc., Sunderland, MA
2. Bezanilla, F. (2008) How membrane proteins sense voltage. *Nat. Rev. Mol. Cell Biol.* **9,** 323–332
3. Tombola, F., Pathak, M. M., and Isacoff, E. Y. (2006) How Does Voltage Open an Ion Channel? *Annu. Rev. Cell Dev. Biol.* **22,** 23–52
4. Lee, S. Y., Lee, A., Chen, J., and MacKinnon, R. (2005) Structure of the KvAP voltage-dependent K+ channel and its dependence on the lipid membrane. *Proc. Natl. Acad. Sci. U.S.A.* **102,** 15441–15446
5. Long, S. B., Campbell, E. B., and Mackinnon, R. (2005) Crystal structure of a mammalian voltage-dependent Shaker family K+ channel. *Science* **309,** 897–903
6. Lainé, M., Lin, M. C., Bannister, J. P., Silverman, W. R., Mock, A. F., Roux, B., and Papazian, D. M. (2003) Atomic proximity between S4 segment and pore domain in Shaker potassium channels. *Neuron* **39,** 467–481
7. Jiang, Y., Lee, A., Chen, J., Ruta, V., Cadene, M., Chait, B. T., and MacKinnon, R. (2003) X-ray structure of a voltage-dependent K+ channel. *Nature* **423,** 33–41
8. Long, S. B., Tao, X., Campbell, E. B., and MacKinnon, R. (2007) Atomic structure of a voltage-dependent K(+) channel in a lipid membrane-like environment. *Nature* **450,** 376–382
9. DeCaen, P. G., Yarov-Yarovoy, V., Sharp, E. M., Scheuer, T., and Catterall, W. A. (2009) Sequential formation of ion pairs during activation of a sodium channel voltage sensor. *Proc. Natl. Acad. Sci. U.S.A.* **106,** 22498–22503
10. Papazian, D. M., Shao, X. M., Seoh, S. A., Mock, A. F., Huang, Y., and Wainstock, D. H. (1995) Electrostatic interactions of S4 voltage sensor in Shaker K+ channel. *Neuron* **14,** 1293–1301
11. Tao, X., Lee, A., Limapichat, W., Dougherty, D. A., and MacKinnon, R. (2010) A gating charge transfer center in voltage sensors. *Science* **328,** 67–73
12. Hoshi, T., Zagotta, W. N., and Aldrich, R. W. (1994) Shaker potassium channel gating. I: Transitions near the open state. *J. Gen. Physiol.* **103,** 249–278
13. Schoppa, N. E., and Sigworth, F. J. (1998) Activation of Shaker potassium channels. II. Kinetics of the V2 mutant channel. *J. Gen. Physiol.* **111,** 295–311
14. Zagotta, W. N., Hoshi, T., Dittman, J., and Aldrich, R. W. (1994) Shaker potassium channel gating. II: Transitions in the activation pathway. *J. Gen. Physiol.* **103,** 279–319
15. Delemotte, L., Tarek, M., Klein, M. L., Amaral, C., and Treptow, W. (2011) Intermediate states of the Kv1.2 voltage sensor from atomistic molecular dynamics simulations. *Proc. Natl. Acad. Sci. U.S.A.* **108,** 6109–6114
16. Jensen, M. Ø., Jogini, V., Borhani, D. W., Leffler, A. E., Dror, R. O., and Shaw, D. E. (2012) Mechanism of voltage gating in potassium channels. *Science* **336,** 229–233
17. Jogini, V., and Roux, B. (2007) Dynamics of the kv1.2 voltage-gated k+ channel in a membrane environment. *Biophys. J.* **93,** 3070–3082
18. Pathak, M. M., Yarov-Yarovoy, V., Agarwal, G., Roux, B., Barth, P., Kohout, S., Tombola, F., and Isacoff, E. Y. (2007) Closing in on the resting state of the Shaker K(+) channel. *Neuron* **56,** 124–140
19. Vargas, E., Yarov-Yarovoy, V., Khalili-Araghi, F., Catterall, W. A., Klein, M. L., Tarek, M., Lindahl, E., Schulten, K., Perozo, E., Bezanilla, F., and Roux, B. (2012) An emerging consensus on voltage-dependent gating from computational modeling and molecular dynamics simulations. *J. Gen. Physiol.* **140,** 587–594
20. Kim, M., Baro, D. J., Lanning, C. C., Doshi, M., Farnham, J., Moskowitz, H. S., Peck, J. H., Olivera, B. M., and Harris-Warrick, R. M. (1997) Alternative splicing in the pore-forming region of shaker potassium channels. *J. Neurosci.* **17,** 8213–8224
21. Jegla, T., Grigoriev, N., Gallin, W. J., Salkoff, L., and Spencer, A. N. (1995) Multiple Shaker potassium channels in a primitive metazoan. *J. Neurosci.* **15,** 7989–7999
22. Ramaswami, M., Gautam, M., Kamb, A., Rudy, B., Tanouye, M. A., and Mathew, M. K. (1990) Human potassium channel genes: molecular cloning and functional expression. *Mol. Cell. Neurosci.* **1,** 214–223
23. Schmidt, D., Jiang, Q. X., and MacKinnon, R. (2006) Phospholipids and the origin of cationic gating charges in voltage sensors. *Nature* **444,** 775–779
24. Xu, Y., Ramu, Y., and Lu, Z. (2008) Removal of phospho-head groups of membrane lipids immobilizes voltage sensors of K+ channels. *Nature* **451,** 826–829
25. Tiwari-Woodruff, S. K., Lin, M. A., Schulteis, C. T., and Papazian, D. M. (2000) Voltage-dependent structural interactions in the Shaker K(+) channel. *J. Gen. Physiol.* **115,** 123–138
26. Tiwari-Woodruff, S. K., Schulteis, C. T., Mock, A. F., and Papazian, D. M. (1997) Electrostatic interactions between transmembrane segments mediate folding of Shaker K+ channel subunits. *Biophys. J.* **72,** 1489–1500
27. Klassen, T. L., O'Mara, M. L., Redstone, M., Spencer, A. N., and Gallin, W. J. (2008) Non-linear intramolecular interactions and voltage sensitivity of a KV1 family potassium channel from Polyorchis penicillatus (Eschscholtz 1829). *J. Exp. Biol.* **211,** 3442–3453
28. Gonzalez, C., Rosenman, E., Bezanilla, F., Alvarez, O., and Latorre, R. (2000) Modulation of the Shaker K(+) channel gating kinetics by the S3-S4 linker. *J. Gen. Physiol.* **115,** 193–208
29. Gonzalez, C., Rosenman, E., Bezanilla, F., Alvarez, O., and Latorre, R. (2001) Periodic perturbations in Shaker K+ channel gating kinetics by deletions in the S3-S4 linker. *Proc. Natl. Acad. Sci. U.S.A.* **98,** 9617–9623
30. Dominguez, I., Itoh, K., and Sokol, S. Y. (1995) Role of glycogen synthase kinase 3 beta as a negative regulator of dorsoventral axis formation in *Xenopus* embryos. *Proc. Natl. Acad. Sci. U.S.A.* **92,** 8498–8502
31. Baumgartner, W., Islas, L., and Sigworth, F. J. (1999) Two-microelectrode voltage clamp of *Xenopus* oocytes: voltage errors and compensation for local current flow. *Biophys. J.* **77,** 1980–1991
32. Grigoriev, N. G., Spafford, J. D., and Spencer, A. N. (1999) Modulation of jellyfish potassium channels by external potassium ions. *J. Neurophysiol.* **82,** 1728–1739
33. Huang, Q. Q., Harvey, C. M., Paterson, A. R., Cass, C. E., and Young, J. D. (1993) Functional expression of Na(+)-dependent nucleoside transport systems of rat intestine in isolated oocytes of *Xenopus laevis*. Demonstration that rat jejunum expresses the purine-selective system N1 (cif) and a second, novel system N3 having broad specificity for purine and pyrimidine nucleosides. *J. Biol. Chem.* **268,** 20613–20619
34. Miledi, R., and Parker, I. (1984) Chloride current induced by injection of calcium into *Xenopus* oocytes. *J. Physiol.* **357,** 173–183
35. Sand, R. M., Atherton, D. M., Spencer, A. N., and Gallin, W. J. (2011) jShaw1, a low-threshold, fast-activating Kv3 from the hydrozoan jellyfish *Polyorchis penicillatus*. *The J. Exp. Biol.* **214,** 3124–3137
36. Hodgkin, A. L., and Huxley, A. F. (1952) A quantitative description of membrane current and its application to conduction and excitation in nerve. *J. Physiol.* **117,** 500–544
37. Chen, X., Wang, Q., Ni, F., and Ma, J. (2010) Structure of the full-length Shaker potassium channel Kv1.2 by normal-mode-based x-ray crystallographic refinement. *Proc. Natl. Acad. Sci. U.S.A.* **107,** 11352–11357
38. Bordoli, L., Kiefer, F., Arnold, K., Benkert, P., Battey, J., and Schwede, T. (2009) Protein structure homology modeling using SWISS-MODEL

workspace. *Nat. Protoc.* **4,** 1–13

39. DeLano, W. L. (2010) *The PyMOL Molecular Graphics System*, version 1.5.0.4, Schrödinger, LLC, New York

40. Hess, B., Kutzner, C., van der Spoel, D., and Lindahl, E. (2008) GROMACS 4: Algorithms for highly efficient, load-balanced, and scalable molecular simulation. *J. Chem. Theory Comput.* **4,** 435–447

41. Bennett, C. H. (1976) Efficient Estimation of Free-Energy Differences from Monte-Carlo Data. *J. Comput. Phys.* **22,** 245–268

42. Khalili-Araghi, F., Jogini, V., Yarov-Yarovoy, V., Tajkhorshid, E., Roux, B., and Schulten, K. (2010) Calculation of the gating charge for the Kv1.2 voltage-activated potassium channel. *Biophys. J.* **98,** 2189–2198

43. Kwon, Y. D., Finzi, A., Wu, X., Dogo-Isonagie, C., Lee, L. K., Moore, L. R., Schmidt, S. D., Stuckey, J., Yang, Y., Zhou, T., Zhu, J., Vicic, D. A., Debnath, A. K., Shapiro, L., Bewley, C. A., Mascola, J. R., Sodroski, J. G., and Kwong, P. D. (2012) Unliganded HIV-1 gp120 core structures assume the CD4-bound conformation with regulation by quaternary interactions and variable loops. *Proc. Natl. Acad. Sci. U.S.A.* **109,** 5663–5668

44. Radley, T. L., Markowska, A. I., Bettinger, B. T., Ha, J. H., and Loh, S. N. (2003) Allosteric switching by mutually exclusive folding of protein domains. *J. Mol. Biol.* **332,** 529–536

45. Xu, Y., Ramu, Y., and Lu, Z. (2010) A shaker K+ channel with a miniature engineered voltage sensor. *Cell* **142,** 580–589

46. Hilser, V. J., Wrabl, J. O., and Motlagh, H. N. (2012) Structural and energetic basis of allostery. *Annu. Rev. Biophys.* **41,** 585–609

47. Ma, B., Tsai, C. J., Haliloglŭ, T., and Nussinov, R. (2011) Dynamic allostery: linkers are not merely flexible. *Structure* **19,** 907–917